SCUOLA DI DOTTORATO

UNIVERSITÀ DEGLI STUDI DI MILANO-BICOCCA

Dipartimento di / Department of

Scienze dell'Ambiente e della Terra

Dottorato di Ricerca in / PhD program Scienze Chimiche, Geologiche e Ambientali,
Ciclo / Cycle 35, *Curriculum in* Scienze Geologiche

The influence of land temperatures on the winter mid-latitude atmospheric circulation

TESI IN COTUTELA

Cognome / Surname: Portal *Nome / Name:* Alice

Matricola / Registration: 854559

Tutore / Tutor: Eduardo Garzanti

Supervisor: Claudia Pasquero

Co-supervisor: Fabio D'Andrea

Coordinatore / Coordinator: Marco Giovanni Malusà

ANNO ACCADEMICO / ACADEMIC YEAR 2021/2022

Università degli Studi di Milano-Bicocca (UNIMIB)
Dipartimento di Scienze dell'Ambiente e della Terra

Scuola di Dottorato *Università degli Studi di Milano-Bicocca*, XXXV cycle
PhD program in *Scienze Chimiche, Geologiche e Ambientali*, Curriculum *Scienze Geologiche*

École Normale Supérieure (ENS), Université Paris Sciences & Lettres (PSL)
Laboratoire de Météorologie Dynamique

École Doctorale *Science de l'Environnement d'Ile-de-France* (ED n° 129)
Specialisation in *Instrumentation, télédétection, observation et techniques spatiales pour l'océan, l'atmosphère et le climat*

The influence of land temperatures on the winter mid-latitude atmospheric circulation

Alice Portal

Supervisors: Claudia Pasquero (UNIMIB),
Fabio D'Andrea (ENS, PSL)

Submitted March 2023

Abstract

The first attempts to determine the role of orography and longitudinally varying heat sources for the mid-latitude atmospheric circulation date back to more than half a century ago. Whilst we have reached a good understanding of their interaction with the atmosphere, climate change and the wide use of climate models, characterised by common or individual biases, pose new interesting questions. Because of the long time scales and large impact of ocean-based signals, the interaction of the atmosphere with the sea surface temperature has been studied extensively. Less so for the land surface which, when inducing persistent low-level warming or cooling, may nonetheless become important for the atmospheric circulation. However, the persistence of the forcing by a land-based thermal source is not always sufficient to determine an important dynamical response in the atmosphere. Some examples are developed in the thesis. In a warmer climate the surface of the continents are expected to warm faster than the surface of the oceans, producing changes in the large-scale temperature contrast. During the winter season of the Northern Hemisphere (NH), chosen as the setting for our analysis, the thermal contrast is projected to reduce. A set of perpetual-winter atmospheric simulations with prescribed surface conditions featuring an intense NH extratropical land warming reveals a strong reduction in the strength of the large-scale features of the mid-latitude atmosphere, i.e. stationary waves and jet streams. Interestingly, the response is induced mainly by the warming of the Asian continent, with North America playing only a secondary role. Prompted by this result, we examine the representation of Asian temperatures in a set of state-of-the-art climate models, and detect a large inter-model temperature spread over the Tibetan Plateau and Siberia. We show that anomalously low temperatures over the Tibetan Plateau - a region that is often affected by a cold model bias - reinforce the East Asia winter monsoon and have a strong impact on the mean atmospheric conditions downstream of the orography. Anomalous Siberian temperatures, on the other hand, do not produce substantial changes in the Pacific sector, but, through local changes in the low-level atmospheric conditions, influence the winds over the continent. Consistent dynamical changes are detected in climate projections featuring different degrees of warming over the regions of the Tibetan Plateau and Siberia. The results presented in the thesis identify the Asian orography as a hotspot of land–atmosphere interaction, highlighting the importance of land modelling over complex orography (e.g. the Tibetan Plateau) for the atmospheric circulation.

Summary of the thesis for the general public. The first attempts to model the impact of orography and longitudinally varying heat sources on mid-latitude atmospheric circulation date back more than half a century. While we have reached a good understanding of their interaction with the atmosphere, climate change and biases in climate models pose new questions, such as the role of land surface temperature, as opposed to sea surface temperature, in the mid-latitude climate. The thesis examines the response of the atmospheric circulation to large-scale changes in surface temperature over extratropical continents in the Northern Hemisphere. Results show that East Asia is a hotspot of land-atmosphere interaction, highlighting the importance of land modeling over complex orography for atmospheric circulation.

Key words: climate, large-scale atmospheric variability, mid latitudes, land-sea thermal contrast, land surface temperature.

Versione in italiano. Risalgono a più di mezzo secolo fa' i primi studi sul ruolo dell'orografia e delle variazioni longitudinali delle sorgenti di calore per la circolazione atmosferica delle medie latitudini. Nonostante sia stato raggiunto un buon livello di conoscenza del tema, nuove domande stanno nascendo per via del cambiamento climatico e dell'ingente utilizzo di modelli climatici, interessati da varie tipologie di errori. I tempi scala lunghi e l'impatto importante dei segnali termici oceanici hanno permesso uno studio approfondito delle interazioni tra la temperatura della superficie del mare e l'atmosfera. La superficie delle terre emerse ha ricevuto meno attenzione, sebbene possa diventare rilevante per la circolazione quando induce un riscaldamento o raffreddamento persistente nella bassa atmosfera. La persistenza del segnale termico terrestre non costituisce però una condizione sufficiente per determinare una risposta dinamica forte in atmosfera. Nella tesi ne sviluppiamo alcuni esempi. Con il riscaldamento climatico la superficie dei continenti dovrebbe scaldarsi più velocemente della superficie degli oceani; di conseguenza anche il contrasto termico tra i due dovrebbe cambiare. Decidiamo di concentrarci sulla stagione invernale dell'emisfero boreale. Un set di simulazioni a inverno perenne, girate con condizioni superficiali caratterizzate da un riscaldamento anomalo della superficie terrestre negli extratropici, mostra una riduzione degli elementi principali che contraddistinguono l'atmosfera delle medie latitudini, ovvero le correnti a getto e le onde stazionarie. È interessante notare che la risposta atmosferica è prevalentemente forzata dal riscaldamento del continente asiatico, con un ruolo secondario dell'America settentrionale. Partendo da questi risultati, esaminiamo la rappresentazione delle temperature asiatiche medie in un insieme di modelli climatici allo stato dell'arte, e troviamo ampie differenze tra i modelli soprattutto nell'altopiano tibetano e in Siberia. Mostriamo che la temperature della regione dell'altopiano tibetano, che nei modelli è spesso eccessivamente fredda, ha un ruolo nella modulazione del monsone invernale dell'Asia orientale, e quindi influenza le condizioni atmosferiche a valle dell'orografia. D'altro canto, le temperature in Siberia non hanno particolari conseguenze sul settore del Pacifico, ma influenzano i venti sul continente. Inoltre i modelli caratterizzati da Siberia calda mostrano un riscaldamento anomalo ai Tropici, quelli con Siberia fredda mostrano anomalie nella copertura nuvolosa dalle medie latitudini al Polo Nord. I risultati presentati nella tesi sono concordi nell'identificare l'orografia asiatica come una regione chiave per le interazioni tra superficie terrestre e atmosfera. Ulteriori simulazioni che analizzino l'impatto atmosferico della temperatura superficiale di regioni più circoscritte, potrebbero contribuire ad una visione completa sull'interazione tra anomalie termiche e orografia in Asia. Inoltre, in base ai risultati qui pre-

sentati, crediamo che avanzamenti nella modellizzazione della terraferma, particolarmente in zone dove l'orografia è complessa (come l'altopiano tibetano), possano avere un impatto positivo anche sulla rappresentazione della circolazione atmosferica.

Sintesi della tesi per il grande pubblico in italiano. I primi tentativi di modellare l'impatto dell'orografia e delle variazioni longitudinali delle sorgenti di calore sulla circolazione atmosferica delle medie latitudini risalgono a più di mezzo secolo fa. Sebbene sia stata raggiunta una buona comprensione dell'interazione con l'atmosfera, il cambiamento climatico e i bias nei modelli climatici introducono nuovi argomenti di ricerca, come ad esempio il ruolo della temperatura della superficie terrestre, rispetto a quella della superficie del mare, nel clima delle medie latitudini. La tesi esamina la risposta della circolazione atmosferica ai cambiamenti della temperatura superficiale sui continenti extratropicali nell'emisfero settentrionale. I risultati mostrano che l'Asia orientale è un hotspot dell'interazione terra-atmosfera, evidenziando quanto la modellizzazione di alcune regioni terrestri caratterizzate da orografia complessa sia importante per la circolazione atmosferica.

Parole chiave: clima, variabilità atmosferica a grande scala, medie latitudini, contrasto termico terra-mare, temperatura superficiale delle terre emerse.

Version en français. Les premières tentatives pour déterminer le rôle de l'orographie et des variations longitudinales des sources de chaleur pour la circulation atmosphérique extratropical remontent à plus d'un demi-siècle. Bien que nous ayons une bonne compréhension de leur interaction avec l'atmosphère, le changement climatique et les biais des modèles numeriques posent de nouvelles questions. Si l'interaction de l'atmosphère avec la température de surface de la mer a été largement étudiée, on ne peut pas en dire autant pour l'interaction avec la surface des terres qui, par un réchauffement ou un refroidissement persistant de la basse troposphère, peut devenir importante pour la circulation atmosphérique. Cependant, la persistance d'une source thermique terrestre n'est pas toujours efficace pour déterminer une réponse dynamique importante. Des exemples sont développés dans la thèse. Dans un climat plus chaud, on s'attend que la surface des continents se réchauffe plus rapidement que la surface des océans, produisant des changements à grande échelle dans le contraste de température terre-mer. Pendant la saison d'hiver de l'hémisphère nord, choisi comme cadre pour notre analyse, le contraste thermique devrait diminuer. Un ensemble de simulations atmosphériques en condition d'hiver perpétuel, avec des conditions de surface présentant un réchauffement intense des continents extratropicales, révèle une forte réduction des structures de l'atmosphère aux moyennes latitudes: les ondes stationnaires et les courants-jets. La réponse se produit principalement par le réchauffement du continent asiatique, l'Amérique du Nord ne jouant qu'un rôle secondaire. Motivés par ce résultat, nous avons examiné la représentation des températures asiatiques dans un ensemble de modèles climatiques, où une large dispersion de température superficiale a été détecté parmi les modèles, en particulier sur le Plateau Tibétain et en Sibérie. Nous montrons que les températures anormalement basses sur le Plateau Tibétain - une région souvent affectée par un biais froid - renforcent la mousson d'hiver d'Asie de l'Est et ont un impact fort sur les conditions atmosphériques moyennes en aval de l'orographie. Les températures anormales de Sibérie, en revanche, ne déterminent pas de changements substantiels dans le secteur du Pacifique, mais, par des changements locaux dans les basses couches atmosphériques, influencent les vents sur le continent. Des changements dynamiques cohérents sont détectés dans les projections climatiques présentant différents degrés de réchauffement sur les régions du Plateau Tibétain et de la Sibérie. Les résultats présentés dans la thèse identifient l'orographie asiatique comme un "hotspot" de l'interaction terre-atmosphère, soulignant l'importance de la modélisation de ces interactions dans le contexte d'une orographie complexe (comme le Plateau Tibétain) pour la circulation atmosphérique.

Résumé de thèse pour le grand public en français. Les premières tentatives de modélisation de l'impact de l'orographie et des variations longitudinales des sources de chaleur sur la circulation atmosphérique des latitudes moyennes remontent à plus d'un demi-siècle. Bien que nous ayons une bonne compréhension de leur interaction avec l'atmosphère, le changement climatique et les biais des modèles climatiques posent de nouvelles questions, telles que le rôle de la température de la surface terrestre, par opposition à la température de la surface de la mer, dans le climat des latitudes moyennes. La thèse examine la réponse de la circulation atmosphérique aux changements de la température de surface sur les continents extratropicaux de l'hémisphère nord. Les résultats montrent que l'Asie de l'Est est un "hotspot" pour l'interaction entre la surface terrestre et l'atmosphère, soulignant l'importance de la modélisation de certaines régions terrestres caractérisées par une orographie complexe pour la circulation atmosphérique.

Mots clés: climat, variabilité atmosphérique à grande échelle, moyennes latitudes, contraste thermique terre-mer, température de surface des terres.

Acknowledgements

It feels as if it was only a few months ago when Fabio created our first shared folder on Google Drive (named `Alice-Claudia-Fabio`, quite poetic), but more than three years have gone past and a lot of things have happened in the meantime. Covid-19 is what will remain most impressed in our memories, and the endless video-calls which played an impressive role in my PhD. Mostafa and Paolo were soon included in a sort of "SPEEDY dream team", hosting occasional visitors such as Franco and Gwendal. Even though the first year or so was a bit like driving blindfold in New Dehli (I'm joking!), we had fun, and - apart from the scientific discussions - I will miss your spirit and your ways. Claudia, with her frequent "No, io non ho capito!", which were actually useful to understand that I was in the same position and disposition, taught me to look into the logics of relations, and to not give for granted what is usual or obvious. Simple things sometimes hide interesting problems. Fabio, often in a hurry to fetch some kid in some place, was the last to be convinced of my convictions, and taught me caution and rightful doubt. The great enthusiasm in science and the care of personal relations is what characterises them both and makes them most precious.

The PhD was also a wonderful opportunity to make new friends out of collegues, or non-collegues. The gentle ways of Anna, the abrupt loving Vinita, Yanxu with her phylosophical brain, calm and rational Ago, with the right word in every situation, Fabien's political anger contrasted by his smile, brilliant Mostafa, Marion, Matteo, Lisa, Chiara, Pablo and all the other nice people that I met during this period. Friends from the Parisian Cité U (Avi, Luisa, Amar, Jess) will always feel close even when geographically far, and Paris in itself will remain a place of good memories and discoveries.

Finally, my heart is always in the hands of my dear parents, Franci, Luigi and Cristina, and, of course, Federico, loving and lovely husband.

— Qui aimes-tu le mieux, homme énigmatique, dis ? ton père, ta mère, ta sœur ou ton frère ?
— Je n'ai ni père, ni mère, ni sœur, ni frère.
— Tes amis ?
— Vous vous servez là d'une parole dont le sens m'est resté jusqu'à ce jour inconnu.
— Ta patrie ?
— J'ignore sous quelle latitude elle est située.
— La beauté ?
— Je l'aimerais volontiers, déesse et immortelle.
— L'or ?
— Je le hais comme vous haïssez Dieu.
— Eh ! qu'aimes-tu donc, extraordinaire étranger ?
— J'aime les nuages... les nuages qui passent... là-bas... là-bas... les merveilleux nuages !

Charles Baudelaire, Petits poèmes en prose, 1869

Contents

List of Tables

List of Figures

Chapter 1

Introduction

In the extratropical atmosphere the balance between the strong meridional pressure gradient force, induced by the Equator-to-pole temperature difference, and the Coriolis force, arising from Earth's rotation, drive a strong westerly mean flow, which we call *mid-latitude jet stream* or simply *jet*. Were the Earth axisymmetric (i.e. symmetric around the axis connecting the two poles), as in the case of an *aquaplanet*, the mean mid-latitude flow would turn on a plane parallel to the Equator and its intensity would be zonally uniform (independent of longitude). However, due to the alternation of land and water masses and to the presence of orography, the surface boundary conditions of the atmospheric system are far from axisymmetric. Such irregular surface forcing modifies the atmospheric circulation aloft, but also adjusts itself to the zonally asymmetric features developed by the atmosphere, in a continuously evolving feedback between the atmosphere and the surface (cf. Figure 1.1 and Figure 1.2). An explicit example of the stationary atmospheric response to surface forcing is the difference between the climatological[1] mid-latitude circulation in the Northern and Southern Hemisphere: the former, characterised by the presence of large continents and important orography, presents a mean flow with conspicuous deviations from the zonal mean. The deviations from zonal symmetry are altogether less relevant to describe the Southern Hemisphere jet stream (see Figure 1.1).

[1] long-term (climate) mean

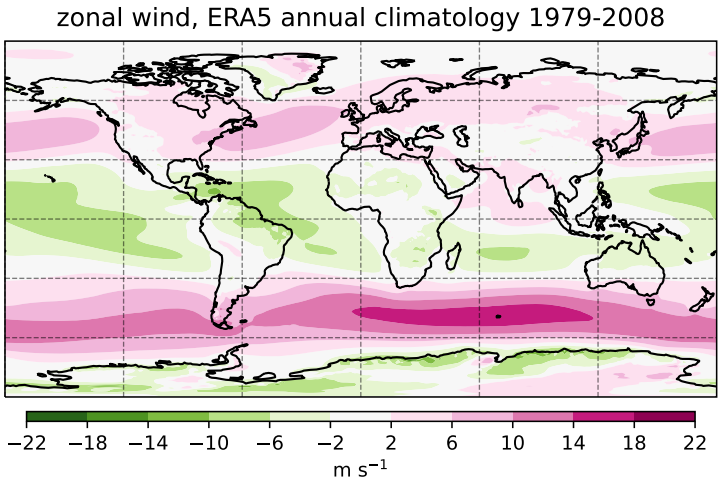

Figure 1.1: Annual zonal wind climatology at the pressure level 850 hPa from ERA5 Reanalysis 1979–2008. To note, the stronger zonal asymmetry of the wind patterns in the Northern Hemisphere compared to the Southern Hemisphere

Smagorinsky (1953) first represented the effect of the alternation of land and ocean on the mean mid-latitude flow. In his analytical model a spatially fixed sinusoidal distribution of heat sources and sinks of limited depth acts on a horizontally uniform zonal current confined between rigid horizontal planes; the speed of the flow increases linearly with height. For the case of NH winter the heat sinks are over the continents, due to predominant radiative heat loss, the heat sources are over the oceans, which transfer heat to the atmosphere through turbulent fluxes (negative and positive lobes of the sinusoidal distribution, respectively). See as a reference the climatological winter column-integrated heating in Figure 2.6. For realistic length and warming parameters, the theory predicts the presence of a surface low-pressure center approximately 25 degrees east of the heat source and a mid-tropospheric trough slightly west of the source (details on the model and parameters in Section 2.3.2). This is entirely consistent with the circulation induced by the ocean heat fluxes to the east of the Asian and North American continents (Figure 2.6), giving rise to Aleutian and Icelandic lows centered approximately 30 degrees to their east (Figure 1.3). The position of the Siberian surface high-pressure system, i.e. to the east of the maximum continental cooling, is also coherent with the theory. Before the use of atmospheric general circulation models (AGCMs), Smagorinsky's simplified analytical calculations were surprisingly accurate in predicting the longitudinal variations of the winter mid-latitude climate.

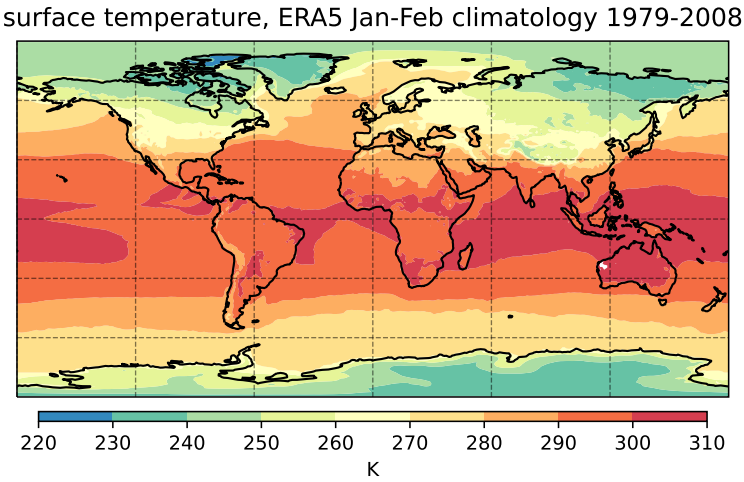

Figure 1.2: January-February climatology of surface (skin) temperature from ERA5 Reanalysis 1979–2008

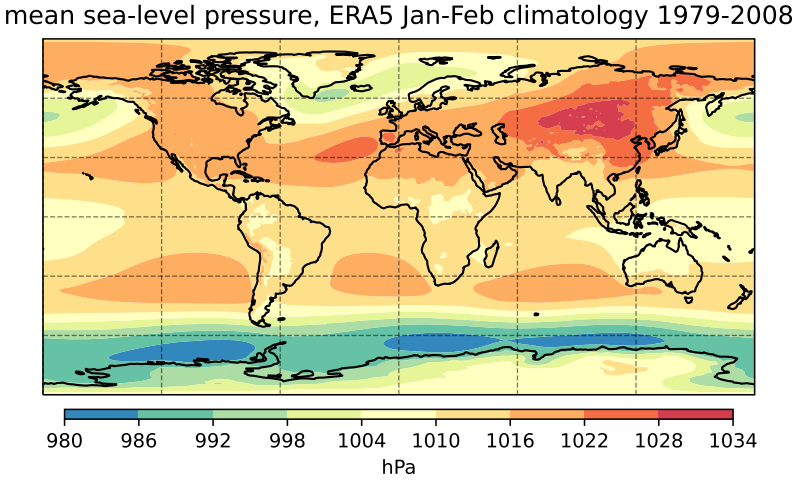

Figure 1.3: January-February climatology of mean sea-level pressure from ERA5 Reanalysis 1979–2008

A mid-latitude circulation theory based on large-scale[2] heat sources and sinks fails when considering the transition from the winter to the summer season. While in summer the inverted thermal effect of land and ocean would advocate for a reversal of the low and high pressure systems and of the related circulation patterns, observations detect - in some regions of the mid latitudes - only small changes in the direction and intensity of the mean flow throughout the year (e.g. east of the Andes Mountains, see Boffi, 1949). The mechanical forcing by orography, acting on the jet in all seasons, is a second fundamental ingredient necessary to explain stationary large-scale atmospheric systems in the Extratropics (Charney and Eliassen, 1949; Bolin, 1950).

[2]spatial scale of the order of 2000 km or more

Quite early in the development of the theory for mid-latitude planetary[3] waves, it was noted - at first from an analytical point of view - that the largest-size waves, specifically the stationary disturbances of zonal wavenumber 1 and 2, propagate vertically to the stratosphere where they transport heat to the cold polar core of the stratospheric polar vortex and slow down the strong climatological winds turning eastwards around the pole (Matsuno, 1971). This happens in winter, when the intense radiatively-forced temperature gradient sustains the stratospheric polar vortex, while in summer the vortex turns westwards and stops supporting the vertical propagation of tropospheric waves (the mechanism is explained by the *Charney-Drazin criterion*, see Chapter 2,2.2). The upward propagation to the stratosphere concerns, hence, the largest possible extratropical waves, which coincide mainly with those produced by the land-sea thermal contrast. Large-scale waves can be modulated by extensive perturbations generated by mid-latitude signals or propagating from other latitudinal regions, e.g. the Tropics.

The influence of the Tropics is twofold. Because of the reversal in the direction of the mean flow at these latitudes, it acts firstly as a meridional boundary with marked reflective properties, affecting the meridional propagation of disturbances out of the Extratropics; secondly it constitutes an active wave source reaching far polewards to influence the higher-latitude perturbations. The tropical wave source is mainly stationary, from the presence of a climatological zonal circulation (known as Walker circulation) fostered by deep convection over the warm oceans, but also undergoes long-lasting variations, as for the notable ENSO - El Niño-Southern Oscillation.

Complex general circulation models provide the possibility to study the non-linear interaction between large-scale atmospheric waves and the other elements of the climate system. Feedbacks influencing the planetary waves at many temporal and spatial scales are thus included. An example of feedback between time scales is given by the interaction between planetary stationary waves and the mid-latitude storm tracks. The latter are extratropical regions located mainly over the western oceanic basins that are characterised by the passage of transient synoptic[4] disturbances - eddies - sustaining the zonal flow, called the *eddy-driven jet* in the lower-to-

[3] large-scale ($\geq$ 2000 km)

[4] spatial scale of the order of 1000 km

mid troposphere. The development of the eddies in specific geographical areas is favored by the large-scale features of the climate system and, at the same time, induces persistent atmospheric conditions (i.e. heat and momentum fluxes) that help to shape the large-scale atmospheric waves.

Although the theory of planetary atmospheric waves is valid for the Southern and Northern Hemisphere without distinction, it is certainly most important for explaining the average NH conditions, where land occupies a considerable fraction of the extratropical surface, and mountain ranges such as the Rocky Mountains and the Tibetan Plateau obstruct the mean mid-latitude flow. Moreover, the NH planetary waves reach their maximum amplitude in winter as a result of (i.) the intensified mean flow that increases the effect of orography and (ii.) the strong thermal contrast between cold continental land and warm oceans. For the reasons listed above, throughout the thesis we focus on the winter season of the NH mid latitudes.

Details on the theory of planetary waves and of their interaction with the climate system are provided in Chapter 2. We present the basic equations in the mid-latitudes, the propagation of Rossby waves and the first analytical models representing thermal and orographic wave forcing, and we discuss the modern concept of stationary waves derived from experiments using state-of-the-art climate models (Sections 2.1-2.3). The relation between stationary and transient waves and the influence of surface conditions on the large-scale atmospheric circulation (Sections 2.4, 2.5) conclude the chapter.

Much as the role of mid-latitude sea surface temperature (SST)s has been broadly investigated because of the vigourous effect of oceans on the atmospheric system in terms of sensible and latent heat release, less attention has been dedicated to the effect of large-scale land surface temperature on the atmospheric circulation, constituting the winter heat sink in Smagorinsky's model. The topic is specially compelling in light of ongoing and projected modifications in the intensity of the contrast between land and sea temperatures. In fact, as a consequence of climate change, land surface is warming faster than the sea surface, thereby reducing the winter thermal contrast and amplifying the summer contrast. Here we posit the following research questions:

- how does a reduction of the winter land-sea thermal contrast by land warming influence the large-scale mid-latitude circulation?
- what is the role of the land temperature individually over Asia and North America?

We elaborate on this subject in Chapter 3, where we show the results of idealised simulations run with a present-day climate characterised by intensive warming over the NH continents. It is found that the intensity of the atmospheric response is extremely sensitive to the geographical location (i.e. the continent) where the warming is imposed, specifically it is sensitive to East-Asia land warming while the response to North-America land-temperature anomalies is weak.

The extensive work done since the mid XXth century to unravel the topic of large-scale surface forcing and its interaction with the atmosphere agrees on the importance of thermally forced waves for the winter mid-latitude climate. Even so, state-of-the-art climate models exhibit a wide spread in representing large-scale patterns of land temperature in the winter NH, which may easily result in modifications of the models' climate over a range of spatial scales. Based on the findings of Chapter 3, where we show evidence for the impact of land temperature over East Asia for the global atmospheric circulation, in Chapter 4 we analyse the interaction between East-Asia near-surface temperatures and the large-scale winter circulation in the context of the Coupled Model Intercomparison Project - Phase 6 (CMIP6) simulations. The results indicate that the well-known cold model bias over the Tibetan Plateau strongly modifies the average circulation over the Pacific sector (Section 4.1), while model spread in Siberian temperatures may be connected to anomalies in the mid-latitude or tropical regions, and determine local low-level changes that do not affect the Pacific jet streams (Section 4.2). Consistent patterns are identified in CMIP6 projections of the future atmospheric circulation, despite different amplitudes of land warming over East Asia (Section 4.3). Furthermore, in the Conclusions (Chapter 5) we discuss the role of orographic elevation in setting the atmospheric response.

In brief, after presenting the theoretical background to atmospheric planetary (stationary) waves in Chapter 2, we first approach the topic of land-temperature forcing from an idealised point of view in Chapter 3, in order to isolate its impact on the winter NH atmosphere. Secondly in Chapter 4, after having identified East Asia as a hot-spot of land–atmosphere interaction, we

apply the main findings from the idealised setting to interpret the role of large-scale temperature patterns in state-of-the-art models, using the CMIP6 simulations for the purpose. A summary of the main findings and of future perspectives of this work is provided in Chapter 5.

Chapter 2

Theoretical background

In this chapter, after introducing the primitive equations for the mid latitudes in Section 2.1 and Rossby waves and their vertical propagation in Section 2.2, two analytical models are presented serving as example to understand the effect of orography and large-scale heat sources on the mean mid-latitude flow. The first is Charney and Eliassen's barotropic model for orographic waves (Section 2.3.1), the second is Smagorinsky's baroclinic model forced by an idealised distribution of heat sources and sinks (Section 2.3.2). Both analyse the zonal disturbances in a channel of limited meridional width or on an infinitely extended plane where the Coriolis term varies linearly with latitude (β-plane approximation presented in Section 2.1). For simplicity, the meridional propagation of waves and, with this, the contribution of the Tropics and Subtropics to the mid-latitude planetary waves, are not included in the analytical models. In Section 2.3.3 the discussion is extended to detail the debate on the relative importance of thermal and orographic forcing of stationary waves, and to discuss the sensitivity of the atmospheric response to the depth and position of the thermal forcing, with comparisons of the linear model results with those obtained with full AGCM simulations. The contribution of transient eddies to deep thermal forcing of planetary waves is examined in Section 2.4. In Section 2.5 we present a short overview of the land-atmosphere feedback, with a focus on the relation between near-surface processes and the winter atmospheric circulation. Specific details on some of these topics will be provided in the introductions to the Chapters of the thesis.

2.1 Governing equations in the mid-latitudes

The primitive Navier–Stokes equations describing the evolution of the atmosphere can be approximated differently depending on the choice of scale and latitudinal setting. For mid-latitude synoptic and large-scale phenomena the primitive equations can be reduced to

$$\frac{D\mathbf{u}}{Dt} + f\hat{k} \times \mathbf{u} + \nabla_h \Phi = (X, Y) \qquad \text{horizontal momentum} \qquad (2.1a)$$

$$\frac{\partial \Phi}{\partial z^*} = -g \qquad \text{hydrostatic balance} \qquad (2.1b)$$

$$\frac{\partial u}{\partial x} + \frac{\partial v}{\partial y} + \frac{\partial w^*}{\partial z^*} + w^* \frac{d}{dz^*}(\ln \rho_r) = 0 \qquad \text{mass conservation} \qquad (2.1c)$$

$$c_p \frac{D \ln T}{Dt} - R \frac{D \ln p}{Dt} = \frac{J}{T} \qquad \text{energy conservation} \qquad (2.1d)$$

$$\text{with material derivative} \qquad \frac{D}{Dt} \equiv \frac{\partial}{\partial t} + u\frac{\partial}{\partial x} + v\frac{\partial}{\partial y} + w^*\frac{\partial}{\partial z^*},$$

$$\text{horizontal gradient} \qquad \nabla_h \equiv \frac{\partial}{\partial x} + \frac{\partial}{\partial y}$$

where x is the eastward distance along $\hat{\mathbf{i}}$, y the northward distance along $\hat{\mathbf{j}}$, z^* the geometric height above the surface, $\mathbf{u} = u\hat{\mathbf{i}} + v\hat{\mathbf{j}}$ the horizontal velocity, w^* the velocity along the vertical $\hat{\mathbf{k}}$, (X, Y) the horizontal components of nonconservative mechanical forcing, $f = 2\Omega \sin\phi$ the Coriolis parameter (Ω angular rotation velocity of the Earth, ϕ latitude), Φ the geopotential defined as $d\Phi \equiv g dz^* = -\rho_r^{-1} dp$, $\rho_r = \rho_r(z^*)$ the reference density of the atmospheric fluid, J the rate of diabatic heating per unit mass (Andrews et al., 1987, p. 118).

It is convenient to introduce two new variables:

- the log-pressure vertical coordinate z, instead of the geometric height z^*

$$z \equiv -H \ln(p/p_s)$$

where $H = \frac{R\langle T \rangle}{g} \approx 7$ km is the standard scale height at the mean atmospheric temperature $\langle T \rangle \approx 240$ K and p_s is a standard reference pressure ($\approx 10^5$ Pa). It is convenient to use the

vertical coordinate z because it depends only on the pressure value (in the stratosphere the magnitude of z is similar to the difference between the geometric height [z^*] and the geopotential height [$Z = -R \langle T(p, p_s) \rangle / g \cdot \ln(p/p_s)$]);

- the potential temperature θ, defined as the temperature that a parcel of dry air at pressure p and temperature T would acquire if it were expanded or compressed adiabatically to $p_s = 10^5$ Pa

$$\theta = T(p_s/p)^\kappa \quad \Rightarrow \quad \theta = Te^{\kappa z/H}$$

where $\kappa \equiv \frac{R}{c_p}$. An important property of potential temperature is that it is conserved for adiabatic flow (Holton and Hakim, 2013, Eq. 2.45), allowing to separate non-conservative diabatic terms in the governing equations.

We insert the variables z and θ in the primitive equations (2.1)

$$\frac{Du}{Dt} - fv + \frac{\partial \Phi}{\partial x} = X \tag{2.2a}$$
$$\frac{Dv}{Dt} + fu + \frac{\partial \Phi}{\partial y} = Y \tag{2.2b}$$
$$\frac{\partial \Phi}{\partial z} = \frac{R\theta}{H} e^{-\kappa z/H} \tag{2.2c}$$
$$\frac{\partial u}{\partial x} + \frac{\partial v}{\partial y} + \frac{1}{\rho_r} \frac{\partial (\rho_r w)}{\partial z} = 0 \tag{2.2d}$$
$$\frac{D\theta}{Dt} = Q \tag{2.2e}$$

$$\text{with} \qquad Q \equiv \frac{J}{c_p} e^{\kappa z/H}$$

Further manipulation of these equations is useful when studying large-scale phenomena in the Extratropics. In particular here we apply the *β-plane approximation* and enter the *quasi-geostrophic framework*.

The β-plane approximation

The β-plane approximation consists in restricting the flow domain to the neighborhood of the latitude ϕ_0, where the value of the Coriolis parameter is well approximated by a linear expansion

$$f = (f)_{\phi=\phi_0} + y \left(\frac{\partial f}{\partial y}\right)_{\phi=\phi_0} = 2\Omega \sin(\phi_0) + 2\Omega a^{-1} \cos(\phi_0) y = f_0 + \beta y$$

with $f_0 \equiv 2\Omega \sin(\phi_0)$ and $\beta \equiv 2\Omega a^{-1} \cos(\phi_0)$, a the average radius of the Earth.

The quasi-geostrophic framework

At extratropical latitudes the dominant synoptic and global scale dynamics is the geostrophic flow, which balances the zero order Coriolis terms ($-f_0 v$, $+f_0 u$) and the pressure gradient terms ($\frac{\partial \Phi}{\partial x}$, $\frac{\partial \Phi}{\partial y}$), when Eqs (2.2a) and (2.2b) are stationary ($\frac{\partial \mathbf{u}}{\partial t} = 0$) and un-forced ($(X, Y) \approx 0$). By defining the streamfunction $\Psi \equiv f_0^{-1}(\Phi - \Phi_0)$, with $\Phi_0(z)$ reference geopotential profile, the geostrophic wind is written

$$\mathbf{u}_g = (u_g, v_g) \equiv (-\frac{\partial \Psi}{\partial y}, \frac{\partial \Psi}{\partial x}) = \hat{\mathbf{k}} \times \nabla_h \Psi.$$

The relation $\nabla_h \cdot \mathbf{u}_g \equiv -\partial^2 \Psi / \partial y \partial x + \partial^2 \Psi / \partial x \partial y = 0$ implies that the vertical geostrophic velocity must be $w_g = 0$ in order to guarantee mass conservation in Eq. (2.2d). Note that on a zonally symmetric, unperturbed planet the geopotential gradient is purely meridional and gives a zonal geostrophic flow $\mathbf{u}_g = u_g \hat{\mathbf{i}} = \overline{u}\, \hat{\mathbf{i}} = -f_0^{-1} \frac{\partial \Phi}{\partial y} \hat{\mathbf{i}}$.

The thermal wind relation, obtained by deriving $\mathbf{u}_g$ along the vertical, relates the vertical profile of the geostrophic wind with the horizontal derivative of the potential temperature

$$\frac{\partial \mathbf{u}_g}{\partial z} = \frac{g}{f_0} \hat{k} \times \nabla_h \ln \theta, \tag{2.3}$$

and is obtained by combining Eq. (2.2c) with the definition $H = R \langle T \rangle / g$.

The *geostrophic flow* is the zero order approximation of the synoptic[1] and large scale[2] atmosphere dynamics in the Extratropics. The first order approximation is called *quasi-geostrophic flow* (q.-g. flow), and corresponds to the ageostrophic deviation from the balanced state. The definitions of (i.) ageostrophic velocities, (ii.) material derivative following geostrophic wind, and (iii.) departure from a reference potential temperature profile

$$\begin{aligned}
&\text{(i.)} \quad \mathbf{u}_a \equiv \mathbf{u} - \mathbf{u}_g, \;\; w_a \equiv w \\
&\text{(ii.)} \quad D_g \equiv \frac{\partial}{\partial t} + u_g \frac{\partial}{\partial x} + v_g \frac{\partial}{\partial y} \\
&\text{(iii.)} \quad \theta_e \equiv \theta - \theta_0(z)
\end{aligned}$$

are necessary to write the q.-g. equations

$$D_g u_g - f_0 v_a - \beta y v_g = X \tag{2.5a}$$

$$D_g v_g + f_0 u_a + \beta y u_g = Y \tag{2.5b}$$

$$\frac{\partial u_a}{\partial x} + \frac{\partial v_a}{\partial y} + \frac{1}{\rho_r}\frac{\partial(\rho_r w_a)}{\partial z} = 0 \tag{2.5c}$$

$$\theta_e = \frac{H f_0}{R} e^{\kappa z/H} \frac{\partial \Psi}{\partial z} \tag{2.5d}$$

$$D_g \theta_e + w_a \frac{\partial \theta_0(z)}{\partial z} = Q, \tag{2.5e}$$

These can be combined into the q.-g. vorticity equation by taking the difference between $\partial(2.5\text{b})/\partial x$ and $\partial(2.5\text{a})/\partial y$, then inserting Eq. (2.5c)

$$D_g \zeta_g \equiv D_g(f_0 + \beta y - \frac{\partial u_g}{\partial y} + \frac{\partial v_g}{\partial x}) = \frac{f_0}{\rho_r}\frac{\partial(\rho_r w_a)}{\partial z} - \frac{\partial X}{\partial y} + \frac{\partial Y}{\partial x}. \tag{2.6}$$

In Eq. (2.5e) we define $\theta_{0,z} \equiv \partial\theta_0/\partial z$, to find

$$\rho_r w_a = -D_g \left(\frac{\rho_r \theta_e}{\theta_{0,z}} \right) + \frac{\rho_r Q}{\theta_{0,z}},$$

[1] spatial scale of the order of 1000 km

[2] spatial scale of the order of 2000 km or more

that, in Eq. (2.6), produces the q.-g. potential vorticity equation

$$D_g q_g \equiv D_g(\zeta_g + f_0\rho_r^{-1}\frac{\partial(\rho_r\theta_e/\theta_{0,z})}{\partial z}) = -\frac{\partial X}{\partial y} + \frac{\partial Y}{\partial x} + f_0\rho_r^{-1}\frac{\partial(\rho_r Q/\theta_{0,z})}{\partial z}. \tag{2.7}$$

where the terms on the RHS represent the input of vorticity due to external mechanical forcing (X, Y) and the vortex stretching associated with the heating rate Q.

In log-pressure coordinates the buoyancy or Brunt-Väisälä frequency N (i.e., the angular frequency at which a particle displaced along z oscillates in a stable atmosphere) is defined as $N(z) \equiv \sqrt{H^{-1}\theta_{0,z}e^{-\kappa z/H}}$. Then $\theta_e/\theta_{0,z} = (f_0\,\partial\Psi/\partial z)/N^2(z) + f_0^{-1}\epsilon(z)\partial\Psi/\partial z$ (with $\epsilon(z) \equiv f_0^2/N^2(z)$) and the q.-g. potential vorticity corresponds to an elliptic operator (a stretched Laplacian) of the streamfunction

$$q_g \equiv \zeta_g + f_0\rho_r^{-1}\frac{\partial(\rho_r\theta_e/\theta_{0,z})}{\partial z} = f_0 + \beta y + \frac{\partial^2\Psi}{\partial x^2} + \frac{\partial^2\Psi}{\partial y^2} + \rho_r^{-1}\frac{\partial}{\partial z}(\rho_r\epsilon(z)\frac{\partial\Psi}{\partial z}). \tag{2.8}$$

The variable q_g condenses in one simple expression (Eq. (2.7)) all information on the evolution of the flow. If the flow is frictionless and adiabatic ($X \approx 0$, $Y \approx 0$, $Q \approx 0$) then q_g is conserved following the geostrophic wind under q.-g. conditions.

2.2 Rossby waves

In an adiabatic and frictionless quasi-geostrophic environment characterised by a prevalent zonal flow $\overline{u}(y,z)$ we can linearise the system in terms of the perturbations to the q.g. vorticity (q in the following) and to the streamfunction

$$q = \overline{q}(y,z) + q'(x,y,t), \qquad \Psi = \overline{\psi}(y,z) + \psi'(x,y,z,t).$$

The 0th order equation being the zonally symmetric geostrophic flow ($u_g = \overline{u}$), the 1st order equation gives the q.g. approximation of the flow

$$\frac{\partial q'}{\partial t} + \overline{u}\frac{\partial q'}{\partial x} + v'\frac{\partial \overline{q}}{\partial y} = 0$$

or, in terms of the streamfunction

$$\left(\frac{\partial}{\partial t} + \overline{u}\frac{\partial}{\partial x}\right)\left[\nabla_h^2\psi' + \rho_r^{-1}\frac{\partial}{\partial z}(\rho_r\epsilon(z)\frac{\partial\psi'}{\partial z})\right] + \frac{\partial\psi'}{\partial x}\beta = 0, \tag{2.9}$$

where we have neglected the contribution of the vertical structure of the zonal wind to the meridional gradient $\partial\overline{q}/\partial y = \beta + \rho_r^{-1}\partial/\partial z(\rho_r\epsilon(z)\partial\overline{u}/\partial z)$.

We seek wave solutions travelling zonally (along x) in the form $\psi' = \Re\left(\widetilde{\psi}(z)\, e^{i(kx+ly-\omega t)}\right)$, which we substitute in Eq. (2.9) to obtain

$$(\omega - \overline{u}k)\left[-K^2\widetilde{\psi} + \rho_r^{-1}\frac{d}{dz}(\rho_r\epsilon(z)\frac{d\widetilde{\psi}}{dz})\right] - \beta k\widetilde{\psi} = 0 \qquad \text{where } K^2 = k^2 + l^2.$$

Supposing Γ to be the value solving the eigenvalue problem for the vertical structure (dependent on the top and bottom boundary conditions)

$$\rho_r^{-1}\frac{d}{dz}(\rho_r\epsilon(z)\frac{d\widetilde{\psi}}{dz}) = -\Gamma\widetilde{\psi}, \tag{2.10}$$

the dispersion relation and the group velocity take the form

$$\omega = k\overline{u} - \frac{k\beta}{K^2 + \Gamma}, \tag{2.11a}$$

$$\mathbf{c} = (c_x, c_y) = \left(\overline{u} + \frac{k^2\beta - l^2 - \Gamma}{(K^2+\Gamma)^2}, \frac{2kl\beta}{(K^2+\Gamma)^2}\right). \tag{2.11b}$$

Note that the wave propagates westward against the mean zonal flow $\overline{u}$ with stationary conditions when $K_s = \sqrt{\beta/\overline{u} - \Gamma}$ is satisfied.

2.2.1 Vertical propagation of Rossby waves

Consider a realistic variation of density with height as in $\rho_r = \rho_0 e^{-z/H}$ and constant Brunt-Väisälä frequency in an atmosphere extending from $z = 0$ to $z = +\infty$, then the eigenvalue problem of Eq. (2.10) is equivalent to

$$\rho_r^{-1} \frac{d}{dz}(\rho_r \epsilon(z) \frac{d\widetilde{\psi}}{dz}) = \left(K^2 - \frac{k\beta}{k\overline{u} - \omega} \right) \widetilde{\psi}$$

that, by defining a new function $\phi = \widetilde{\psi}\, e^{-z/2H}$, reduces to a simpler form

$$\frac{d^2\phi}{dz^2} + m^2\phi = 0 \qquad \text{where } m^2 = \epsilon^{-1} \left(\frac{k\beta}{k\overline{u} - \omega} - K^2 - \frac{\epsilon}{4H^2} \right)$$

with solutions $\phi(m) = \phi_0 e^{imz}$, so that the perturbation streamfunction can be written $\psi' = \Re\left(\widetilde{\psi}(z)\, e^{i(kx+ly-\omega t)}\right) = \Re\left(\phi_0\, e^{i(kx+ly+mz-\omega t)+z/2H}\right)$.

To obtain some simple conditions on the upward propagation of Rossby waves we neglect the meridional propagation and write $\omega = ck$. Generally, the waves propagate vertically when the wavenumber m is real, that, under these settings, is equivalent to establishing

$$0 < \overline{u} - c < \frac{\beta}{K^2 + \frac{\epsilon}{4H^2}}. \tag{2.12}$$

This is commonly known as the *Charney-Drazin criterion* (Charney and Drazin, 1961), and gives a simple understanding of the propagation of planetary waves from the troposphere to the stratosphere, where the zonal-mean stratospheric wind acts as a filter of stationary and travelling waves based on the wavenumber. The criterion shows that vertical wave propagation to the stratosphere is possible only in presence of a westerly flow ($\overline{u} > 0$), i.e. in winter when the stratospheric polar vortex is strong, whereas in summer the mean flow turns easterly and hinders the penetration of tropospheric disturbances.

2.3 Orographic and thermal forcing of planetary waves

2.3.1 Orographic waves in a barotropic model

The influence of stationary orographic waves on weather systems was considered in Charney and Eliassen (1949) to solve a problem encountered in attempting short-range weather predictions. They found a substantial discrepancy between dynamical calculations, forecasting the presence of a deep mid-tropospheric trough–ridge system travelling westwards over the Pacific sector, and observations, showing the persistence of such a system in time. The presence of mountains downstream of the fixed Pacific waves inspired Charney and Eliassen to consider orography as a fixed wave forcing, and weather patterns downstream as the superposition of stationary waves produced by orography and travelling disturbances.

They tested this idea with a simple shallow-water model in quasi-geostrophic framework - a hydrostatic, homogeneous, depth-independent flow - where the geopotential field is set by the height of the fluid above the flat surface at rest. Consider h_T and h_s the vertical coordinates describing the profile of the lower boundary and of the free surface, the depth of the fluid $h \equiv h_s - h_T$, and $\eta = h_s - h_{s,0}$ the deviation from mean free surface height. The streamfunction, geostrophic velocity and relative vorticity describing the flow are thus

$$\Psi = \frac{g\,\eta}{f_0}, \qquad \mathbf{u}_g = -\frac{g}{f_0}\mathbf{k} \times \nabla_h \eta, \qquad \zeta = \nabla_h^2 \Psi = \frac{g}{f_0}\nabla_h^2 \eta.$$

From the continuity equation in the shallow water approximation

$$0^{\text{th}} \text{ order}: \ \nabla_h \cdot \mathbf{u}_g = 0, \qquad 1^{\text{st}} \text{ order}: \ D_g h + h \nabla_h \cdot \mathbf{u}_a = 0$$

the q.-g. vorticity reduces to

$$q = f_0 + \beta y + \nabla_h^2 \Psi - \frac{f_0}{h_{s,0}}(h_s - h_T)$$

(for the derivation of the shallow-water formulation of the continuity equation and the q.-g.

potential vorticity see Vallis (2017), Sections 3.1, 5.3). Therefore, if we consider an η slanting with y, the geostrophic flow is purely zonal ($\mathbf{u}_g = u_g\hat{\mathbf{i}} = \overline{u}\,\hat{\mathbf{i}}$) and, by indicating perturbations from the zonal flow with the apix $'$, the q.-g. equation is written

$$\left(\frac{\partial}{\partial t} + \overline{u}\frac{\partial}{\partial x}\right)\left(\nabla_h^2\psi' - \frac{f_0}{h_{s,0}}(\eta' - h_T)\right) + v'\left(\beta + \frac{\overline{u}}{\lambda_2}\right) = 0$$

$$\text{where} \qquad \frac{\overline{u}}{\lambda_2 \equiv \frac{f_0^2}{g\,h_{s,0}}\overline{u} = \frac{\partial}{\partial y}(\frac{f_0}{h_{s,0}}\eta),}$$

or, considering the topographic profile as the forcing term and substituting v' with $\partial\psi'/\partial x$

$$\frac{\partial}{\partial t}\left(\nabla^2\psi' - \frac{\psi'}{\lambda^2}\right) + \overline{u}\frac{\partial}{\partial x}\nabla^2\psi' + \beta\frac{\partial\psi'}{\partial x} = -\overline{u}\frac{f_0}{h_{s,0}}\frac{\partial h_T}{\partial x}. \tag{2.14}$$

For unforced disturbances ($h_T = 0$) in the form $\psi' = \Re\left(\widetilde{\psi}\,e^{i(kx+ly-\omega t)}\right)$ the shallow water Rossby wave dispersion is

$$\omega = k\,\frac{\overline{u}K^2 - \beta}{K^2 + \lambda^{-2}} \tag{2.15}$$

(reminiscent of Eq. (2.11a) in the stratified atmosphere), which supports stationary waves only in presence of a westerly geostrophic flow at wavenumber $K^2 = K_s^2 \equiv \beta/\overline{u}$.

The Fourier analysis of Eq. (2.14), obtained by probing the equation over the range of zonal wavevectors $k = k_T$, gives us a relation between the amplitude of the topographic forcing $\widetilde{h}_T$ and the amplitude of the free surface height disturbance $\widetilde{\eta} = f_0\widetilde{\psi}/g$

$$\widetilde{\eta} = \frac{\widetilde{h}_T}{\lambda^2(K^2 - K_s^2)}. \tag{2.16}$$

For $K > K_s$ ($K < K_s$) the wave response is in (out of) phase with the topography. In the first case, based on $K^2\overline{u} > \beta$, the topographic contribution to vorticity is balanced by the zonal advection of relative vorticity by the geostrophic flow (third term on the LHS of Eq. (2.14)) or, with $K^2\overline{u} < \beta$, by the meridional advection of planetary vorticity by the ageostrophic flow (fourth term on the LHS of Eq. (2.14)). To remove unrealistic resonance Charney and Eliassen (1949) introduced a linear damping of vorticity based on Ekman pumping ($-r\nabla^2\psi'$ on RHS of Eq. (2.14)), which adds a new term in the denominator of Eq. (2.16), as in $\widetilde{\eta} = \widetilde{h}_T/[\lambda^2(K^2 -$

$K_s^2 - i\,(rK^2)/(k\overline{u}))]$. The height response computed using a realistic profile of topography for 45° N, $\overline{u} = 17m\,s^{-1}$ and a damping time scale r^{-1} of 5 days gives a strong similarity to the observed profile of 500 hPa geopotential height (see Figure 2.1 and for additional details Held (1983), Section 6.2). The linear damping kills the far-field response to the lower boundary forcing (i.e. the orography), removing unrealistic resonance at $K \approx K_s$ in Eq. (2.16). In the case of realistic topography (Figure 2.1) the damping also decreases the interference between the atmospheric waves generated by the two principal mid-latitude mountain barriers, the Tibetan Plateau and the Rocky Mountains.

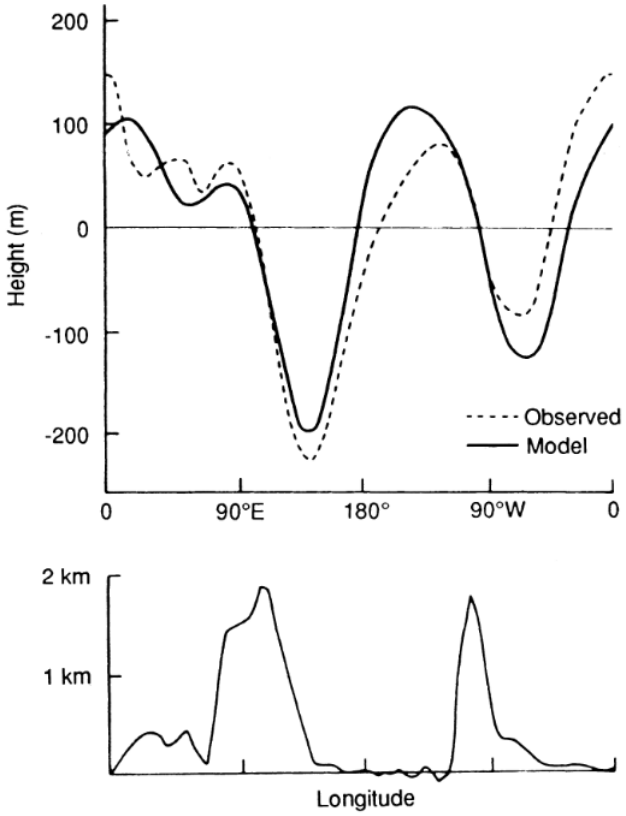

Figure 2.1: (Top) Longitudinal variation of the disturbance geopotential height ($\equiv f_0\,\Psi/g$) in the Charney–Eliassen model for the parameters given in the text (solid line) compared with the observed 500-hPa height perturbations at 45° N in January (dashed line). (Bottom) Smoothed profile of topography at 45° N used in the computation. After Held (1983)

2.3.2 Thermal waves in a baroclinic model

An effective depiction of the impact of low-level, large-scale heat sources on the mid-latitude circulation was presented in Smagorinsky (1953). Notwithstanding the strong idealisation of

his "theoretical heating model", Smagorinsky puts together early observational evidence of heat exchange between the atmosphere and the Earth's surface. For the winter season he recognises the dominant warming contribution of latent heat fluxes above the mid-latitude oceans, particularly in correspondence of the warm currents (Kuroshio and Gulf Stream), and the importance of radiative cooling over large snow-covered continents, with sensible heat fluxes reinforcing the latent and radiative terms, upward over warm oceans and downward over cold continents.

To represent the alternation of continents and oceans in the mid-latitude NH (Asia - Pacific Ocean and North America - Atlantic Ocean), the model features a periodic variation of low-level heat sources and sinks in the longitudinal direction with a wavelength L of 160°. In the meridional direction the conditions are still periodic within a channel of meridional width D, corresponding to 35 or 53.9° latitude, which is meant to represent the observed heating in the mid latitudes. The depth h_Q of the heating was also chosen respectful of observations, varying between 1 and 5 km over a vertical extension H of 8 km with rigid top.

We start from the q.-g. vorticity equation in Eq. (2.9) in presence of a baroclinic mean flow independent of latitude $\mathbf{u}_g = \overline{u}(z)\hat{\mathbf{i}} = (\overline{u}(0) + \Lambda z)\hat{\mathbf{i}}$. By requiring stationarity and considering the linear terms in the perturbations ζ', v', ω'

$$\overline{u}\frac{\partial \zeta'}{\partial x} + \beta v' = \frac{f_0}{\rho_r}\frac{\partial(\rho_r \omega')}{\partial z} \qquad \text{or also} \quad \overline{u}\frac{\partial^2 v'}{\partial^2 x} + \beta v' = \frac{f_0}{\rho_r}\frac{\partial(\rho_r \omega')}{\partial z}. \tag{2.17}$$

By dividing Eq. (2.2e) by the potential temperature θ, the first order terms give a thermodynamic equation related to the rate of change of entropy $c_p\, Q/\theta_0$

$$\frac{D}{Dt}\ln\theta = (\frac{\partial}{\partial t} + \overline{u}\frac{\partial}{\partial x} + v'\frac{\partial}{\partial y})\ln\theta + \omega'\frac{\partial \ln\theta_0}{\partial z} = \frac{Q}{\theta_0}, \tag{2.18}$$

which, combined with the general thermal-wind relation

$$\frac{\partial \mathbf{u}}{\partial z} = \frac{g}{f_0}\hat{\mathbf{k}} \times \nabla_h \ln\theta, \tag{2.19}$$

and assuming steady motions, reads

$$\overline{u}\frac{\partial v'}{\partial z} - v'\frac{\partial \overline{u}}{\partial z} + \frac{g}{f_0}\omega'\frac{\partial \ln\theta_0}{\partial z} = \overline{u}\frac{\partial v'}{\partial z} - v'\Lambda + \frac{N^2}{f_0}\omega' = \frac{g}{f_0}\frac{Q}{\theta_0} \tag{2.20}$$

Here the vertical structure of the potential temperature is expressed by $\theta_0(z) = T_s\, e^{\kappa z/H} + \gamma z$ (T_s is the average surface temperature) and allows to write the Brunt-Väisälä frequency $N^2 = g\,\partial \ln\theta_0/\partial z = \frac{g}{T_s}\,(\gamma_d - \gamma)$, with γ and $\gamma_d \equiv g/c_p$ the total and adiabatic lapse rate, respectively.

The equations are solved assuming a sinusoidal variation of the heat sources in a zonal length L of 160° longitude, a meridional width $D_1 = 35°$ or $D_2 = 53.9°$ ($k = 2\pi/L$ and $l = 2\pi/D$) and a vertical profile $e^{-z/h_Q}\sin(\pi z/H)$, presenting a maximum between the low and mid troposphere. A barotropic boundary layer is included to introduce the effect of friction, which - near the surface - causes variations in the wind stronger than those induced by baroclinicity. In Figure 2.2 we see the longitudinal profile of the sea-level pressure and of the 500-hPa geopotential height responding to a heat perturbation of depth h_Q= 1 and 2 km in channels of width D_1 and D_2. The surface trough is located 25° east of the maximum warming, and is characterised by a low-level cyclonic circulation tilting westwards with height and by vertical ascent almost immediately above. The mid-tropospheric response lags to the west of the surface response by approximately 40° in the narrow channel D_1 and by less (approximately 30°) in the broad channel D_2, where the response is distinctly stronger. Interestingly, the order of magnitude of the surface and mid-tropospheric perturbations (especially using D_2) is comparable to the observed climatological deviations from the zonal mean ($\sim$ 10 hPa & $\sim$ 40 m). The relative position of the observed heat sources (Kuroshio and Gulf Stream currents) or sinks (Siberia), surface pressure lows (Aleutian Low and Icelandic Low) or highs (Siberian High) and the associated 500-hPa height profile also reflect the expectations of Smagorinsky's "theoretical heating model".

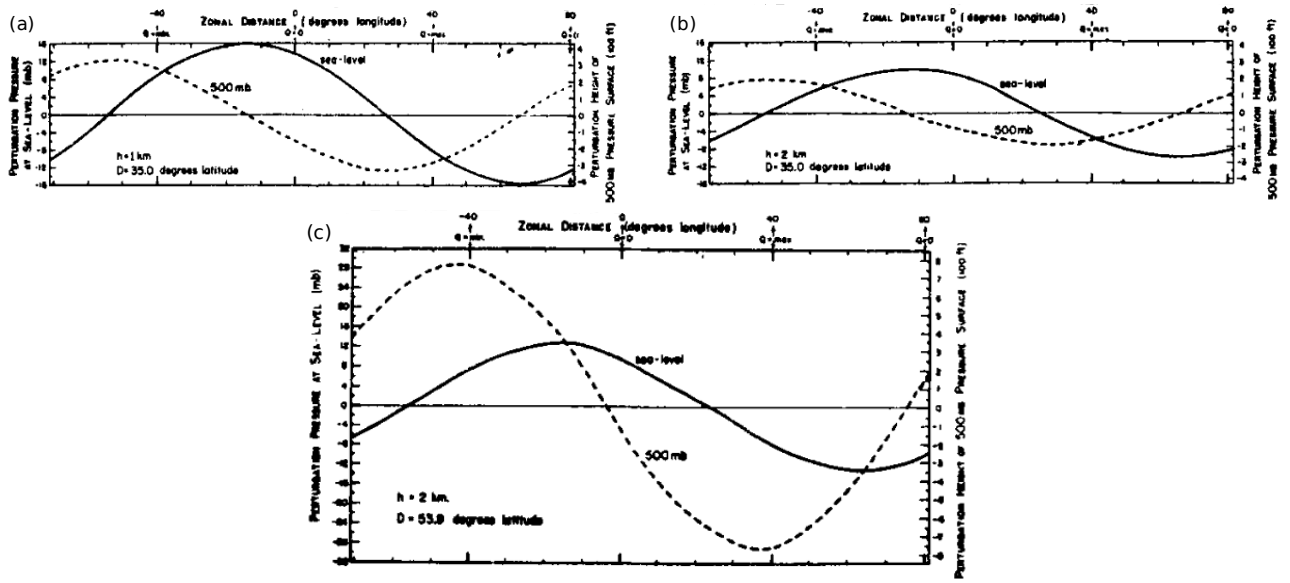

Figure 2.2: "Theoretical heating model" (baroclinic model with rigid tropopause and surface friction). The maximum and minimum heating are at a zonal position of 40 and -40° longitude (on the x-axis). The atmospheric response is represented in terms of the zonal profiles of the perturbation pressure at sea level (solid lines) and of the perturbation height of the 500-hPa pressure surface (dashed lines). Results for parameters (a) $D_1 = 35°$ latitude, $h_Q = 1$ km; (b) $D_1 = 35°$ latitude, $h_Q = 2$ km; (c) $D_2 = 53.9°$ latitude, $h_Q = 2$ km. After Smagorinsky (1953)

2.3.3 Discussion

In light of Smagorinsky's results and of the findings from Charney and Eliassen's barotropic model of orographic waves, in the last section of Smagorinsky (1953) the global observed 45° N profile of alternating atmospheric troughs and ridges is discussed. While the relevance of the distribution of heat sources and orography for the mid-latitude planetary waves has been undisputed, this work gave rise to a long-standing debate on the relative importance of the two forcings. In the context of AGCMs the impact of orography was estimated by running "mountain" versus "no-mountain" simulations (e.g. Manabe and Terpstra, 1974; Held, 1983), an approach which can produce results indicating the dominance of the mountains or the dominance of the heat sources, depending on the details of the numerical experiment (cf. Nigam et al., 1988; Valdes and Hoskins, 1989). Held and Ting (1990) partially solved this dispute by observing that the amplitude of thermally (orographically) forced planetary waves decreases (increases) with the strength of the surface westerlies. The latest studies (Held et al., 2002; Chang, 2009) agree on the main wave features in the NH being set by the distribution of

diabatic heating, but with non-negligible smaller-scale waves from mountain barriers.

The depth of the thermal forcing is a relevant factor determining the atmospheric response. In the introduction to thermal forcing by Hoskins and Karoly (1981) a height scale for the wind and for the heat source are defined as $H_u \equiv \overline{u}/\left\langle \frac{\partial \overline{u}}{\partial z} \right\rangle$ and $H_Q \equiv Q/\left\langle \frac{\partial Q}{\partial z} \right\rangle$ (the average derivative is computed up to the level where $\overline{u}(z) \approx$ const or $Q \approx 0$). In the Extratropics, where the warming is primarily balanced by horizontal motion, we can consider the cases of predominant meridional and zonal vorticity advection in response to variable depths of Q. From Eq. (2.20) the order of magnitude of the meridional velocity is $v' \sim min\{H_Q, H_u\}\, g\, Q/(\theta_0 f_0 \overline{u})$, and takes negative values, with positive $\zeta' = \partial v'/\partial x$ to the east and negative ζ' to the west of Q.

- Deep warming ($H_Q > H_u$). The meridional wind

$$v' \approx -\frac{g\, Q}{\theta_0 f_0 \partial \overline{u}/\partial z}$$

  (Eq. (2.20)) primarily balances the warming. It reaches its maximum intensity above the boundary layer due to strong Q and relatively small values of $\theta_0 \partial \overline{u}/\partial z$, where it creates a zonal ridge-trough system centered at Q. By manipulating the thermal wind equation (Eq. (2.19))

$$\frac{\partial \zeta}{\partial z} \propto \nabla^2 \theta' \sim -\Delta \theta_0, \tag{2.21}$$

  we obtain a relation which shows that, since to the east of Q the vorticity increases from the surface to the mid troposphere, the vertical advection in the mid troposphere will induce a negative perturbation to the mean profile of potential temperature θ_0 downstream of Q. Moreover, using the thermal wind equation itself, $\partial v'/\partial z = (g/f_0\theta_0)\, \partial \theta'/\partial x$ indicates a westward (baroclinic) tilt of the vertical profile of the meridional velocity.

- Shallow warming ($H_Q \approx H_u$). From Eq. (2.20)

$$\overline{u}\frac{\partial v'}{\partial z} \approx \frac{g\, Q}{\theta_0 f_0},$$

  the zonal advection of vorticity balances the heating; the approximation also shows that

the negative perturbation is localised near the surface, since the meridional velocity increases rapidly with height. The circulation anomaly is thus localised in the low troposphere, with a positive vorticity perturbation to the east of Q also reducing in intensity along the vertical. From Eq. (2.21), this induces a positive temperature perturbation ahead of the heat source.

A schematics of the conditions correspondent to deep and shallow mid-latitude warming is provided in Figure 2.3. In both cases, from Eq. (2.17), negative v' corresponds to vortex shrinking at the location of maximum heating ($\partial\omega/\partial z < 0$).

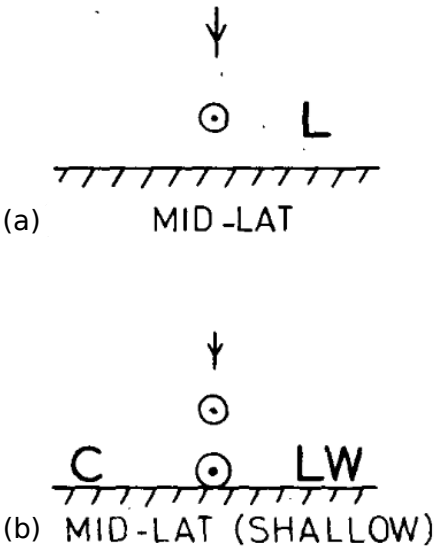

Figure 2.3: Longitude-height sections showing the different mid-latitude response to (a) deep thermal forcing (meridional advection dominates) and (b) shallow thermal forcing (zonal advection dominates). The arrow depicts vertical motion, circled dots motion out of the section, L the pressure trough, C and W cold and warm air. From Hoskins and Karoly (1981)

Since the dominant mechanism is the one requiring the smallest possible v', for deep warming ($H_Q > H_u$) meridional advection prevails, while for shallow warming ($H_Q \approx H_u$) zonal advection is important. The scale of the waves is also determinant in setting the relative role of meridional and zonal advection: in the dispersion equation for horizontal Rossby waves (Eq. (2.11a)) the meridional advection leads when the waves are large in scale ($K \sim k$ small compared to $\sqrt{\beta/\overline{u}}$).

We note that a deep heat source with peak intensity in the mid-troposphere, apart from being balanced by a different term in the vorticity equation, is much more effective in producing

planetary waves compared to a source near the surface (Trenberth, 1983). This becomes important when combining waves produced by orographic and thermal forcing. In fact, within an idealised extratropical setting Ringler and Cook (1999) show that a heat sink combined with a Gaussian mountain profile amplifies non-linearly the orographic wave, i.e. the response to the combined forcing is stronger than the sum of the two separate responses, enhancing the zonal wave train.

The description of the prevalent dynamical response to heat sources (Hoskins and Karoly, 1981; Smagorinsky, 1953), although merely based on the linear quasi-geostrophic equations, corresponds well with the patterns obtained from AGCM integrations forced with deep and shallow warming (see Hoskins and Karoly, 1981; Ting, 1991; Hall et al., 2001; Kushnir et al., 2002). It is equally important to note that the response of the atmosphere shows a strong non-linear dependence on the position of the forcing with respect to the mid-latitude jets and storm tracks, be the forcing orographic (White et al., 2017) or thermal (Hall et al., 2001).

We mention briefly the role of the asymmetric heat distribution in the Tropics for the mid-latitude stationary waves (for a review see Held et al., 2002, 6a. and references therein). Warm tropical heat sources are balanced by strong vertical motions that give rise to deep convection and strong upper-level divergence. The divergence in the upper troposphere produces a Rossby-wave train which amplifies in scale as it moves polewards, due to vortex stretching with increasing planetary vorticity. Although the extratropical response to tropical wave sources is weaker in intensity than the response to large-scale orographic and thermal forcing, it remains relevant; moreover, it depends strongly on the climatological state of the mid latitutudes.

2.4 Interaction between stationary and transient waves

Up to this point we have ignored the interactions between the large-scale stationary waves and the synoptic (transient) waves - here referred to as eddies. The latter grow as instabilities in locations where the flow is strongly non-uniform due to horizontal temperature gradients, i.e. in the presence of baroclinic conditions (see Holton and Hakim, 2013, Chapter 7). Hence

synoptic eddies are organised along what we call the *mid-latitude storm tracks* and, much as the thermal and orographic forcing, induce a geographically-fixed field of average heat and momentum convergence. Saltzman (1962) was among the first to understand that the average eddy distribution is an important factor shaping the larger mid-latitude waves and that, at the same time, the presence of the large-scale forcings discussed in Section 2.3 modulates the baroclinicity, suppressing or amplifying the development of synoptic eddies. Indeed, diabatic heating is important for the intensity and position of the storm tracks over the Pacific and Atlantic oceans, while the presence of mountains suppresses the growth of instabilities upslope and enhances it downslope (see Hoskins and Valdes, 1990; Chang et al., 2002; Chang, 2009). Stationary waves self-induced by the storm track are also relevant in confining longitudinally the eddy activity, as shown by the aquaplanet experiments in Kaspi and Schneider (2011, 2013).

The effect of transient eddies was first included in the study of stationary waves by Youngblut and Sasamori (1980) and Opsteegh and Vernekar (1982), and was referred to as "internal forcing" relative to the atmosphere, as opposed to "external forcing" by orography and diabatic heating. "Internal forcing" shows a dissipative or constructive effect on the stationary waves produced by "external forcing" - the feedback is non uniform in space because it depends on the position relative to the climatological state (Branstator, 1995; Hall et al., 2001). The component of the stationary wave forced by the transient momentum fluxes is relatively weak in intensity (Held et al., 2002), however, since a change in the eddies has a direct feedback on the position and strength of the mid-latitude jets (Lau and Holopainen, 1984) and, in turn, the jet is important for shaping the large-scale waves (Hall et al., 2001), the effect of the eddies cannot be neglected. As emerges from the analyses by Chang (2009), their contribution is particularly relevant for the strengthening of the main oceanic surface-pressure patterns, i.e. the Aleutian Low and the Icelandic Low (see Figure 1.3).

The linear contribution to stationary planetary waves from the three terms here discussed, i.e. thermal (diabatic) forcing, orographic forcing and transient eddy forcing, is shown in Figure 2.4, where the heat flux by transient eddies is included in the thermal forcing. As often mentioned in works trying to separate the different components of the stationary wave forcing (e.g. Held et al., 2002; Chang, 2009), the limitation of this approach lies in the fact that the three terms are

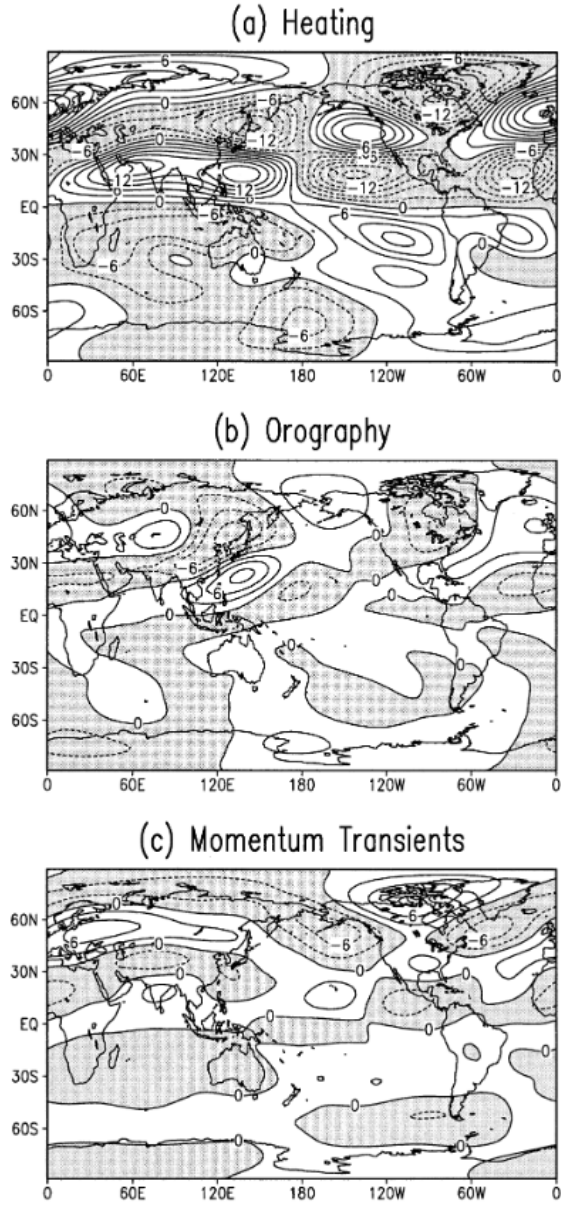

Figure 2.4: The decomposition of the total linear response of the eddy streamfunction at 300 mb into parts forced by (a) heating plus transient eddy fluxes in the temperature equation, (b) orography, and (c) transients in the momentum equations. The responses are obtained by relaxing towards a steady state a non-linear primitive equation model on the sphere forced by (a) diabatic heating and heat-flux convergence, (b) orography, and (c) transient vorticity convergence. The forcing fields are taken from the January climatology of the 1948–1999 NCEP-NCAR reanalysis. Contour interval is 3×10^6 m^2 s^{-1}. From Held et al. (2002)

not truly independent, since the thermal patterns of the mid latitudes depend on the average circulation which itself responds to orography and synoptic eddy activity, and equally so for orography and storm tracks.

2.5 Surface–atmosphere interactions

It is noted in the previous paragraphs that during the NH winter the oceans release heat to the atmosphere thanks to sensible and latent fluxes, especially in the regions of the warm Kuroshio and Gulf Stream currents. At the same time, surface sensible heat fluxes cool the atmosphere over land regions characterised by strong radiative cooling and low insolation, i.e. as a general approximation north of 40° N. These features are evident from winter maps of surface latent and sensible fluxes in Figure 2.5. While the surface provides heat sources and sinks at the bottom of the atmosphere, sources/sinks are also present within the atmosphere because of the interaction of its chemical constituents with radiation (e.g. water vapour and droplets, ozone, carbon dioxide, etc). Furthermore, atmospheric processes such as boundary layer turbulence, convection and synoptic eddies, redistribute the warming and cooling in the vertical and horizontal directions, to give a column-integrated heating pattern such as the one represented in Figure 2.6. For a description of the heat budget and its geographical distribution see (Peixoto et al., 1992, Chapter 13).

The response of the mid-latitude atmosphere to ocean surface temperature patterns (SSTs) has been investigated in detail. It is well established that oceanic frontal regions of intense SST gradients release a large quantity of heat into the atmosphere (Figures 2.5, 2.6), modulate the baroclinicity and the development of storms in the atmosphere (Inatsu et al., 2003; Nakamura et al., 2008; Omrani et al., 2019), and ultimately interact with the eddy-driven jets. Further examination of the topic is beyond the scope of this discussion, but can be found in the review studies by Kushnir et al. (2002); Czaja et al. (2019).

On the contrary, the subject of land–atmosphere interaction (see reviews by Betts et al., 1996; Seneviratne et al., 2010) is less developed for the reasons following. Firstly, the thermal influence of the land surface on the atmosphere is overall weaker and is expected to produce a limited response with respect to ocean warming or cooling. This is linked to the depth and intensity of the heat fluxes over land, which are generally small compared to those produced by oceans (Figures 2.5, 2.6). In fact, over land the surface temperature equilibrates faster towards the atmospheric temperature, reducing the vertical thermal gradients on which sensible heat fluxes

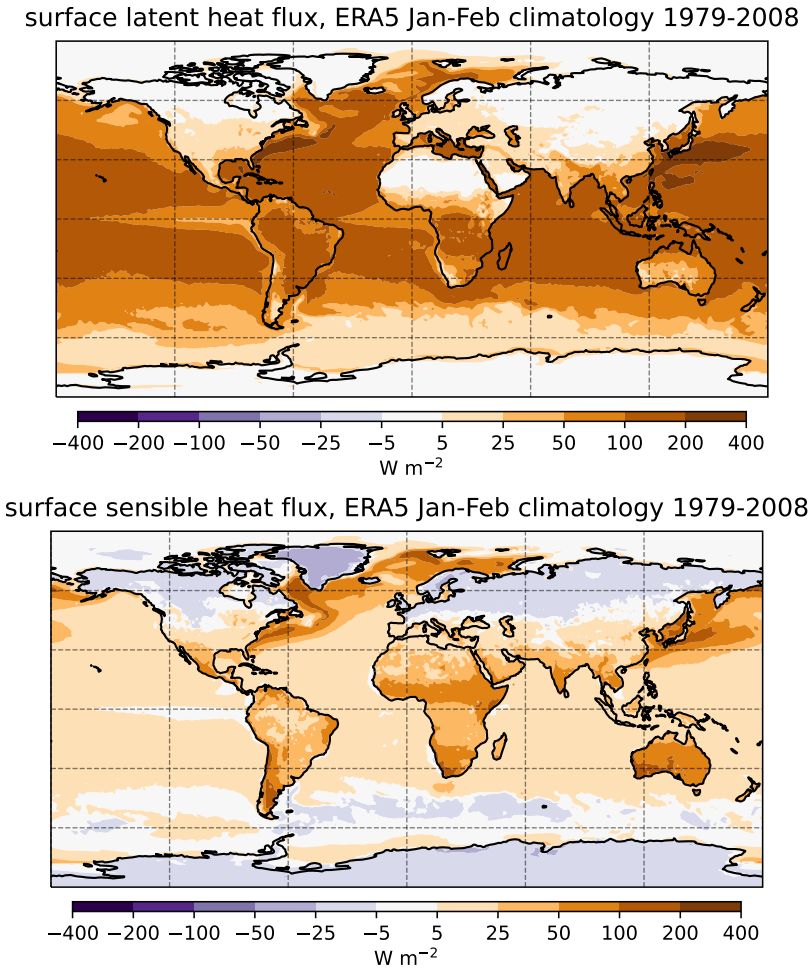

Figure 2.5: January-February climatology of (top) surface latent heat flux, (bottom) surface sensible heat flux from the ERA5 Reanalysis 1979–2008

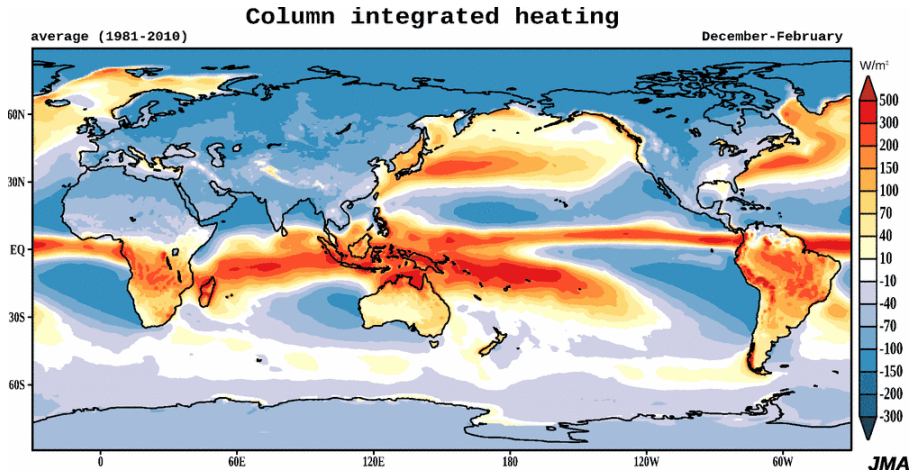

Figure 2.6: December-January-February climatology of column-integrated heating (includes surface sensible heating, condensation latent heating, net longwave and shortwave radiative heating) based on the JRA-55 Reanalysis 1981–2010. From `https://jra.kishou.go.jp/JRA-55/atlas/en`

rely; the finite availability of water vapour restricts the release of latent heat. In the Extratropics weaker small-scale turbulence and synoptic disturbances limit the vertical extension of the heat release in the atmosphere by land-based temperature anomalies. Secondly, a representation of land surface processes and hydrology, hence of the heat fluxes thereby released, is a recent introduction to state-of-the-art coupled general circulation models (CGCMs)[3], and still shows important biases with respect to observations (Van den Hurk et al., 2016; Seneviratne et al., 2010). The distribution of low-level heating depends on many properties of the land surface, e.g. soil moisture, vegetation type, snow cover and snowmelt.

The importance of land temperatures is recognised in the regional circulation systems known as monsoons. A monsoon climate is identified by the annual reversal of surface winds and by the associated seasonal contrasts in precipitation (Webster, 1986, Part I), and is mainly driven by the seasonal variations in insolation at tropical and subtropical latitudes. Notwithstanding the regionality of such climates, at a global scale the annual migration of the ITCZ (InterTropical Convergence Zone) is largely connected with the monsoonal seasonal cycle. The upper-level divergence (uplift), coinciding with the convective rainy season of the monsoons, is roughly co-located with the ITCZ; upper-level convergence inducing subsidence corresponds with the subtropical highs and the dry season of the monsoons. While land-sea thermal contrast alone is neither a necessary nor a sufficient condition for the formation of monsoon climate (Chao and Chen, 2001), together with other surface features (e.g. orography) it modulates the intensity of oceanic and continental highs and lows, influencing the local atmospheric circulation, hence the low-level wind and precipitation patterns. This is particularly important in the case of Asia, because of the size and structure of the continent. For example, along its eastern coastline the formation of a strong summer pressure contrast between the oceanic subtropical high and the continental low drives an anticyclonic circulation centered on the ocean, characterised by a southerly flow carrying moist air and precipitation into East Asia, far northward with respect to the location of the ITCZ. The Tibetan Plateau is considered as an intensification factor for the East Asia summer monsoon (Wu et al., 2007; Hoskins and Rodwell, 1995). See Wang et al. (2017) and references therein for a detailed review on the topic of global monsoons.

[3]coupled indicates the coupling between the atmosphere and ocean / land models. In coupled climate models ocean and land processes are computed - not prescribed as in AGCMs

While the role of land conditions for regional weather systems such as monsoons has been explored in some detail, we find a limited selection of works on the potential impact of land temperatures (or of land-sea thermal contrast) on the large-scale atmospheric circulation. An example is given by the potential influence on the winter atmosphere of autumn Siberian snow cover. Anomalous snow cover, associated with enhanced thermal cooling induced by the local increase in the surface albedo (Cohen and Rind, 1991), is thought to cause the amplification of the largest mid-latitude stationary planetary waves (Cohen et al., 2014). Its influence may propagate to the stratosphere (Gong et al., 2003a, 2004), where the waves break into the stratospheric polar vortex and heat the core of the vortex. For thermal wind balance, the vortex wind slows down and may induce a negative Northern Annular Mode (NAM) signal down to the surface by its coupling with the troposphere (Baldwin and Dunkerton, 1999; Kidston et al., 2015). The whole process starts in Autumn with anomalous snow cover in the mid-latitude regions of Central Asia and affects the NAM at the beginning of the winter season. However, the direction and robustness of the link between Eurasian snow-cover anomalies and the large-scale atmosphere is currently matter of debate (discussed in more detail in Section 4.2; for a complete review see Henderson et al., 2018).

An additional example of the influence of land on the atmospheric circulation is the link between the surface temperature over the Tibetan Plateau and weather patterns over downstream East Asia, extending elsewhere through global teleconnections (e.g. Xue et al., 2022). Recently, several works focused on the winter season have identified a possible downstream impact of the Tibetan Plateau snow cover over different time scales (Liu et al., 2017; Li et al., 2018; Chen et al., 2021). The role of the high elevation of such extended land areas may be relevant in determining the strong atmospheric responses (see Gong et al., 2004, and General Outlook in Chapter 5).

Chapter 3

Effects of mid-latitude land warming

Chapter Summary

Winter land-sea thermal contrast (LSC) is expected to undergo a strong weakening because of a faster land surface warming in the future warmer climate. Yet its effects on the atmospheric circulation have been poorly investigated. Here we run a set of idealised winter simulations featuring reduced LSC in the Northern Hemisphere (NH) extratropics, or in individual extratropical sectors of the NH (Atlantic and Pacific), using an intermediate-complexity atmospheric general circulation model. Reduced LSC is obtained by imposing a warming of surface land temperatures in East Asia and North America. For similar warming intensities over the two regions, the response of the model to East Asia forcing is significantly stronger and dominates the response to the sum of the two forcing patterns. We find that the LSC reduction causes a weakening and poleward shift of the mid-latitude jet streams, and a strong interference with zonal wavenumbers 1 and 2. In particular, East-Asia warming reduces the amplitude of wave 1 and 2 producing a strengthening of the stratospheric vortex, while a weaker vortex due to a moderate amplification of wave 1 is detected when warming North America. Eventually, stratospheric signals propagate downward in the troposphere affecting the midlatitude winter NH even remotely from the forcing. In this work we pinpoint some mechanisms by which weakened winter LSC influences the NH extratropical circulation: the results may become useful

to interpret the response to long-term projections displaying reduced LSC along with other climate-change forcing patterns.

Chapter 3 is adapted from the following article.

Title: Influence of winter land-sea contrast on mid-latitude atmospheric circulation.

Status: Research article published in *Journal of Climate* on the 8th September 2022 online, on the 1st October 2022 in print. DOI: `https://doi.org/10.1175/JCLI-D-21-0941.1`

Authors: Alice Portal[1,2], Claudia Pasquero[1,3], Fabio D'Andrea[2], Paolo Davini[3], Mostafa Hamouda[4,5], Gwendal Rivière[2].

3.1 Introduction

The winter thermal contrast between the cold continents and the relatively warmer oceans determines a consistent part of the diabatic heating pattern in the atmosphere (Smagorinsky, 1953; Held, 1983). This is of fundamental importance for the dynamics of the mid-latitude atmosphere and, along with orography and tropical forcing, sets the shape of planetary waves throughout the troposphere (Held, 1983; Held and Ting, 1990; Held et al., 2002; Garfinkel et al., 2020). At synoptic frequencies, the strong thermal gradients between land and sea located at the eastern coasts of Asia and North America are a prominent source of baroclinicity and trigger the eastward-extending storm tracks feeding the jet streams across the Pacific and Atlantic basins (Hoskins and Valdes, 1990; Brayshaw et al., 2009). At longer time scales the thermal-equilibration theory introduced by Charney and DeVore (1979) posits that the global-scale wave-like thermal structure generated by the asymmetric surface-temperature pattern induces a succession of equilibrated and forced regimes, where the mid-latitude circulation resonates with the temperature structure or else is predominantly zonal (Marshall and So, 1990; Mitchell and Derome, 1983).

Among the features of long-term climate change projections, the most relevant in the mid and

[1]Department of Earth and Environmental Sciences, Università di Milano - Bicocca, Milan, Italy
[2]Laboratoire de Météorologie Dynamique/IPSL, École Normale Supérieure, PSL Research University, Sorbonne Université, École Polytechnique, IP Paris, CNRS, Paris, France
[3]Consiglio Nazionale delle Ricerche, Istituto di Scienze dell'Atmosfera e del Clima (CNR-ISAC), Torino, Italy
[4]Astronomy and Meteorology Department, Faculty of Science, Cairo University, Cairo, Egypt
[5]Institute for Atmospheric and Environmental Sciences, Goethe University Frankfurt, Frankfurt am Main, Germany

high latitudes are Arctic Amplification of warming (AA) (Serreze and Barry, 2011; Previdi et al., 2021) and changes in the thermal land-sea contrast (LSC), which is expected to decrease in winter and increase in summer due to the faster warming of land surface compared to ocean surface (Sutton et al., 2007; Wallace and Joshi, 2018; He et al., 2018). A number of studies addresses the impact of LSC changes on regional atmospheric dynamics, e.g. on tropical monsoons (Shaw and Voigt, 2015; Zhuang et al., 2022), temperature variability (de Vries et al., 2012; Gregory and Mitchell, 1995), tropospheric circulation (Kamae et al., 2014; Day and Hodges, 2018). Despite the rich literature assessing the importance of extratropical LSC for mid-latitude dynamics (e.g. Smagorinsky, 1953; Held, 1983; Valdes and Hoskins, 1989; Held and Ting, 1990; Held et al., 2002), limited attention is given to the influence of LSC on the future large-scale atmospheric circulation. The predicted variation in extratropical LSC is similar, in order of magnitude, to AA (IPCC-*WGI*, 2021), which, conversely, has been extensively studied for its links with the mid-latitude circulation (e.g. Cohen et al., 2020; Blackport and Screen, 2020; Labe et al., 2020, just to cite some of the most recent articles).

Mid-latitude LSC is also known to play a role in the interannual-to-interdecadal atmospheric variability. He et al. (2014, 2018) find an impact of winter LSC on atmospheric circulation and atmospheric blocking using reanalysis and models. Molteni et al. (2011) use a different approach to investigate the role of the thermal contrast in forcing interdecadal variations in the NAM during the second half of the 20th century. By running idealised experiments with an intermediate-complexity atmospheric model, they show evidence for the effects of a Cold-Ocean/Warm-Land pattern on the winter planetary-scale variability.

Here we use a similar procedure and the same model as Molteni et al. (2011) to study the large-scale tropospheric and stratospheric response to reduced winter mid-latitude LSC, with a large-scale analysis covering frequencies from the stationary to the synoptic. In long-term climate projections a different warming of the Pacific and Atlantic oceans is foreseen for the NH mid latitudes due to the so-called North Atlantic Warming Hole, i.e. a deficit in the North Atlantic warming rate (Drijfhout et al., 2012). Such an asymmetry in the ocean-surface warming implies a substantially weaker LSC over the mid-latitude East America coast compared with the East Asia one in the future climate. For this reason, and because the interannual evolution

of Atlantic and Pacific LSC appears to be independent (i.e. the correlation between two basin-dependent indices of LSC is very low), we investigate the circulation response to reduced LSC over each basin independently. The individual-basin approach is reminiscent of analyses of the atmospheric response to individual topographic structures, e.g. the Rockies and the Tibetan plateau (Held et al., 2002, and references therein). The results of this work may be valuable for the interpretation of long-term climate-change scenarios and for determining the role of LSC in the extratropical interannual variability.

Section 3.2 provides a description of the model and of the set of sensitivity experiments, as well as a definition for Atlantic and Pacific LSC and of the main diagnostics; in Section 3.3 we present the responses to different patterns of reduced LSC; in Section 3.4 we summarise and discuss the main findings.

3.2 Methods

Model

We use an 8-level Atmospheric General Circulation Model (AGCM) developed at the International Centre for Theoretical Physics (ICTP), known as SPEEDY (for Simplified Parametrization, primitivE-Equation DYnamics). The model is spectral on the sphere, with triangular truncation at total wavenumber 30 (T30) and with an associated Gaussian grid of 96 by 48 points. Despite the low horizontal and vertical resolution, SPEEDY displays an adequate performance for the analysis of large-scale features of the climate system (Kucharski et al., 2013) (see Molteni (2003) and Kucharski et al. (2006) for a comprehensive description of the model and its climatology). In the Methods' Sections *Stratospheric levels in SPEEDY* (p. 36) and *Land-temperature and ice-temperature schemes* (p. 36) we also supply a focus on the model's stratosphere and we report the details of the land-surface-temperature (LST) and sea-ice-temperature (SIT) schemes, including how the latter interacts with the sea surface temperature (SST). The schemes are switched on or off depending on the target of each simulation.

Stratospheric levels in SPEEDY

The stratosphere in SPEEDY includes two atmospheric levels at 100 and 30 hPa. In the top level (30 hPa) a drag on the zonal-mean winds with relaxation time of 1 month is implemented to obtain a climatology close to the observed one; this level also acts as a "sponge layer" thanks to additional diffusion with a relaxation time of 12 hours. The model is not equipped with an atmospheric chemistry scheme, hence the absorption of radiation in the stratosphere is prescribed by a zonally-symmetric function with a suitable seasonal cycle. Hence, the top two levels of the model provide a "bulk" representation of the stratosphere, which serve as boundary conditions for reproducing the effects of the stratosphere on the troposphere (King et al., 2010). As reported in King et al. (2010); Herceg-Bulić et al. (2017); Ruggieri et al. (2017), the stratospheric variability and troposphere–stratosphere coupling are remarkably well represented in SPEEDY considered the scarcity of stratospheric levels, and are comparable with results from higher-complexity and finer-resolution atmospheric models (see Figure 11 in King et al. (2010)); however, the vertical coupling develops faster in SPEEDY than in finer-resolved models and in reanalysis (Herceg-Bulić et al., 2017).

Land-temperature and ice-temperature schemes

The skin temperature over land (T_{skin}), computed separately from the land-surface temperature (LST, i.e. the temperature in the upper layer of soil), follows the equation of energy balance at the surface

$$k_l(T_{skin} - \mathrm{LST}) = F^{SR} + F^{LR} + \mathrm{SHF}_l + \mathrm{LHF}_l = \mathrm{GHS}_l, \tag{3.1}$$

where the ground heat flux on land (GHS_l) is the sum over short-wave and long-wave radiation fluxes (F^{SR}, F^{LR}), sensible heat flux over land (SHF_l), latent heat of evaporation over land (LHF_l), all computed assuming $T_{skin} = \mathrm{LST}$; k_l is the coefficient for land heat flux. Further details on the solution of Eq. (3.1) and on the form of the different heat-flux components can be found in Molteni and Kucharski (2016). The LST adjusts to the incoming heat flux and, at

the same time, relaxes towards a prescribed monthly seasonal cycle LST_{cl}, as in

$$d_s\, c_s\, \frac{\partial \mathrm{LST}}{\partial t} = \mathrm{GHS}_l - d_s\, c_s\, \tau_s^{-1}(\mathrm{LST} - \mathrm{LST}_{cl}), \tag{3.2}$$

where d_s is the depth of the interactive soil layer (1 m), c_s is the heat capacity of the soil and τ_s is the damping time scale for soil temperature anomalies (40 days). When the land-temperature scheme in Eq. 3.2 is deactivated then LST is fixed to its climatological value.

The model includes a scheme for sea-ice temperature (SIT) analogous to that of land-surface temperature

$$d_i\, c_i\, \frac{\partial \mathrm{SIT}}{\partial t} = \mathrm{GHS}_s - d_i\, c_i\, \tau_i^{-1}(\mathrm{SIT} - \mathrm{SIT}_{cl}), \tag{3.3}$$

characterised by GHS_s the ground heat flux on sea, computed using the SST, c_i the heat capacity of sea ice, a depth varying according to $d_i = d_M + (d_m - d_M)cos(\phi)^2$ (d_M =2.5 m, d_m =1.5 m, ϕ being the latitude), and a damping time scale τ_i of 30 days. The anomaly of SIT from its climatology adjusts to the incoming heat-flux, while the SIC is always fixed to its prescribed climatology. As in the case of the land surface temperature, SIT corresponds to its climatological value (SIT_{cl}) when the sea-ice scheme is suppressed.

Despite the sea-surface temperature (SST) being prescribed in all experiments, when the sea-ice scheme is activated the SST may deviate in some areas from its prescribed climatology (SST_{cl}) by the quantity $(\mathrm{SIT} - \mathrm{SIT}_{cl}) \cdot \mathrm{SIC}_{cl}$, where SIT and SIT_{cl} are the sea-ice temperature and its climatology, SIC_{cl} the climatological sea-ice concentration. Moreover, SST_{cl} corresponds to the grid-box average over the climatological values of liquid water temperature (ST_{cl}) and SIT_{cl}, weighted by their respective concentrations ($1-\mathrm{SIC}_{cl}$ and SIC_{cl}). While SST_{cl} and SIC_{cl} are provided as an input, ST_{cl} and SIT_{cl} are computed directly by the model by fixing SIT_{cl} / ST_{cl} to 271.4 K, sea-water freezing temperature, when SST_{cl} is above / below freezing. Moreover, the minimum SIC_{cl} is 0.1 when SST_{cl} is below freezing.

Model and Experiments

We first perform an ensemble of ten 30-year simulations with realistic SST and sea-ice cover (SIC) conditions and with active land-surface-temperature scheme and inactive sea-ice-temperature scheme. [6] The ensemble-mean monthly-averaged LST from this set of simulations, hereafter referred to as $\mathrm{LST}_{mod}(m)$ with m indicating the month, is used to compute the forcing for a set of perpetual-winter simulations. The perpetual-winter integrations have LST fixed to the prescribed values, and SST set to the 1979–2008 HadISST climatology, with only its SIT component free to evolve.[7] The procedure for the construction of the perpetual-winter runs is similar to that in Molteni et al. (2011) and is described in the following.

i. *Control*: two perpetual-winter control simulations (hereafter CONTROL), one for January and one for February, are run separately for 400 months with fixed SST, SIC and LST – the first two being the monthly HadISST climatologies, the latter being LST_{mod}. The CONTROL surface temperature is shown in Figure 3.1a.

ii. *Reduced land-sea contrast*: two perpetual-winter experiments, one for January and one for February, for each different forcing (hereafter TOTAL, ASIA and NAMERICA) are run for 400 months with fixed LST, SST and SIC. Whereas SST and SIC are as in (i.), the LST for TOTAL forcing is constrained to a weighted mean between the January / February and the April LST_{mod} (see Section *Forcing patterns* (p. 40) for details on the computation). The forcing patterns are constructed in order to obtain similar intensities of the zonally integrated temperature anomaly and of LSC reduction over the two continents (see Figure 3.1b for the TOTAL forcing, Figure 3.1c for the zonal-mean forcing considering East-Asia or North-America anomaly). Individual-continent patterns are selected from the TOTAL forcing to run experiments ASIA and NAMERICA.

When compared to Molteni et al. (2011), our experiments differ for two main reasons. Firstly,

[6] Each of the ten ensemble members is forced by observed SST and by climatological SIC from the 1979–2008 monthly fields of HadISST reanalysis (see Rayner et al. (2003)), with different initial conditions taken from the 1st-January fields of a simulation constrained by climatological SST and SIC.

[7] The difference in average SIT between the forcing and control experiments is found to be negligible with respect to the amplitude of the LST forcing, hence is not examined in the Results.

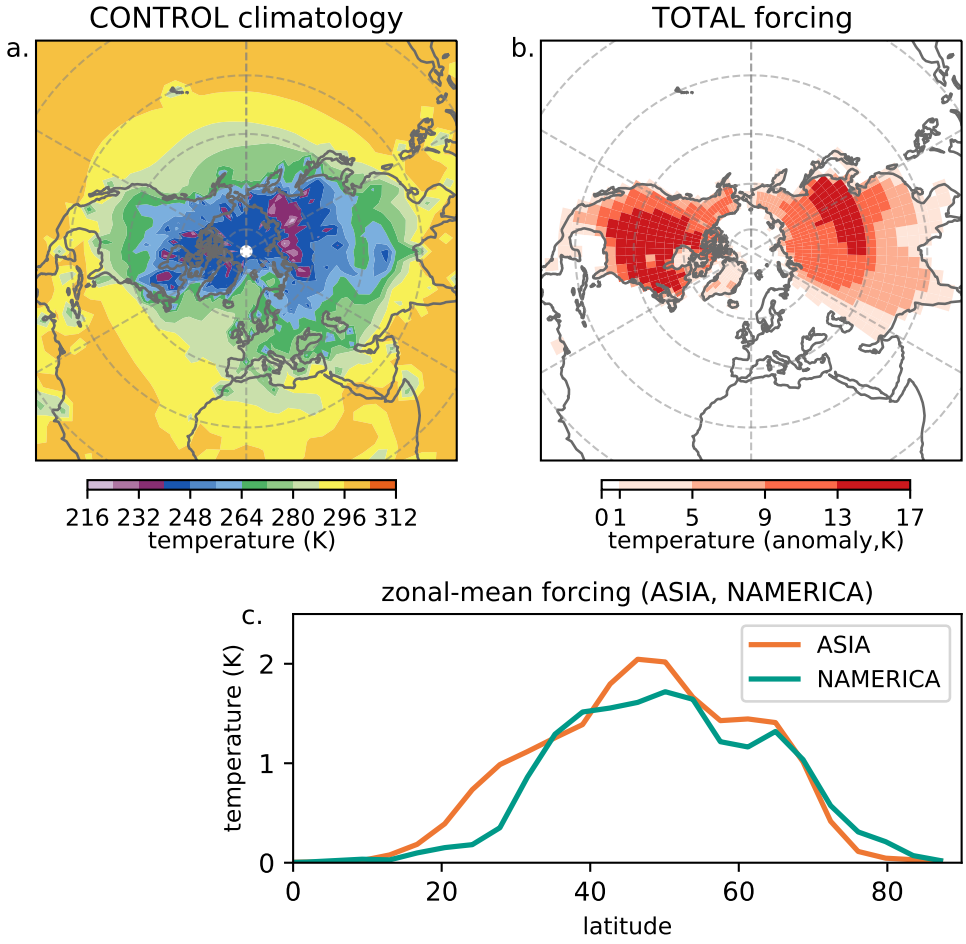

Figure 3.1: (a) Surface temperature in CONTROL and (b) TOTAL forcing anomaly, averaged over January and February; (c) zonal-mean anomaly for individual-continent forcing – ASIA and NAMERICA – weighted by the cosine of latitude

a regional difference is applied in the forcing (details in Forcing patterns) in order to obtain anomalies of similar intensity over the Pacific and Atlantic sectors; secondly, SST (apart from the SIT component) is kept as in the CONTROL so as not to influence the meridional temperature gradients over the mid-latitude oceans. This means that in the reduced-LSC experiments the NH is subject to a net heating with respect to the CONTROL.

Forcing patterns

The pattern of LST forcing shown in Figure 3.1b is computed from a mean between the January / February and the April LST_{mod}

$$\mathrm{LST}_{\mathrm{TOT}}(m, C) = \frac{\mathrm{LST}_{mod}(m, C) + \mathcal{A}(C) \cdot sin(\phi) \cdot \mathrm{LST}_{mod}(\mathrm{Apr}, C)}{1 + \mathcal{A}(C) \cdot sin(\phi)}, \tag{3.4}$$

where m indicates the month (January or February), $\mathcal{A}(C)$ is a coefficient depending on the continent C ($\mathcal{A}$ is set to 8 for C = North America, 4 for C = Asia), and the weight of the April LST grows with the sine of the latitude ϕ. This is done to obtain a large mid-latitude LST forcing that becomes unimportant in the Tropics. In addition, the anomaly $\Delta\mathrm{LST}_{\mathrm{TOT}} = \mathrm{LST}_{\mathrm{TOT}} - \mathrm{LST}_{mod}$ is multiplied by a factor 1.5 over the region of North America (experiments TOTAL and NAMERICA). Both the amplification factor and the coefficient $\mathcal{A}$ are modulated to obtain zonal-mean forcing and LSC reduction of similar intensity over the two continents so as to compare experiments ASIA and NAMERICA (run with the individual continental anomalies from Figure 3.1b). We note that the April LST is chosen instead of summer LST because its temperature pattern is reflective of a dynamics which is reminiscent of the winter one, e.g. in terms of stationary planetary waves (Wang and Ting, 1999); moreover, the latitudinal profile of the forcing pattern (weighted by the sine of latitude) recalls that of NH land-surface warming in scenarios of the future climate (IPCC-*WGI*, 2021).

Thermal land-sea contrast

We define LSC over the extratropical Atlantic and Pacific sectors as the skin-temperature difference between two boxes placed west and east of the western continental coastline (Figure 3.2). Note that the forcing is applied in terms of LST, while the LSC is computed on the basis of skin-temperature averages – the difference between the two variables is illustrated in Section *Land-temperature and ice-temperature schemes*. The values of LSC_{Atl} and LSC_{Pac} for the perpetual winter simulations are shown in Table 3.1, where they are compared to recent January-February LSC (1979–2008 climatology from ECMWF ERA5, Hersbach et al. (2020a)) and to January-February LSC in 2200–2300 climate change projections (mean over models CCSM4, CNRM-CM5, GISS-E2-R, MPI-ESM-LR participating in the CMIP5 Extended Concentration Pathways – RCP 8.5, Taylor et al. (2012)). While in the CONTROL and TOTAL simulations and in the reanalysis (first three columns of Table 3.1) the values of LSC_{Atl} and LSC_{Pac} are of comparable amplitude, the long-term projections show a thermal contrast that is reduced in both ocean sectors, but less over the western Pacific than over the western Atlantic (fourth column of Table 3.1). This is an effect of the slower warming predicted for the subpolar North Atlantic (North Atlantic Warming Hole) in response to the predicted change in the North Atlantic circulation (Keil et al., 2020; Rahmstorf et al., 2015), which, matched with the high warming rate of the North American continent, is expected to cause a strong reduction of the winter contrast between the cold continent and the relatively warmer ocean. A reduction in both Pacific and Atlantic winter LSC is already seen in observations, e.g. a linear regression on ERA5 data shows a weakening of both $\mathrm{LSC}_{Pac}(t)$ and $\mathrm{LSC}_{Atl}(t)$ by 1.2 K ($\pm$1.0 K); however, the evolution of the two indices displays a weak correlation coefficient (r=0.07). We note that these calculations were performed using time series of yearly winter (January-February) averages between 1979 and 2020 (not shown).

Diagnostics

Daily model output is averaged over the January and February runs, excluding a spin-up period of 165 days for each run. Here we introduce some daily-field diagnostics, useful for the analyses

Table 3.1: Atlantic and Pacific January-February LSC in the CONTROL simulations and in the TOTAL experiments, in the 1979–2008 ERA5 climatology and in the RCP 8.5 CMIP5 long-term projections for 2200–2300 (the differences "TOT - CTRL" and "CMIP5 - ERA5" in square brackets, the standard deviation for ERA5 in rounded brackets). For experiments ASIA and NAMERICA the LSC is reduced only over one basin, Pacific and Atlantic respectively

	CTRL	TOTAL	ERA5 1979–2008	CMIP5 - RCP8.5 2200–2300
LSC_{Atl}	22.4 K	13.9 [-8.5] K	23.3 (± 1.8) K	11.1 [-12.2] K
LSC_{Pac}	21.6 K	12.8 [-8.8] K	21.7 (± 1.9) K	16.6 [-5.1] K

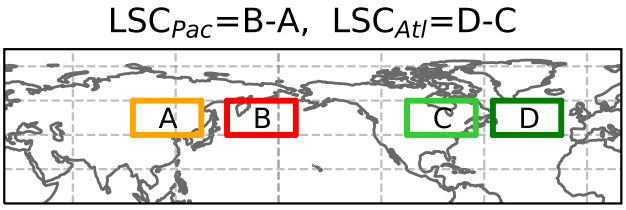

Figure 3.2: Longitude-latitude boxes used to compute LSC_{Pac} (B-A) and LSC_{Atl} (D-C). The boxes are comprised between latitudes $40-60°$ N and are 40-degrees longitude wide (A: $95-135°$ E, B: $150-190°$ E, C: $65-105°$ W, D: $15-55°$ W)

presented in Section 3.3. Firstly, the vertical component of the Eliassen-Palm flux is used to estimate the vertical propagation of planetary waves

$$\mathrm{EPf}_z \equiv a \cdot cos(\phi)\ \frac{f}{\partial\overline{\theta_{cl}}/\partial p}\ \overline{v^*T^*}, \tag{3.5}$$

where a is the radius of the Earth, f is the Coriolis parameter dependent on latitude, θ_{cl} is the climatological potential temperature and $\overline{v^*T^*}$ is the meridional eddy heat flux, with $\bar{\cdot}$ denoting the zonal mean and * the deviation from the zonal mean (eddy component). Similarly, the 200-hPa v^*T^* evidences the longitudinal features of the vertical wave propagation in the lower stratosphere.

A measure for baroclinicity is provided by the maximum Eady growth rate, as in the expression by Hoskins and Valdes (1990) comprising the modulus of the vertical derivative of the horizontal wind velocity $\mathbf{u}$ (not only the zonal component)

$$\sigma_{BI} \equiv 0.31 \cdot f \cdot |\frac{\partial \mathbf{u}}{\partial z}| \cdot \mathcal{N}^{-1}, \tag{3.6}$$

with $\mathcal{N} \equiv \sqrt{\frac{g}{\theta}\frac{d\theta}{dz}}$ the Brunt-Väisälä frequency (θ is the potential temperature, g is Earth's gravitational acceleration).

The high-frequency (HF) components of the geopotential-height, wind and potential-temperature fields are selected using a 2-6 day Fourier bandpass filter in order to represent the high-frequency geopotential-height variance, i.e. the storm track, and the eddy total energy flux (TEF, Drouard et al., 2015). The latter is used to estimate the downstream propagation of eddy total energy and is defined as

$$\text{TEF} \equiv \mathbf{u} \cdot (\text{EKE} + \text{EAPE}) + \mathbf{u}_a^{\text{HF}} Z^{\text{HF}}, \qquad \mathbf{u}_a \equiv \mathbf{u} - \frac{g\mathbf{k}}{f} \times \nabla Z \tag{3.7}$$

with contributions from the advective flux of EKE $\equiv (\mathbf{u}^{\text{HF}})^2/2$ (eddy kinetic energy), from EAPE $\equiv (h^2/s^2)(\theta^{\text{HF}})^2/2$ (eddy available potential energy), and from the ageostrophic geopotential flux, described in terms of Z (geopotential height) and $\mathbf{u}_a$ (ageostrophic horizontal wind). The EAPE parameters $s^2 = -h\,\partial\theta_{cl}/\partial p$ and $h = (R/p)(p/p_s)^{R/C_p}$ depend on pressure (R is the gas constant, p_s is 1000 hPa, C_p is the specific heat of the air at constant pressure).

3.3 Results

a. Stationary waves

The stationary response of the model to the three configurations of surface forcing described in Section 3.2 (TOTAL, ASIA, NAMERICA) is depicted in Figure 3.3. The simulations with the TOTAL forcing are characterised by negative mean sea-level pressure (MSLP) anomalies extending up to 60° N over North America and Asia and by a weakening of the Aleutian and Icelandic low-pressure systems (Figure 3.3a). The attenuation of the low-pressure systems is linked to the decrease of the diabatic heating from the oceanic western-boundary currents (surface heat flux in Figure 3.4) and to the weakening of the mid-latitude jets in Figure 3.3j (Wang and Ting, 1999; Held et al., 2002; Chang, 2009; Kaspi and Schneider, 2011). In the mid troposphere we find a general increase of the geopotential height in the mid and high latitudes,

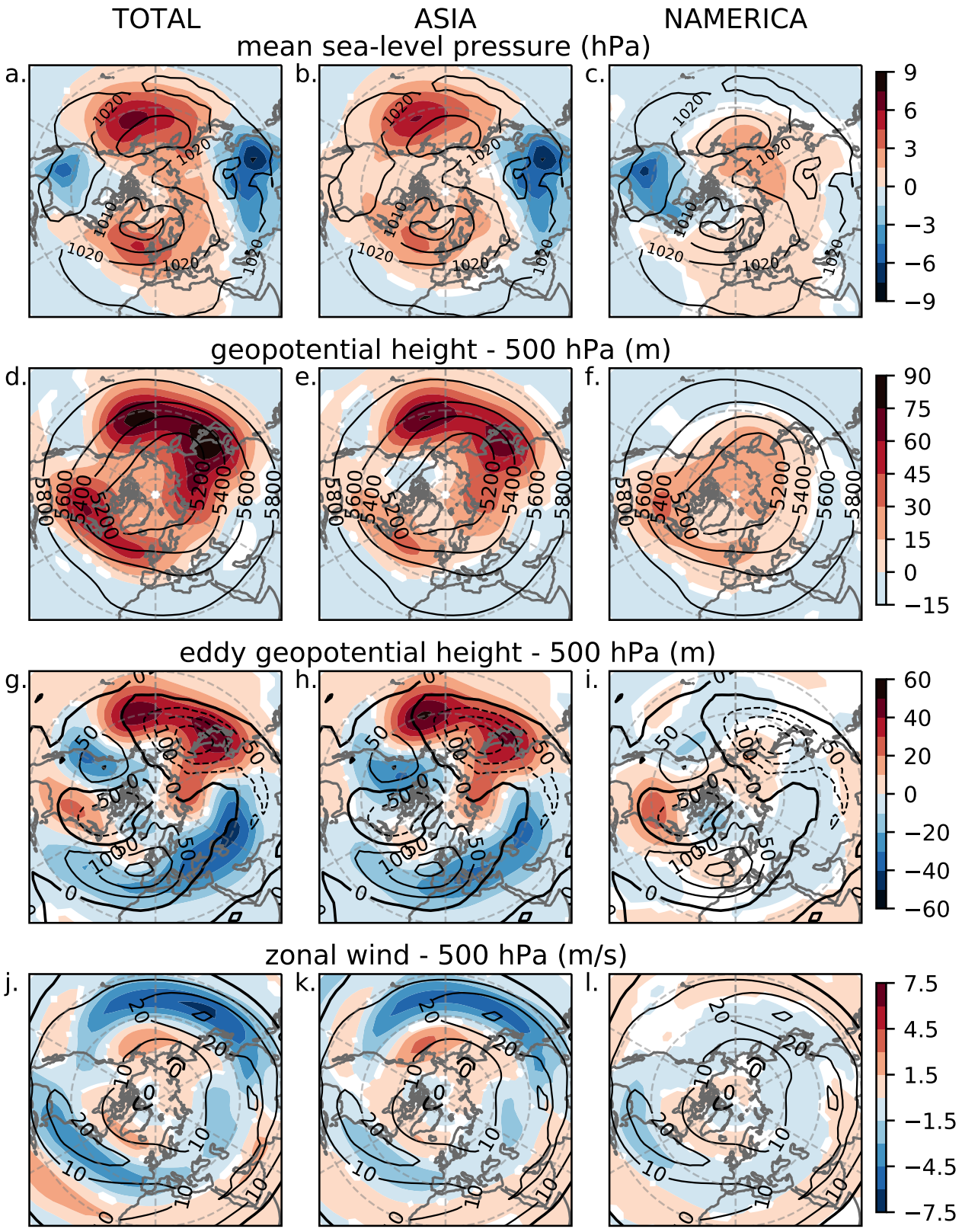

Figure 3.3: The response of TOTAL, ASIA, and NAMERICA (shading) with respect to the CONTROL climatology (contours) for (a–c) mean sea-level pressure, (d–f) geopotential height at 500 hPa and (g–i) its eddy component, (j–l) zonal wind at 500 hPa. Shading indicates significant anomalies at a 95% confidence level according to a permutation test repeated 1000 times (Wilks, 2011)

peaking downstream of the forcing, over the adjacent mid-latitude basins (Figure 3.3d). The surface-pressure low to the east of the warming and the downstream high in geopotential height are found also in individual ASIA and NAMERICA experiments (Figure 3.3b,e & c,f); both features are expected in response to low-level heating anomalies in the mid latitudes (Kushnir et al., 2002). Moreover, the stationary eddy component (deviation from the zonal mean) of the geopotential height is strongly reduced (Figure 3.3g), with a weakening of the cyclonic structure over Asia / Pacific and of the anticyclonic eddy over western North America. The pattern is reminiscent of the "thermal" stationary wave in Figure 6.22 of Held (1983).

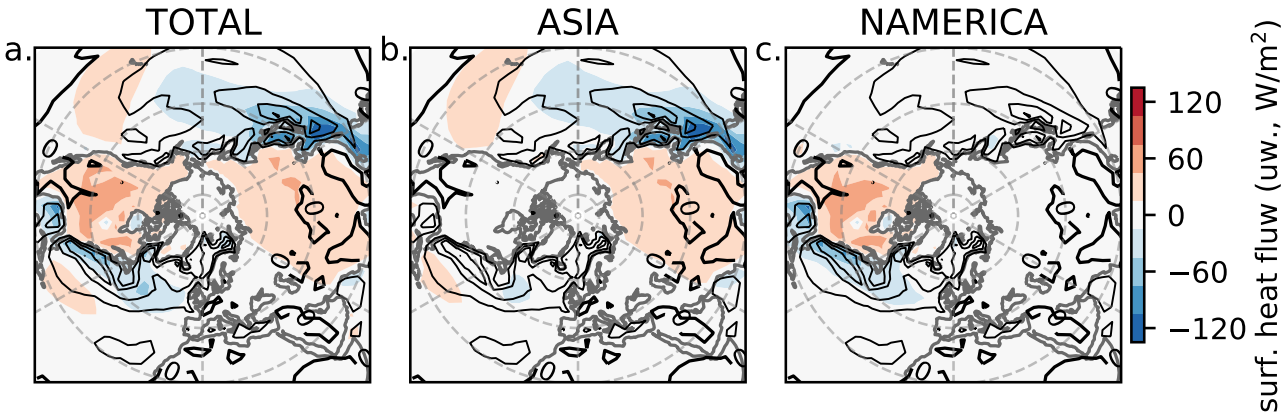

Figure 3.4: Surface heat flux (upwards), in shading the response of (a) TOTAL, (b) ASIA, and (c) NAMERICA with respect to the CONTROL climatology (contours every 100 $\mathrm{W\,m^{-2}}$)

The resemblance of experiments TOTAL and ASIA (cf. panels a,d,g,j and b,e,h,k in Figure 3.3) proves that the global signal in TOTAL is dominated by the changes in Pacific LSC, and in particular that the Siberian surface-pressure high is of great relevance in setting the shape of stationary planetary waves (Cohen et al., 2001). In fact, the widespread anomalies in experiment ASIA tend to reduce the stationary planetary waves in the mid troposphere, including the orographic wave over North America (cf. eddy geopotential height in Figure 3.3h to the response to Rocky Mountain topography in Figure 6.9, Held (1983)). This last effect is linked to the weakening of the low-level Pacific jet impinging on the Rockies (Held and Ting, 1990, discussed in more detail in Section 3.3b). Despite the similar intensity of the zonal-mean surface forcing in the NAMERICA and ASIA experiments (see Figure 3.1c), the global response to the Atlantic LSC, consisting of a deepening of the geopotential-height field over the North

Atlantic sector and at high latitudes (Figure 3.3f), is at least 50% weaker. On top of this, we see that, apart from a few regional exceptions, the response to TOTAL is approximately linear with respect to the responses to NAMERICA and ASIA forcings (cf. Figure 3.5 to Figure 3.3).

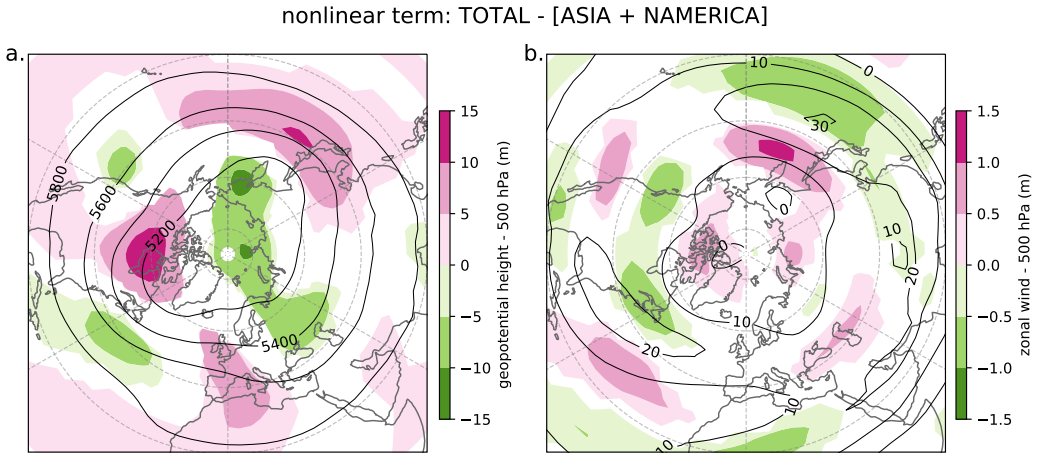

Figure 3.5: The nonlinear component of the 500-hPa (a) geopotential-height and (b) zonal-wind response, calculated as "TOTAL - (ASIA + NAMERICA)", is represented by the shading. The CONTROL climatology is shown in contours. Shading indicates significant anomalies at a 95% confidence level according to a permutation test on "TOTAL" and "ASIA + NAMERICA" repeated 1000 times (Wilks, 2011)

Large stationary waves (wave 1 and 2 in particular) are mainly attributable to extratropical thermal contrasts and orographic forcing (Held, 1983; Held and Ting, 1990), with the position of wave 1 related to the large-scale and high-amplitude signal generated by the Eurasian continent (cf. Figure 3.6a,b, showing first two zonal wavenumbers of the surface and mid-troposphere CONTROL climatology, with the contours in Figure 3.3a,g, comprehensive of all wavenumbers). While ASIA forcing induces a weakening of stationary wave 1 (by $\sim 30\%$ at the surface, $\sim 5\%$ in the mid troposphere[8]) and wave 2 (by $\sim 20\%$ at the surface and in the mid troposphere), the NAMERICA response consists of a wave-2 attenuation (by $\sim 15\%$ at the surface, $\sim 5\%$ in the mid troposphere) and wave-1 amplification near the surface (by $\sim 30\%$ stronger, cf. the positive anomaly over Siberia and North Pacific in Figure 3.3c and the positive lobe of wave-1 in Figure 3.6a). A general feature, particularly noticeable in experiment NAMERICA, is that the influence of the surface forcing on waves 1 and 2 is less evident in the mid troposphere (cf. Figure 3.3 to Figure 3.6).

[8]The estimate is computed by considering the ratio between the wave amplitude in ASIA or NAMERICA and that in the CONTROL, averaged over latitudes $40 - 70°$N. We use the fields of MSLP and of 500-hPa

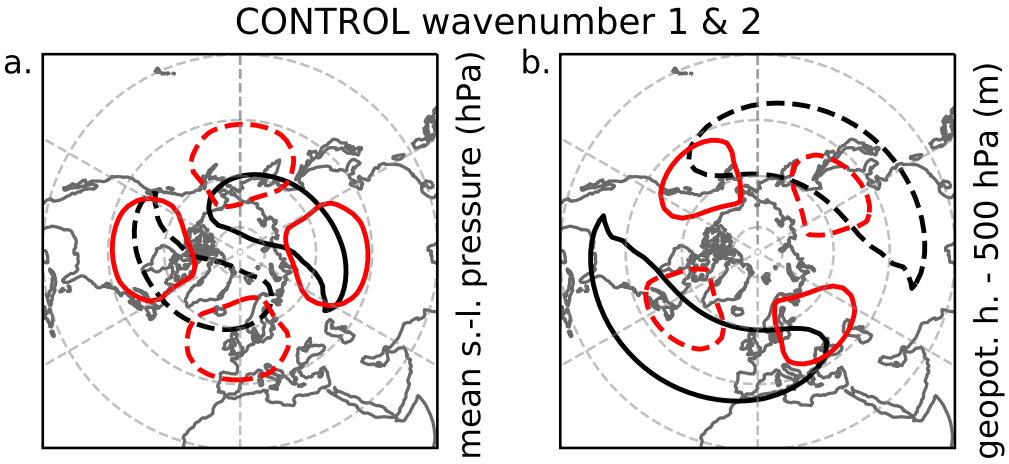

Figure 3.6: Decomposition of the CONTROL climatology in zonal-wavenumber 1 (black) and 2 (red) for (a) mean sea-level pressure with contours at ±4 hPa and (b) 500-hPa geopotential height with contours at ± 40 m

A focus on the meridional cross sections of the atmosphere shows a different warming pattern when comparing experiment ASIA, where the positive temperature anomaly is strong in the mid troposphere at around 40° N but hardly reaches latitudes above 70° N, to experiment NAMERICA, showing a positive anomaly that extends to most of the high-latitude atmospheric column up to the stratosphere (see air temperature in the Atlantic and Pacific sector, shading in Figure 3.7). The northward extension of the low-troposphere temperature anomalies in NAMERICA (Figure 3.7d,h) is coherent with the amplification of MSLP wave 1 favouring poleward heat transport through the North-Atlantic sector (Graversen and Burtu, 2016). The polar-cap heating decays in the mid-troposphere, together with the amplification of wave 1, to become again relevant in the top levels. In the stratosphere the temperature profiles are linked to the dynamic response, as the westerly mean flow weakens with positive polar-latitude temperature anomalies and viceversa, following the thermal-wind relation.

To study the nearly opposite response of the mid-latitude and polar stratosphere to the two individual-continent forcings, i.e. stratospheric cooling and vortex strengthening in ASIA – also applicable to TOTAL – and the opposite conditions in NAMERICA, we compute the vertical component of the Eliassen-Palm flux (hereafter E-P flux). The vertical E-P flux is proportional to the meridional eddy heat flux (Eq. (3.5)) and represents the vertical wave propagation (arrows

geopotential height.

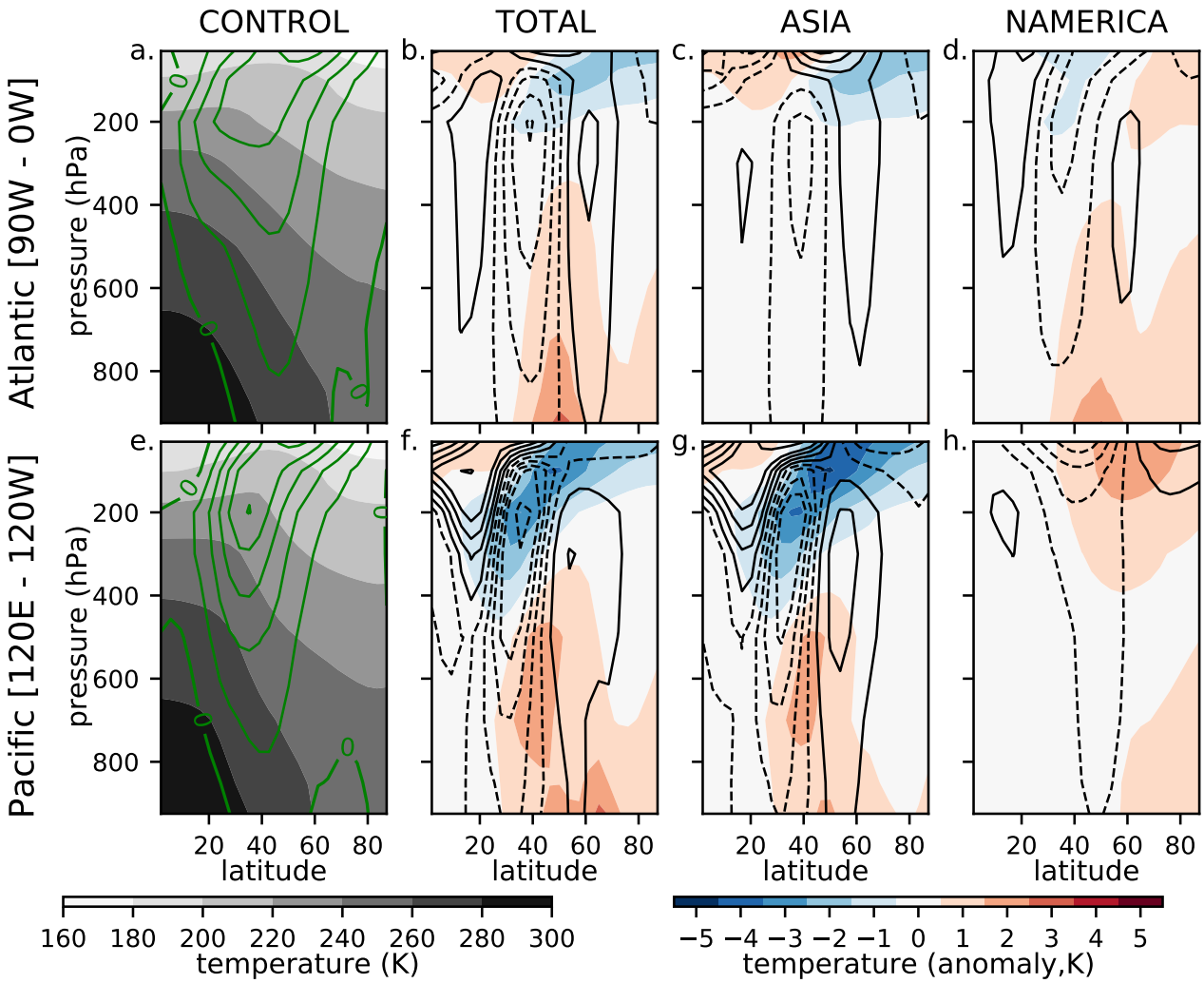

Figure 3.7: Meridional cross sections of temperature (shading) and zonal wind (contours) in the (a–d) Atlantic sector, and (e–h) Pacific sector. The response of (b & f) TOTAL, (c & g) ASIA and (d & h) NAMERICA is shown with respect to the CONTROL climatology (a & e). Contours are drawn every 10 $\mathrm{m\,s^{-1}}$ in (a & e), every 1.2 $\mathrm{m\,s^{-1}}$ in (b–d & f–h)

in Figure 3.9a). Since the convergence of the E-P flux in the stratospheric levels corresponds to a deposition of easterly momentum into the westerly mean flow (negative shading above 200 hPa at $40 - 70^\circ$ N in Figure 3.9a), we expect an enhanced upper-level convergence to be associated to a weak stratospheric vortex and a warm polar stratosphere, the opposite for reduced stratospheric convergence. As a caveat, the small number of stratospheric levels in SPEEDY (see Forcing patterns) limits the sensitivity of the EP-flux convergence diagnosis.

For the ASIA and TOTAL experiments we find a net reduction of the meridional eddy heat flux into the stratosphere (Figure 3.9b,c) at $\sim 40{-}60^\circ$ N, the latitudes corresponding to the strongest climatological upward propagation (Figure 3.9a). Note that this type of signal resembles that of strong stratospheric-vortex events (Figure 4f in Díaz-Durán et al., 2017) and, indeed, in the topmost model level we find a weakening of the E-P flux convergence associated with an acceleration of the zonal-mean zonal wind. In the NAMERICA simulations a weak convergence anomaly in the stratospheric E-P flux and a vortex deceleration are detected (Figure 3.9d). To better understand the mechanism leading to vortex weakening in NAMERICA we plot zonal wavenumbers 1 and 2 of the vertical E-P flux (Figure 3.8), as these are known to dominate the wave propagation from the troposphere to the stratosphere (Charney and Drazin, 1961; Andrews et al., 1987; Haklander et al., 2007). It is thus evident from panels d,h,l of Figure 3.8 that the slowing down of the stratospheric vortex in NAMERICA is caused by a moderate amplification of wave-1 E-P flux into the stratosphere; the reduction of the wave 2 component in the low troposphere hardly reaches stratospheric levels. Differently, for ASIA the wave-1 and wave-2 components of the E-P flux are reduced through the troposphere (Figure 3.8g,k), where the strong tropospheric signal is linked to the mid-tropospheric warming in the Pacific sector (Figure 3.7g). Again, it is mainly wave 1 which influences the strength of the stratospheric vortex.

In both the ASIA and NAMERICA experiments the low-wavenumber anomalies in the upward E-P flux originate in the lower troposphere and decay in the mid-troposphere, but nonetheless reach the topmost atmospheric layers. This is in agreement with the previous analysis on waves 1 and 2 at the surface (MSLP field) and in the mid troposphere (500-hPa geopotential-height field).

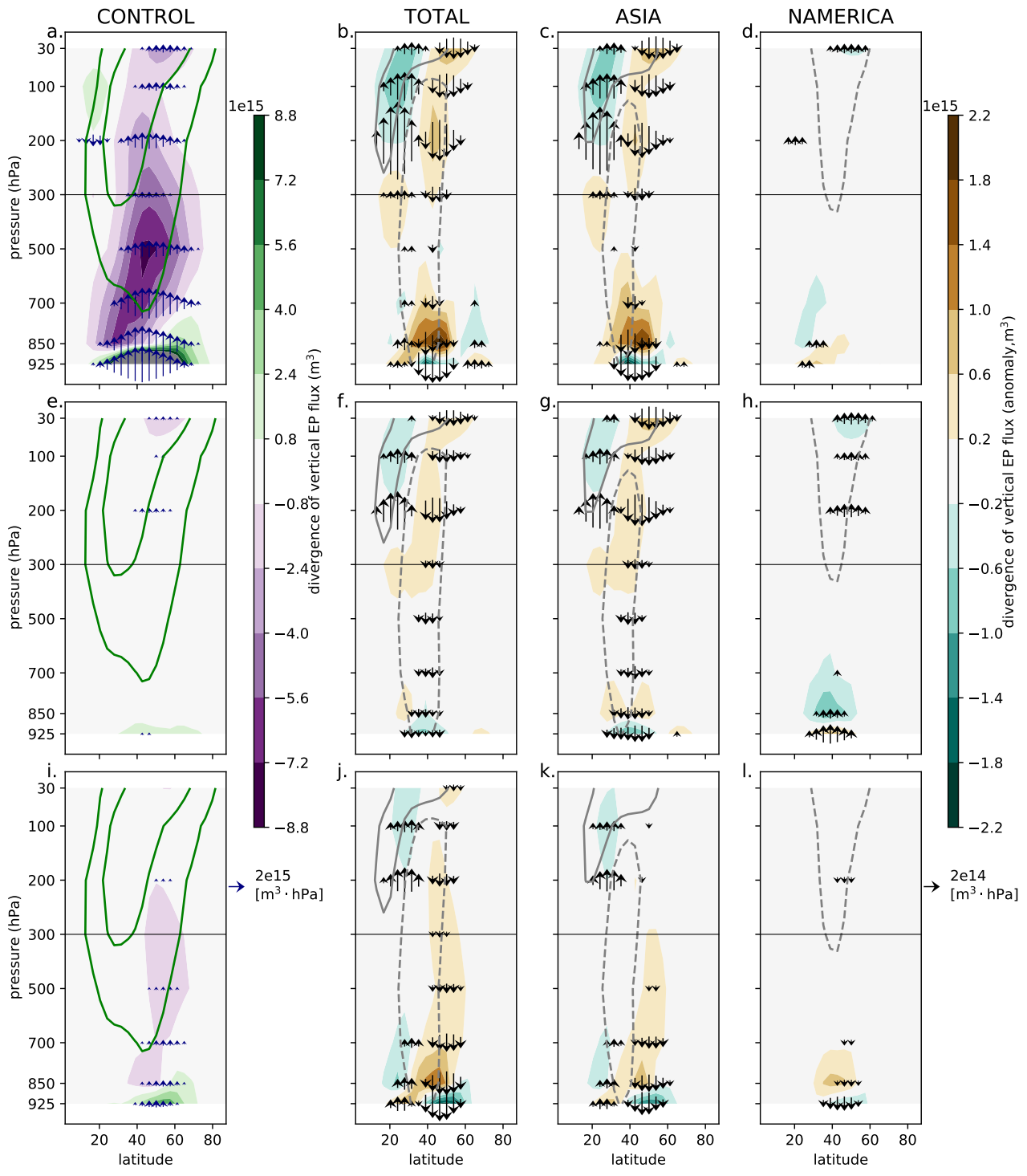

Figure 3.8: Meridional cross sections of the vertical Eliassen-Palm flux (arrows) and of its divergence (shading), anomalies of (b) TOTAL, (c) ASIA and (d) NAMERICA with respect to (a) CONTROL climatology; the same is shown for the (e-h) wave-1 and (i-l) wave-2 contributions. E-P fluxes above the 300-hPa horizontal line are multiplied by a factor 5. The zonal-mean zonal wind contours—control climatology in green [10m/s,30m/s] and anomaly in grey [±1m/s]—are superimposed on to the EP-flux plots

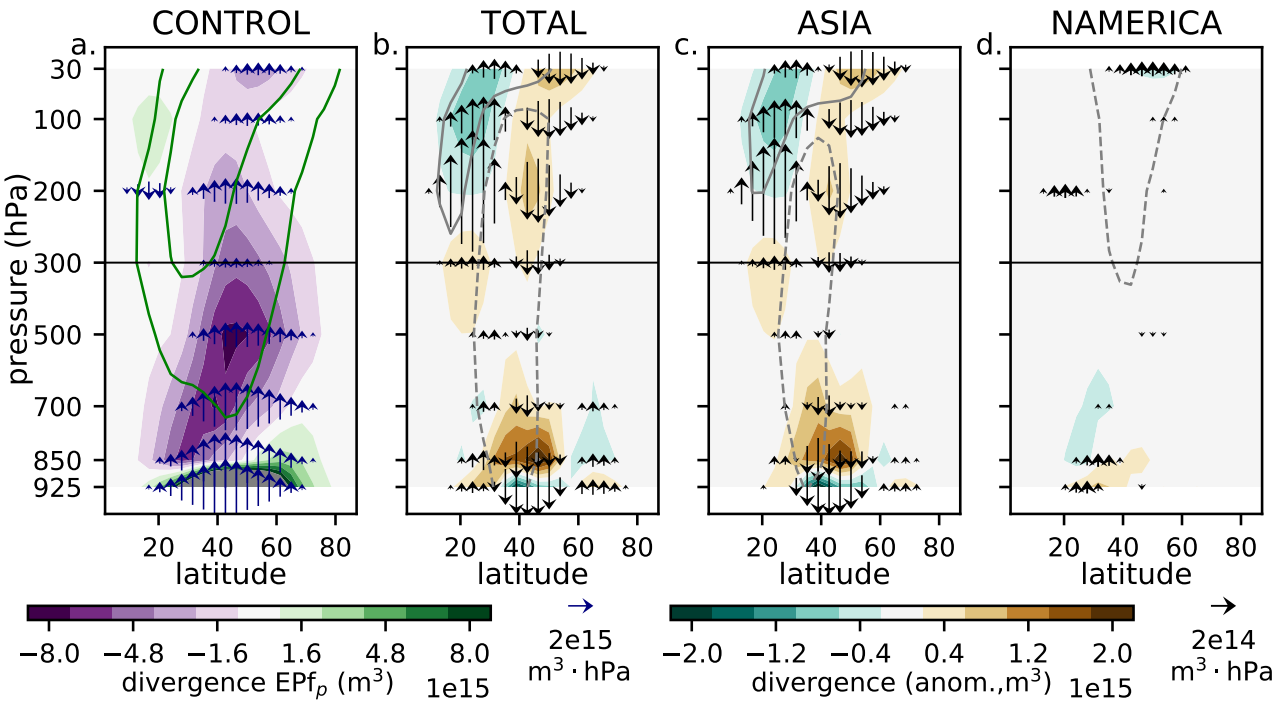

Figure 3.9: Meridional cross sections of the vertical Eliassen-Palm flux (arrows) and its divergence (shading) for (a) CONTROL climatology, (b) TOTAL, (c) ASIA and (d) NAMERICA anomalies. E-P fluxes above the 300-hPa horizontal line are multiplied by a factor 5. Green contours in (a) show the zonal-mean zonal wind at 10 and 30 m s^{-1} levels, grey contours in (b–d) the anomaly of each experiment for levels ±1 m s^{-1}

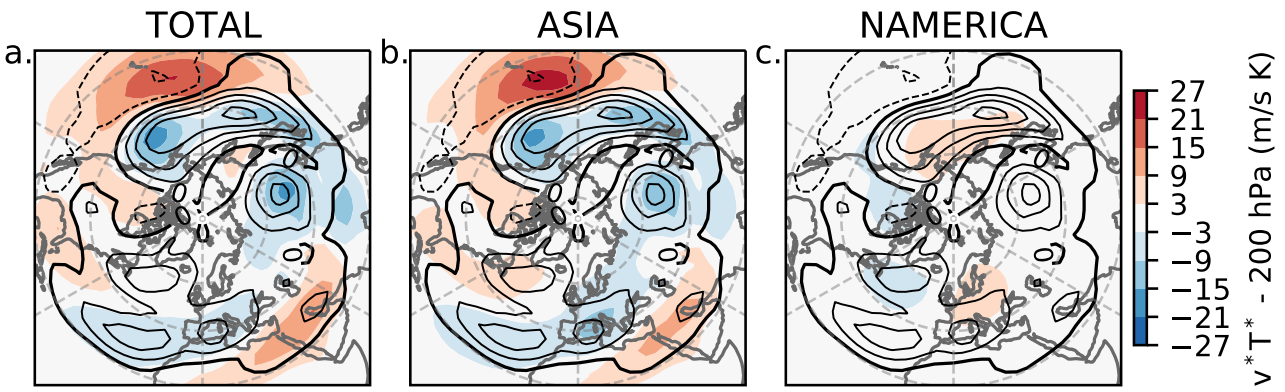

Figure 3.10: v^*T^* at 200 hPa, in shading the response of (a) TOTAL, (b) ASIA, and (c) NAMERICA with respect to the CONTROL climatology (contours every 10 $\mathrm{m\,s^{-1}\,K}$)

The change in the wave activity propagating into the stratosphere is also detected in the v^*T^* anomaly at 200 hPa. In TOTAL and ASIA (Figure 3.10a,b) the three centers of strongest positive v^*T^* (Central Siberia, North Pacific and western North Atlantic) are weaker by $\sim 50\%$ due to the reduction in the eddy components of the temperature field and to the weakening of the meridional circulation (discussed in Section 3.3b). Differently, in NAMERICA the v^*T^* centers over the North Pacific – positive – and over North America – negative – are moderately amplified, while the positive v^*T^* over the North Atlantic–European region weakens over the ocean and strengthens over the continent. Since the meridional circulation is nearly unchanged (see Section 3.3b), such signal is dominated by the changes in the eddy temperature pattern.

b. Mid-latitude jets

The general response to the reduction of extratropical LSC consists of a weakening and poleward shift of the mid-latitude jets. Specifically, the zonal winds weaken south of 50° N (Figure 3.3j) following the reduction of the meridional gradients in the mid troposphere at $\sim 30-50°$ N (Figure 3.3d), while they strengthen along the northern flanks of the jets ($\sim 50-70°$ N) associated with reinforced meridional gradients (cf. panels d and j of Figure 3.3). The signal is coherent in the vertical up to ∼200 hPa (Figure 3.7); once more it is evident that the ASIA response, extending to the Atlantic sector, has a large influence on the mid-latitude zonal flow

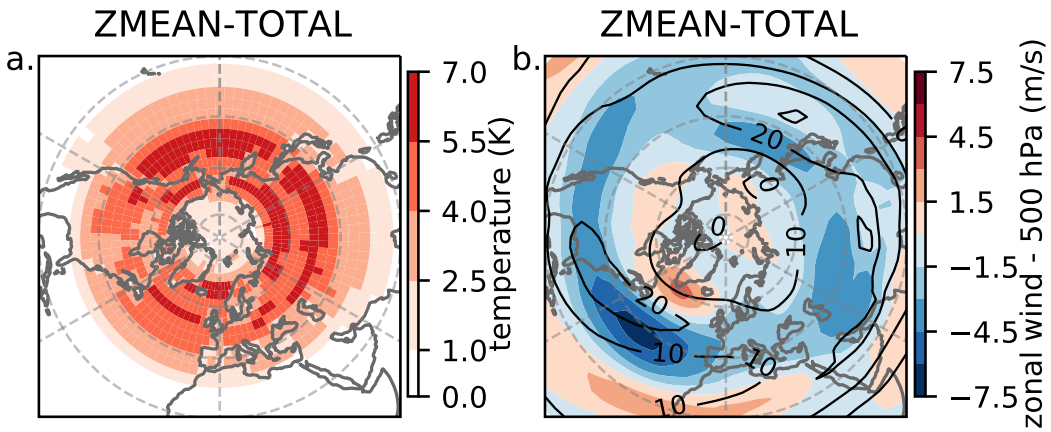

Figure 3.11: (a) ZMEAN-TOTAL forcing anomaly averaged over January and February and (b) response of the zonal wind at 500 hPa (shading) with respect to the CONTROL climatology (contours)

(Figure 3.7c).

The question might arise whether the modifications in the zonal flow are an effect of the LSC reduction or if they constitute a response to the generalised extratropical warming introduced by the forcing. To investigate this we devise a new experiment – ZMEAN-TOTAL – where the zonal-mean forcing from TOTAL is retained and spread uniformly over sea and land surface[9] (Figure 3.11a). Such a configuration produces a zonal-mean forcing equal to that in experiment TOTAL in spite of a zonal LSC similar to that in the CONTROL. The results indicate that the Pacific LSC is relevant for the atmospheric circulation, independent of the generalised warming generated by the forcing. In fact, while in TOTAL the reduction of the Atlantic jet is to a certain extent similar to that in ZMEAN-TOTAL, suggesting a significant role of the generalised meridional temperature gradient, the TOTAL and ZMEAN-TOTAL Pacific-jet responses are different in position and intensity (cf. Figure 3.3j and Figure 3.11b).

The response to ASIA forcing is strong also in the Atlantic sector, where the damping of the Rockies' wave train crossing North America reduces the western ridge and eastern trough. This orographic wave is decisive for the localisation of the Atlantic storm track along the south-eastern coast of North America, i.e. where the baroclinicity is strongest (Brayshaw et al., 2009; Chang, 2009). The attenuation of the Rockies' wave train (see stationary eddy component

[9]We impose two times the zonal-mean ASIA forcing in the sector $60-240°$ E, and two times the zonal-mean NAMERICA forcing in the sector 120° W−60° E

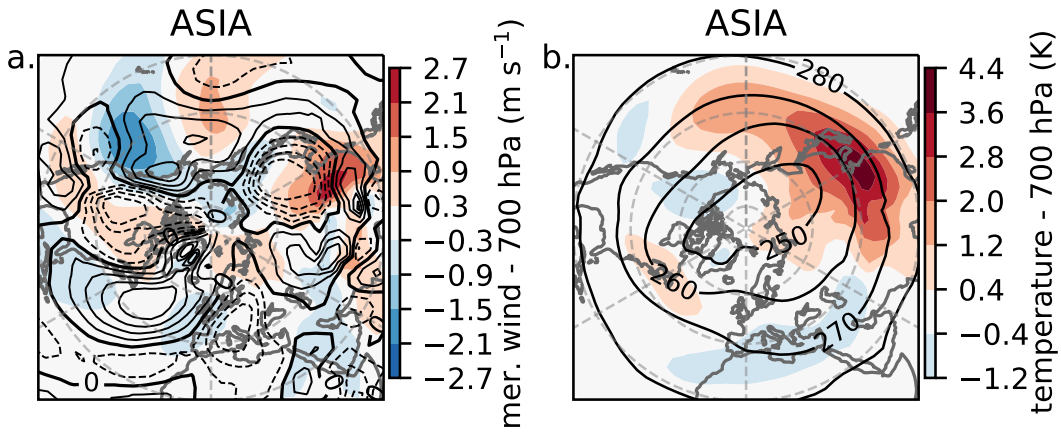

Figure 3.12: (a) Meridional wind and (b) temperature at 700 hPa, response of ASIA (shading) with respect to the CONTROL climatology (contours). In (a) contours are drawn every 1 $\mathrm{m\,s^{-1}}$

of the geopotential height field in Figure 3.3h and meridional wind field in Figure 3.12a) is caused by the weakening of the low-troposphere Pacific jet impinging on the Rocky Mountains (Held and Ting, 1990; Held et al., 2002), with a pattern such as the one in Figure 3.3k. The response to the altered orographic wave consists of a more zonal circulation in the North American region, with a weakened meridional wind over eastern North Pacific and over the continent (Figure 3.12a) and a positive zonal-wind anomaly at latitudes higher than 50° N (Figure 3.3h). West of the Rockies the limited northward advection of warm air results in colder temperatures, while, in the area comprising the Hudson Bay, the diminished advection from the Arctic implies a warming over the eastern coast of North America (Figure 3.12b) and a reduction in the baroclinicity at the entrance of the Atlantic storm track, as shown in Section 3.3b.

The modification of the meridional circulation also affects the propagation of synoptic-eddy total energy flux downstream of the Pacific (TEF, cf. Figure 3.13b to Figure 3.12a) which is known to play a role in setting the strength and position of the Atlantic jet (Chang, 1993; James and Burkhardt, 2006; Rivière and Orlanski, 2007; Li and Lau, 2012). Specifically, the upper-troposphere TEF is enhanced over the northern part of the Pacific basin and is advected zonally across the American continent, feeding the northward flank of the Atlantic storm track (Figure 3.13b). The excess eddy energy does not reach south-eastern North America, a key region for low-level cyclogenesis, characterised by a negative TEF anomaly induced by the

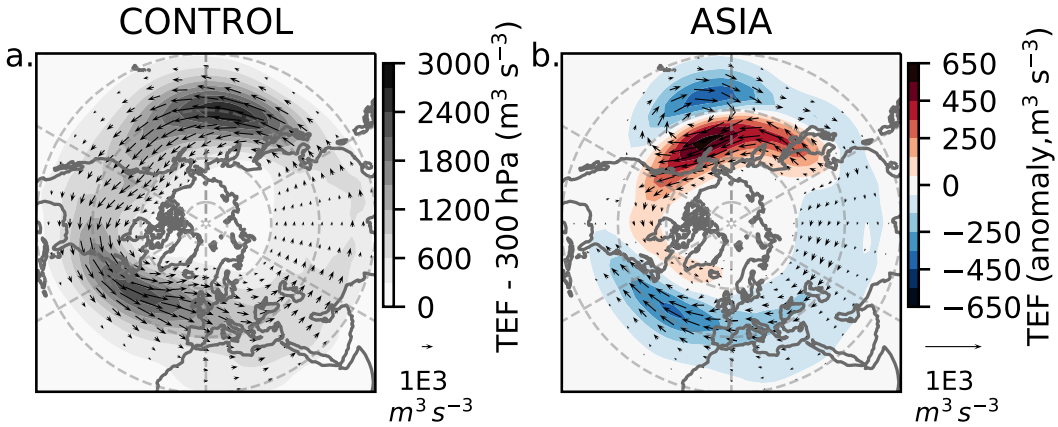

Figure 3.13: Eddy total energy flux at 300 hPa (arrows) and its intensity (shading) for (a) the CONTROL climatology and (b) ASIA anomalies ; in (b) the size of the arrows is amplified by a factor 5

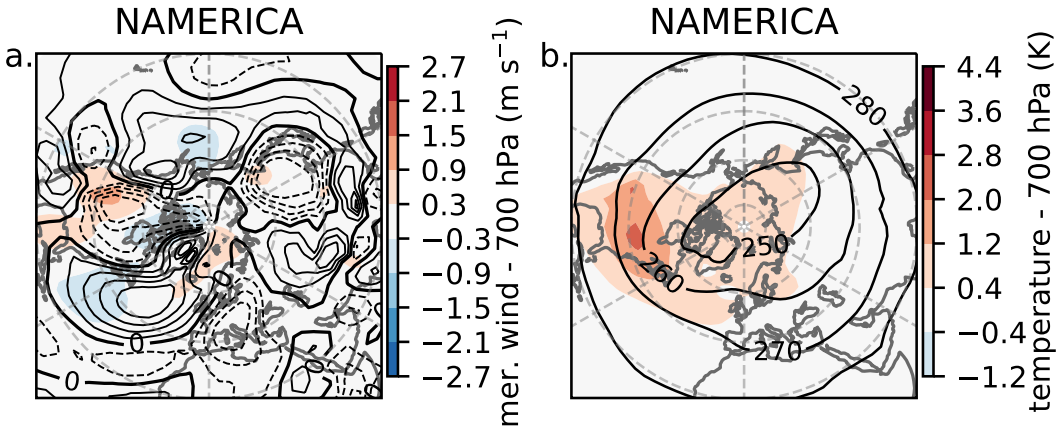

Figure 3.14: (a) Meridional wind and (b) temperature at 700 hPa, response of NAMERICA (shading) with respect to the CONTROL climatology (contours). In (a) contours are drawn every 1 m s^{-1}

weakening of the southward advection downstream of the Rockies (Figure 3.12a) and by the reduction of the Pacific TEF south of 40° N and of its eastward propagation (Figure 3.13b). The decline in synoptic upper-tropospheric disturbances over south-east North-America is thus expected to trigger less low-level cyclogenesis at the entrance of the Atlantic storm track (type-B cyclogenesis in Petterssen and Smebye (1971)).

In summary, in experiment ASIA the attenuation of the North American stationary wave weakens the baroclinicity over the eastern coast of the continent. This, together with less energetic upper-level disturbances entering the Atlantic domain south of 50° N, leads to a reduction in cyclogenesis and storm-track activity and, finally, to a reduction of the Atlantic jet (Figure 3.3k).

In experiment NAMERICA, on the other hand, the response in lower tropospheric warming is strong in the Atlantic sector and extends to the Arctic (Figure 3.14b). However, unlike experiment ASIA, the low-level meridional circulation is weakly impacted (Figure 3.14a), and shows mainly a decrease in amplitude over the Atlantic sector. This confirms the limited influence of North American continental warming on the tropospheric stationary waves (see also EP-flux in Figure 3.9).

c. Storm tracks

The tropospheric temperature anomalies induced by the surface forcings peak between $40-60°$ N and are accompanied by a weakening and poleward shift of the jets (Figures 3.3j,l, 3.7b,f). These changes are associated with modifications in the synoptic variability, and in particular with poleward displaced mid-latitude storm tracks (see shading, i.e. variance of high-frequency geopotential height, in Figure 3.15b,f). ASIA forcing produces a strong, poleward shifted storm track over the Pacific, and a weakened and poleward shifted Atlantic storm track, which are in agreement with the low-level changes in baroclinicity expressed by the maximum Eady-growth rate σ_{BI} (Figure 3.15c,g). Moreover, a weakening of the Pacific storm track on its south-eastern flank is balanced by a positive signal along the north-Asian coast (not shown), giving no net storm-track decrease in the Pacific-sector zonal mean (Figure 3.15g). For NAMERICA forcing

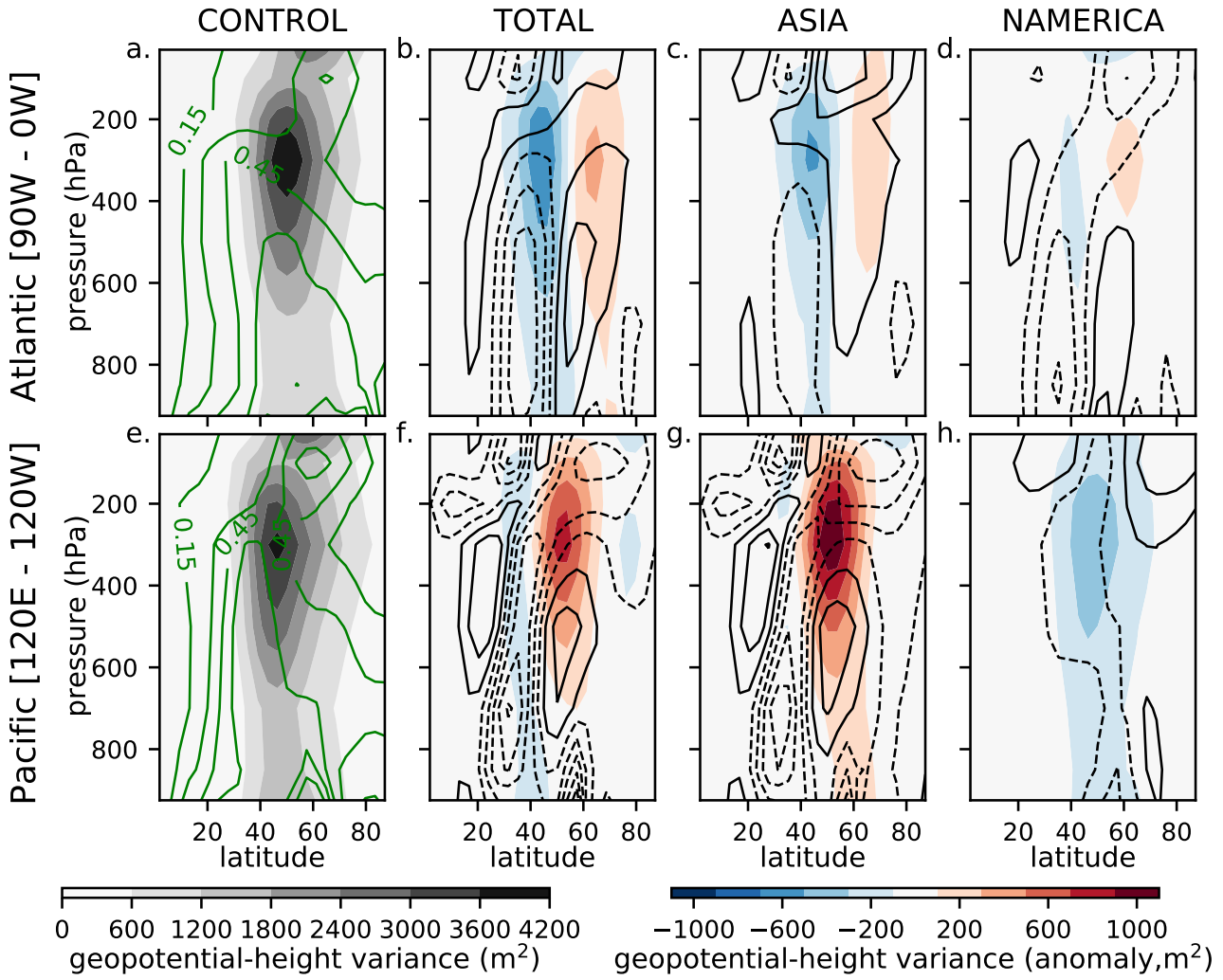

Figure 3.15: Meridional cross sections of high-frequency geopotential-height variance (shading) and maximum Eady growth rate (contours) in the (a–d) Atlantic sector, and (e–h) Pacific sector. The response of (b & f) TOTAL, (c & g) ASIA and (d & h) NAMERICA is shown with respect to the CONTROL climatology (a & e). Contours are drawn every 0.15 d^{-1} in (a & e), every 0.02 d^{-1} in (b–d & f–h)

we find weaker anomalies indicating a poleward shift of the storm track in the Atlantic sector (Figure 3.15d), and a reduction of the storm track and of the jet over the Pacific basin, north of their maximum climatological intensity (Figures 3.7h, 3.15h). Such a negative signal in the storm track is difficult to justify exclusively by the correspondent, moderate decrease in tropospheric baroclinicity (σ_{BI} contours in Figure 3.15h).

Further reasoning for the storm-track and jet weakening could come from the effect of the lower stratosphere on the tropospheric mean state and variability. To give a simplistic picture, the weakening of the stratospheric vortex is known to cause a southward shift of the mid-latitude tropospheric jets, while the opposite happens with a strong stratospheric vortex (Kidston et al., 2015); although regional differences might emerge between the Atlantic and Pacific basin, this behaviour has been detected in models and in reanalysis (e.g. Polvani and Kushner, 2002; Baldwin and Dunkerton, 1999). The mechanisms for the downward propagation of stratospheric anomalies to the mid-latitude troposphere are still debated. Despite a few exceptions (e.g. Smy and Scott, 2009), models characterised by different levels of complexity show that an increase in lower-stratospheric shear tends to amplify the size and strength of baroclinic waves and to favour a northward displacement of the associated jet (see Wittman et al., 2007; Rivière, 2011; Haualand and Spengler, 2021; Rupp and Birner, 2021; Butler et al., 2010).

Returning to the simulations, we note that in the CONTROL at latitudes $0-40^\circ$ N the vertical zonal-wind shear above the tropopause ($\sim$200 hPa) is negative, with $(du/dz)_{str} < 0 < (du/dz)_{tr}$, while at higher latitudes, due to the presence of the stratospheric polar vortex, it turns positive and it exceeds the tropospheric shear $(du/dz)_{tr}$ (Figure 3.16a,e). The patterns of climatological wind shear from reanalysis data are approximately reproduced (not shown). Following the arguments above, we hypothesise that in experiment NAMERICA the negative anomaly of the Pacific-sector lower-stratosphere wind shear (Figure 3.16h), combined with the reduction in the tropospheric baroclinicity (contours in Figure 3.15h), explains the weakening of the Pacific storm track (shading in Figure 3.15h). In addition, the responses of the Atlantic and Pacific sectors to ASIA forcing may be supported by an analogous, opposite influence of the upper-level wind shear on the tropospheric storm tracks. The increase in stratospheric zonal wind (Figure 3.7c) and in its vertical shear (Figure 3.16c) are indeed expected to favour the poleward

shift detected in the NH jets and storm tracks (Figures 3.7c, 3.15c).

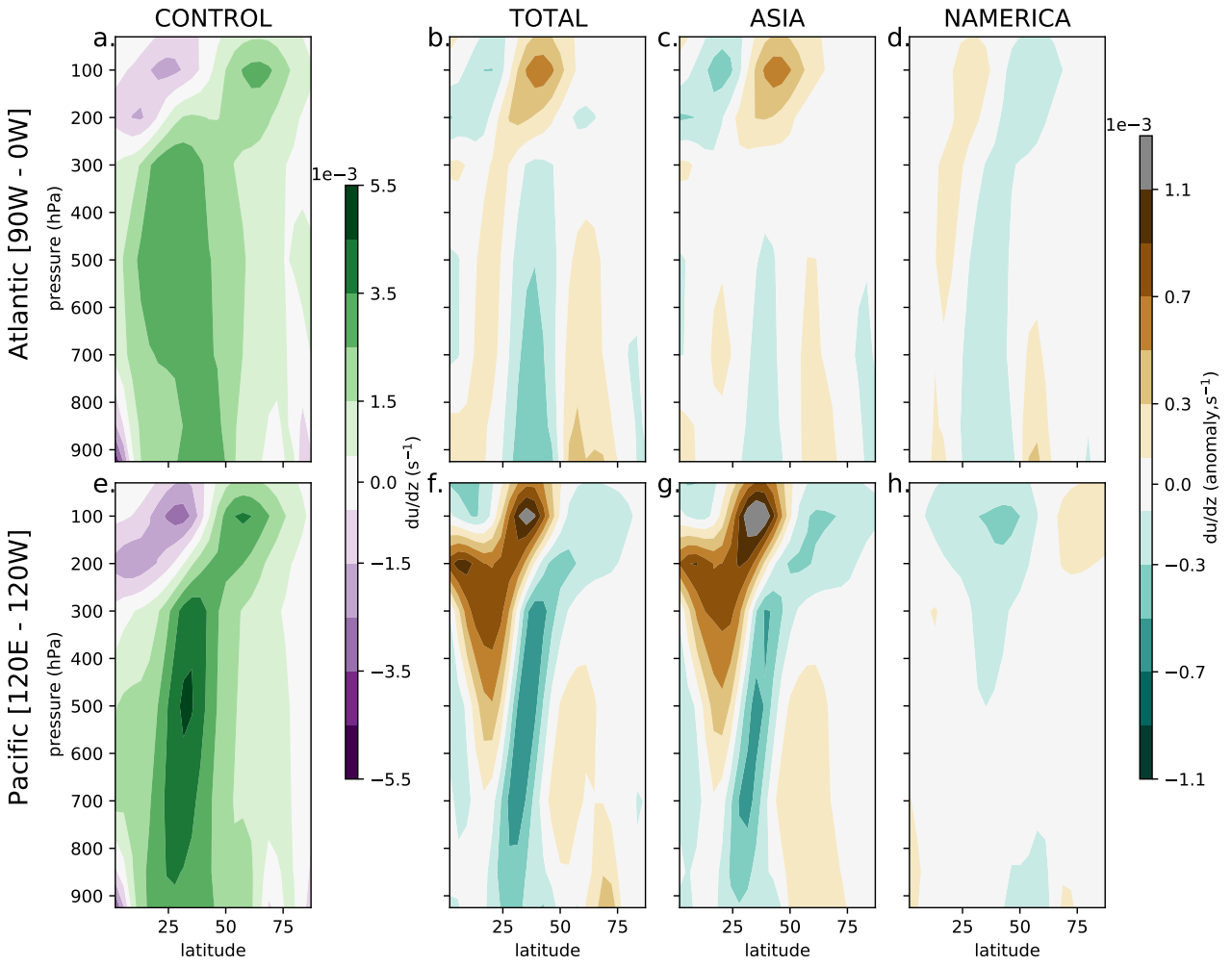

Figure 3.16: Meridional cross sections of zonal-wind shear in the (a-d) Atlantic sector, and (e-h) Pacific sector. The response of (b&f) TOTAL, (c&g) ASIA and (d&h) NAMERICA is shown with respect to the CONTROL climatology (a&e)

3.4 Conclusions

The reduction of mid-latitude thermal land-sea contrast (LSC) is a robust characteristic of long-term climate projections (Table 3.1), with a negative trend already detectable in reanalysis data: ERA5 shows a weakening of LSC_{Pac} and LSC_{Atl} by 1.2 K (±1.0 K) between 1979 and 2020. Here, by running idealised numerical experiments where we impose surface warming over NH continents and climatological SSTs, we find that the response to a reduced boreal winter LSC consists of a reduction of the tropospheric stationary eddies propagating up to the stratosphere

(Figures 3.3g, 3.9b), and a weakening and poleward shift of the mid-latitude jets and of the associated storm tracks (Figures 3.3j, 3.15b,f). This is in line with previous literature on the topic (Brayshaw et al., 2009; Held et al., 2002; Garfinkel et al., 2020), and shows the tendency of the mean NH regime to shift towards a more zonal circulation for a weaker zonal asymmetry in the surface thermal structure (see thermal-equilibration theory, e.g. Charney and DeVore, 1979). In our study for the first time a distinction between the Pacific and Atlantic LSC is applied to disentangle their impact on the mid-latitude atmosphere; note that the responses to individual East-Asia and North-America surface forcings add almost linearly to give the response to the sum of the forcings (Figures 3.3, 3.5).

If over North America the stationary waves are mainly attributable to the presence of the Rockies interacting with the low-level mean flow, the Siberian surface-pressure high forms in winter due to both the Tibetan-plateau orographic wave (Held, 1983; Held et al., 2002) and the vast extent of Eurasia impeding warm-air advection from the oceanic regions (Seager et al., 2002). The large-scale patterns associated with Siberian High / Aleutian Low in the Pacific sector and East-American High / Icelandic Low in the Atlantic sector are reinforced by the atmospheric response to the strong ocean-to-atmosphere heat flux in the western portion of the NH oceans, i.e. a surface upstream high and a downstream low (Kaspi and Schneider, 2011). These circulation systems imply a northerly advection of cold continental air over the western oceans which increases the air-sea temperature difference and enhances the heat flux from the ocean, hence inducing a positive feedback on the circulation. Our results suggest that a reduction of the LSC, Atlantic or Pacific, is consistent with a weakening of the eastern-continents' highs and oceanic lows (Figure 3.3a-c) induced by a decline in the heating effect by the warm western-boundary oceanic currents (see Figure 3.4 and Held et al., 2002; Kaspi and Schneider, 2011).

Our idealised experiments show a dominant impact of East-Asia surface temperatures on stationary planetary waves. Indeed the response to Asian warming interferes destructively with waves 1 and 2 (cf. Figure 3.3 and Figure 3.6) and reduces the propagation of large waves to the stratosphere, making the stratospheric vortex stronger (Figure 3.9c). Hence, we confirm the sensitivity of the NH atmospheric circulation to the Pacific-sector surface conditions, as in

Ayarzagüena et al. (2021), who attest an important impact of the Pacific-sector SST on atmospheric planetary waves up to the stratosphere, or as in Cohen et al. (2014), linking anomalous Siberian snow cover to a weakened stratospheric vortex (this is consistent with the strong vortex in the warm-Asia experiment). The role of Eurasia for the vertical propagation of waves into the stratosphere is important also in model predictions (e.g. Domeisen et al., 2020; Portal et al., 2021). The relevance of the Pacific LSC, as opposed to a generalised mid-latitude warming, is proved by the fact that a widespread reduction of the meridional surface-temperature gradients in the Pacific sector (Figure 3.11) does not reproduce the position and intensity of the Pacific-jet weakening obtained by warming East Asia (Figure 3.3k). Downstream effects of the weakening of the Pacific jet consist of an attenuation of the Rockies' orographic wave and of the baroclinicity and cyclogenesis in the Atlantic jet-entry region (Figures 3.12, 3.13, 3.15), hence in a slower and poleward displaced Atlantic jet (Figure 3.7c).

The impact of reduced Atlantic LSC is less evident in the mid-troposphere and seems to reach remote tropospheric regions mainly through a stratospheric pathway. We note an enhancement in wave-1 vertical propagation which leads to a warming of the stratosphere, a weakening of the vortex (Figure 3.9d) and a reduction of the lower-stratospheric wind shear over the Pacific sector. We hypothesise that the latter is responsible for the negative anomaly in the Pacific storm track and jet (Figures 3.15h, 3.7h). Despite the fact that our results highlight the importance of thermal changes over the mid-latitude Pacific sector, long-term climate projections predict an enhanced reduction of the Atlantic LSC with respect to the Pacific LSC (Table 3.1). Understanding whether the effects of a reduced Atlantic LSC – including the weakening of the stratospheric vortex – would dominate in the projected configuration of LSC is beyond the scope of this thesis.

We indicate some possible shortcomings in this work. Firstly, the surface temperature over the sea is fixed and that over land is relaxed towards the LST forcing patterns. This restricts the two-way interaction between the surface and the atmosphere (see Land-temperature and ice-temperature schemes) and removes the interdependence between the SSTs and the land temperature. While the arrangement is satisfactory for the analysis of a long-term LSC change of amplitude larger than its interannual variations, additional work is necessary to assess whether

our results are also relevant for the impact of LSC on year-to-year variability.

A further limitation derives from the coarse resolution of the model. Kucharski et al. (2013) and the articles there cited show that the model SPEEDY reliably represents the large-scale features of the climate mean and variability in the mid latitudes. According to more recent papers (Ruggieri et al., 2017; Hamouda et al., 2021) the limited representation of the stratospheric system does not inhibit the coupling between the troposphere and the stratosphere (see Stratospheric levels in SPEEDY for an exhaustive discussion). Furthermore, the bias in the representation of the model orography, dependent on the horizontal resolution, may influence the model response.

Our results describe the role played by decreasing LSC in the mid-latitude mean climate and variability. In CMIP6 scenarios the larger land-temperature increase in the NH mid and high latitudes than elsewhere reduces the extratropical LSC by various degrees, with an amplitude comparable to that of Arctic Amplification – AA (IPCC-*WGI*, 2021). However, differently from AA, LSC is rarely cited when analysing the sources of the projected changes in the large-scale mid-latitude circulation, such as those concerning stationary planetary waves (Wills et al., 2019, and references therein) and tropospheric jets and storm-tracks (e.g. Harvey et al., 2020; Oudar et al., 2020; Shaw et al., 2016). Our results suggest that in the "tug of war" for the positioning of the jet stream between AA and the Hadley-cell expansion (Butler et al., 2010; Barnes and Polvani, 2013), a reduced LSC supports the effects of the latter – a poleward jet shift. We therefore encourage research on climate-change scenarios to take into account LSC as a possible source of change for the mid-latitude circulation and to investigate its interplay with AA.

Chapter 4

Interaction with East Asia land temperature in CMIP6 models

Chapter Summary

In the idealised experiments of Chapter 3 the land conditions over East Asia are shown to have a large impact on the mid-latitude circulation. Here we look into the representation of land temperature conditions in a set of higher-complexity climate models and detect a large inter-model spread in their climatologies, computed over a common historical period. The spread is especially broad in East Asia, in particular over the Tibetan Plateau, where a well-documented cold model bias is also present, and over Siberia. The links of these temperature spread hotspots with the large-scale atmospheric circulation are discussed in Sections 4.1 and 4.2. In the last part of Chapter 4 (Section 4.3) East Asia land temperature is also used to constrain model projections of the future low-level circulation.

(Section 4.1) Central Asia orography sets important features of the winter climate over East Asia and the Pacific. By deflecting the mid-latitude jet polewards it contributes to the formation of the Siberian High and, on the lee side, to the advection of dry cold continental air over the East-Asian coast and the Pacific ocean, where atmospheric instability and cyclogenesis thrive. While the mechanical forcing by the orography is assessed in a number of modelling studies, it

is still not clear how near-surface temperature over the two most prominent orographic barriers of the Central Asian continent, namely the Tibetan and Mongolian plateaux, influences the climate downstream. Moreover, a well-known issue of state-of-the art climate models is a cold land temperature bias over the Tibetan Plateau related with the difficulty in modelling land processes and land-atmosphere interaction over complex orography. Here we take advantage of the large spread in representing near surface temperature over the Central Asia plateaux among climate models taking part in the CMIP6 to study how temperatures over these regions impact the atmospheric circulation. Based on a composite of the CMIP6 models' climatologies showing a cold bias over the Tibetan Plateau, we find that negative temperature anomalies over Asian orography intensify the East-Asia winter monsoon and, by enhancing the low-level baroclinicity in the region of the East China Sea, reinforce the southern flank of the Pacific jet. The results of the CMIP6 composite analysis are supported by the response of an intermediate-complexity atmospheric model to a similar pattern of cold surface temperatures over the Central Asia plateaux; we also distinguish the relative influence of the Tibetan and the Mongolian Plateau surface conditions.

(Section 4.2) The interaction between the Siberian near-surface temperature and the atmospheric circulation is investigated by analysing the climatological conditions of 34 simulations from the Coupled Model Intercomparison Project - Phase 6 (CMIP6) historical dataset. We show that the individual models' climatological near-surface temperatures in Siberia interfere with the local atmospheric conditions. The signal is shallow in the subpolar latitudes, while it extends deep in the atmosphere in the mid-latitudes, where the orographic elevation is also high, and over the ocean. The Siberian temperature anomalies do not impact substantially the cold core of the Siberian High, resulting in a weak impact on the downstream tropospheric circulation, and more specifically on the Pacific jet stream. The CMIP6 dataset reveals a possible link between the temperatures over Northern Eurasia and those in the Tropics, which is explained by the anomalous transport of heat and humidity from the low latitudes of the Pacific and Atlantic Oceans to the mid and high latitudes of the Eurasian continent, setting a low-level radiative energy balance over Siberia characterised by warm near-surface conditions and enhanced longwave radiation. The mid-latitude cloud cover is also relevant in the CMIP6 models

displaying colder-than-average Siberian conditions. However, based on the available dataset, it is impossible to understand the reason for the enhanced cloud cover nor the mechanisms by which the high-latitude cooling arises. The comparison of the CMIP6 models' composites with a different composite study based on the interannual variability of Siberian surface temperature in the ERA5 reanalysis supports the hypothesis of a local impact of surface conditions over Northern Eurasia, with insignificant impacts on the atmospheric circulation in the Pacific sector. The differences and analogies between the results of the two approaches are valuable for reviewing the links between Siberian surface temperature and circulation in state-of-the-art climate models.

(Section 4.3) CMIP6 climate projections provide estimates of future changes in the winter low-level circulation, which are however characterised by a high uncertainty due to the large inter-model spread. The identification of plausible drivers of the dynamical changes allows us to constrain the projections conditional to the occurrence of certain climatic conditions. The low-level Arctic and upper-level Tropical temperatures, together with the stratospheric polar vortex, are well-known for their influence on the mid-latitude troposphere; the spread in their future changes affects the dynamical uncertainty in climate projections. Within this framework, we show that also different levels of land warming over East Asia are associated with different future circulation patterns. Consistently with the analyses in Sections 4.1 and 4.2, Tibetan Plateau temperatures are relevant for the North Pacific eddy-driven jet, Siberian temperatures for the intensity of the low-level zonal winds over the continent.

Introduction

In continuity with Chapter 3, where it is shown that the mid-latitude climate is strongly sensitive to a reduced Pacific land-sea thermal contrast produced by the warming of East Asia, we focus our attention on the dynamical influence of the Asian land temperature in state-of-the-art climate models characterised by higher complexity with respect to SPEEDY. The historical simulations from the CMIP6 data collection are chosen for this purpose. The focus here is on the impact of land temperature rather than on LSC because, among the CMIP6 model runs, the differences in LSC are set mainly by the large temperature differences over land. Figures 4.1(a) and 4.2(a) show in fact a large inter-model temperature spread over mid-latitude continents, and a relatively low SST spread. The latter attains its largest values at higher latitudes, probably because of the inter-model variability in the position of the southern boundary of winter sea ice.

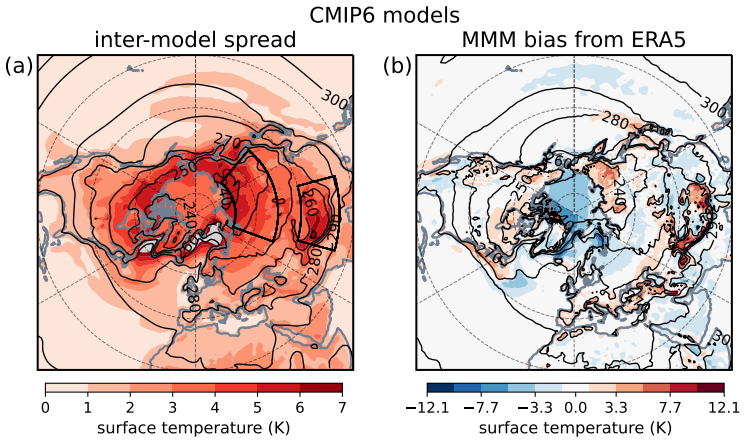

Figure 4.1: (a) The surface temperature spread in CMIP6 historical simulations 1979–2008 for Jan-Feb, with the MMM field in contours, and (b) the bias with respect to ERA5 skin temperature selected over the same period. The black boxes in panel (a) are used to compute the Tibetan-Plateau and Siberia surface temperature indices

The multi-model mean (MMM) surface and near-surface temperature (here corresponding to skin and 2-meter temperature) are in general relatively close to the ERA5 climatology (MMM bias in panels (b) of Figures 4.1 and 4.2), but hide - through MMM flattening - the strong variations among the individual modelling systems (near-surface temperature anomalies with respect to the MMM for each model in Figure 4.5). The individual model surface temperatures, affecting (or affected by) sensible and latent heat flux, radiation and moisture, interact

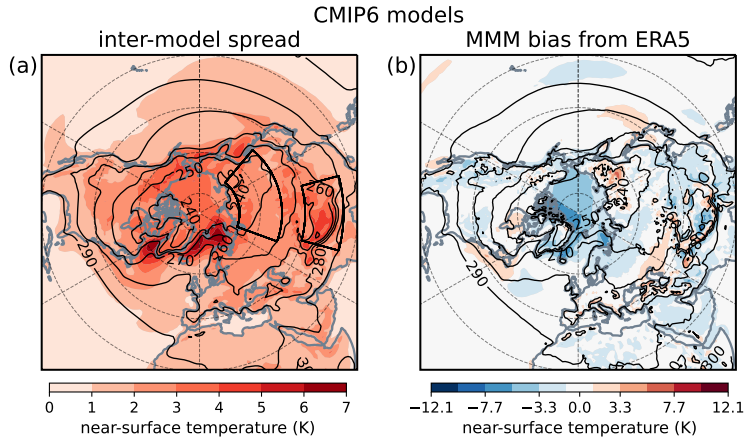

Figure 4.2: (a) The near-surface temperature spread in CMIP6 historical simulations 1979–2008 for Jan-Feb and (b) the bias with respect to ERA5 2m-temperature climatology selected over the same period. The contours represent the MMM and the ERA5 climatology. The black boxes in panel (a) are used to compute the Tibetan-Plateau and Siberia near-surface temperature indices

locally with the low-level troposphere, and, in some cases, are able to influence the large-scale atmospheric circulation. In other cases, it is the anomalous atmospheric circulation which induces biases in the surface temperature field and in the interlinked physical processes. The two possibilities are not mutually exclusive and not easily discernible (see e.g. the dispute about Eurasian snow-cover presented in Henderson et al., 2018).

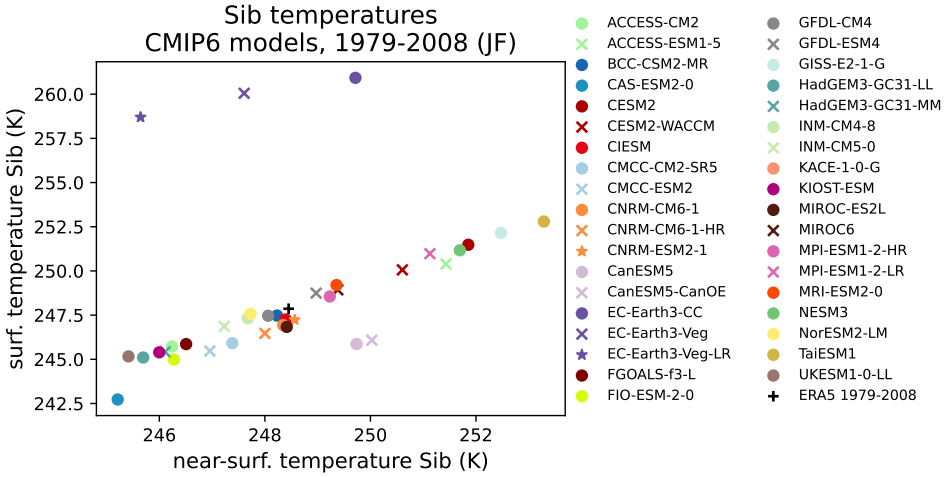

Figure 4.3: Scatter plot representing the Siberian surface temperature and near-surface temperature - area-weighted averages over the Siberian box of Figure 4.1 - for each of the 37 CMIP6 models and for ERA5 (skin temperature and 2-meter temperature are the corresponding reanalysis variable names). The values are computed for January-February over the period 1979–2008

In the CMIP6 historical dataset, considering the months of January and February over the

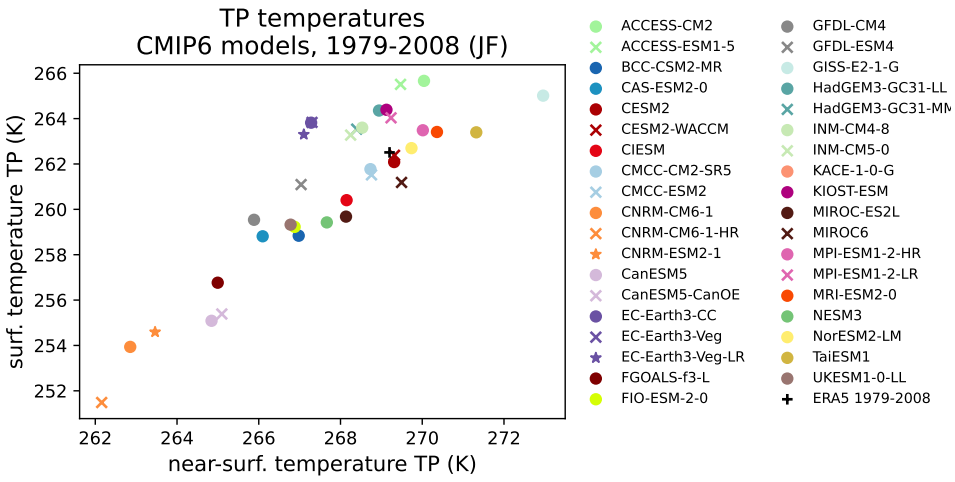

Figure 4.4: Scatter plot representing the Tibetan Plateau surface temperature and near-surface temperature - area-weighed averages over the Tibetan Plateau box of Figure 4.1 - for each of the 37 CMIP6 models and for ERA5 (skin temperature and 2-meter temperature are the corresponding reanalysis variable names). The values are computed for January-February over the period 1979–2008

period 1979–2008 (as in Chapter 3), the highest inter-model spread in climatological surface temperature is found over the Asian regions corresponding to the Tibetan Plateau (TP) and Siberia (Sib) (Figure 4.1(a)). The near-surface temperature variable shows similar patterns, but with a reduced spread over the continental regions, especially at high latitudes (Figure 4.2(a)). Over Siberia, where the land surface temperature varies decidedly more than the near-surface temperature, the scatter plot of the two area-averaged variables for the 37 CMIP6 models (Figure 4.3) denotes that the relation is ostensibly linear. The scatter plot also clarifies that the surface temperature bias is correlated with the near-surface temperature bias, but for the presence of three outliers: the historical simulations of the EC-Earth model (dark purple markers in Figure 4.3). In the region corresponding to the Tibetan Plateau the spread in the two area-averaged variables is similar (Figure 4.4). However, the fact that the relation between surface and near-surface temperature is not as linear as for Siberia (Figure 4.3) is likely associated with issues in the representation of land and near-surface processes in a region characterised by complex orographic features (details in Section 4.1).

In the following sections we develop the topic of the interaction of East Asia winter temperatures with the atmospheric circulation, within the context of CMIP6 historical simulations and future projections. We differentiate between the regions of the Tibetan Plateau (Section 4.1)

and of Siberia (Section 4.2) because the individual climatological anomalies from the MMM (Figure 4.5) or, equivalently, the individual model biases are independent over the two regions - for some models they even attain opposite signs. Similarly, the future warming of the two regions is weakly correlated when the values are scaled by the individual models' global warming (r=0.24, see Table 4.2).

Section 4.1, focusing on the Tibetan Plateau, mainly discusses the dynamical implications of cold low-level winter conditions from the point of view of the atmospheric circulation. Starting from a selection of models charcaterised by anomalously cold Tibetan Plateau, a common pattern in the downstream winds and temperatures is identified; their connection is tested by running an idealised experiment with the atmospheric model SPEEDY.

Section 4.2 addresses the problem of the origin and consequences of Siberian temperature anomalies. The causes of anomalous Siberian warming and cooling are investigated among the CMIP6 climatologies, and are compared with the atmospheric conditions associated with the observed interannual variability of Siberian temperatures.

In Section 4.3 we make use of Zappa and Shepherd's "storyline approach" to constrain the projections of the future low-level circulation on a set of three widely used drivers, to which we add two drivers based on East Asia land temperatures.

List of CMIP6 climate models

Table 4.1: List of CMIP6 climate models by name, member number and institution

Model Name	Member	Institution
ACCESS-CM2 $_{\text{Sib-}}$	1	Australian Research Council Centre of Excellence for Climate System Science & Commonwealth Scientific and Industrial Research Organisation (AUS)
ACCESS-ESM1-5 $_{\text{Sib+}}$	1	Commonwealth Scientific and Industrial Research Organisation (AUS)
BCC-CSM2-MR	1	Beijing Climate Center (CHN)
CAS-ESM2-0 $_{\text{Sib-}}$	2	Chinese Academy of Sciences (CHN)
CESM2 $_{\text{Sib+}}$	2	National Center for Atmospheric Research, Climate and Global Dynamics Laboratory (USA)
CESM2-WACCM $_{\text{Sib+}}$	1	as above
CIESM	1	Department of Earth System Science, Tsinghua University (CHN)
CMCC-CM2-SR5	1	Fondazione Centro Euro-Mediterraneo sui Cambiamenti Climatici (ITA)
CMCC-ESM2	1	as above
CNRM-CM6-1 $_{\text{TP-}}$	1	Centre National de Recherches Meteorologiques & Centre Européen de Récherche et de Formation Avancée en Calcul Scientifique (FRA)
CNRM-CM6-1-HR $_{\text{TP-}}$	1	as above
CNRM-ESM2-1 $_{\text{TP-}}$	1	as above
CanESM5 $_{\text{TP-}}$	1	Canadian Centre for Climate Modelling and Analysis (CAN)
CanESM5-CanOE $_{\text{TP-}}$	1	as above
EC-Earth3-CC	1	EC-Earth consortium (visit `https://ec-earth.org/consortium/`)
EC-Earth3-Veg	1	as above
EC-Earth3-Veg-LR	1	as above
FGOALS-f3-L $_{\text{TP-}}$	1	Chinese Academy of Sciences (CHN)
FIO-ESM-2-0	1	Qingdao National Laboratory for Marine Science and Technology & First Institute of Oceanography (CHN)
GFDL-CM4	1	National Oceanic and Atmospheric Administration, Geophysical Fluid Dynamics Laboratory (USA)
GFDL-ESM4	1	as above
GISS-E2-1-G $_{\text{Sib+}}$	1	Goddard Institute for Space Studies (USA)
HadGEM3-GC31-LL $_{\text{Sib-}}$	1	Met Office Hadley Centre (GBR)
HadGEM3-GC31-MM $_{\text{Sib-}}$	1	as above
INM-CM4-8	1	Institute for Numerical Mathematics (RUS)
INM-CM5-0	1	as above
KACE-1-0-G $_{\text{Sib-}}$	1	National Institute of Meteorological Sciences/ Korea Meteorological Administration (KOR)
KIOST-ESM	1	Korea Institute of Ocean Science & Technology (KOR)
MIROC-ES2L	1	Japan Agency for Marine-Earth Science and Technology & Atmosphere and Ocean Research Institute & National Institute for Environmental Studies & RIKEN Center for Computational Science (JPN)
MIROC6	1	as above
MPI-ESM1-2-HR $_{\text{Sib+}}$	1	Max Planck Institute for Meteorology (DEU)
MPI-ESM1-2-LR	1	as above
MRI-ESM2-0 $_{\text{Sib+}}$	1	Meteorological Research Institute (JPN)
NESM3	1	Nanjing University of Information Science and Technology (CHN)
NorESM2-LM $_{\text{Sib+}}$	1	NorESM Climate modeling Consortium (visit `https://www.noresm.org/consortium/`)
TaiESM1 $_{\text{Sib-}}$	1	Research Center for Environmental Changes (TWN)
UKESM2-0-LL $_{\text{Sib-}}$	1	National Institute of Meteorological Sciences/ Korea Meteorological Administration (KOR)

Models identified as TP- were selected for the "cold Tibetan-Plateau" composite
Models identified as Sib+ / Sib- were selected for the "warm Sib" / "cold Sib" composites

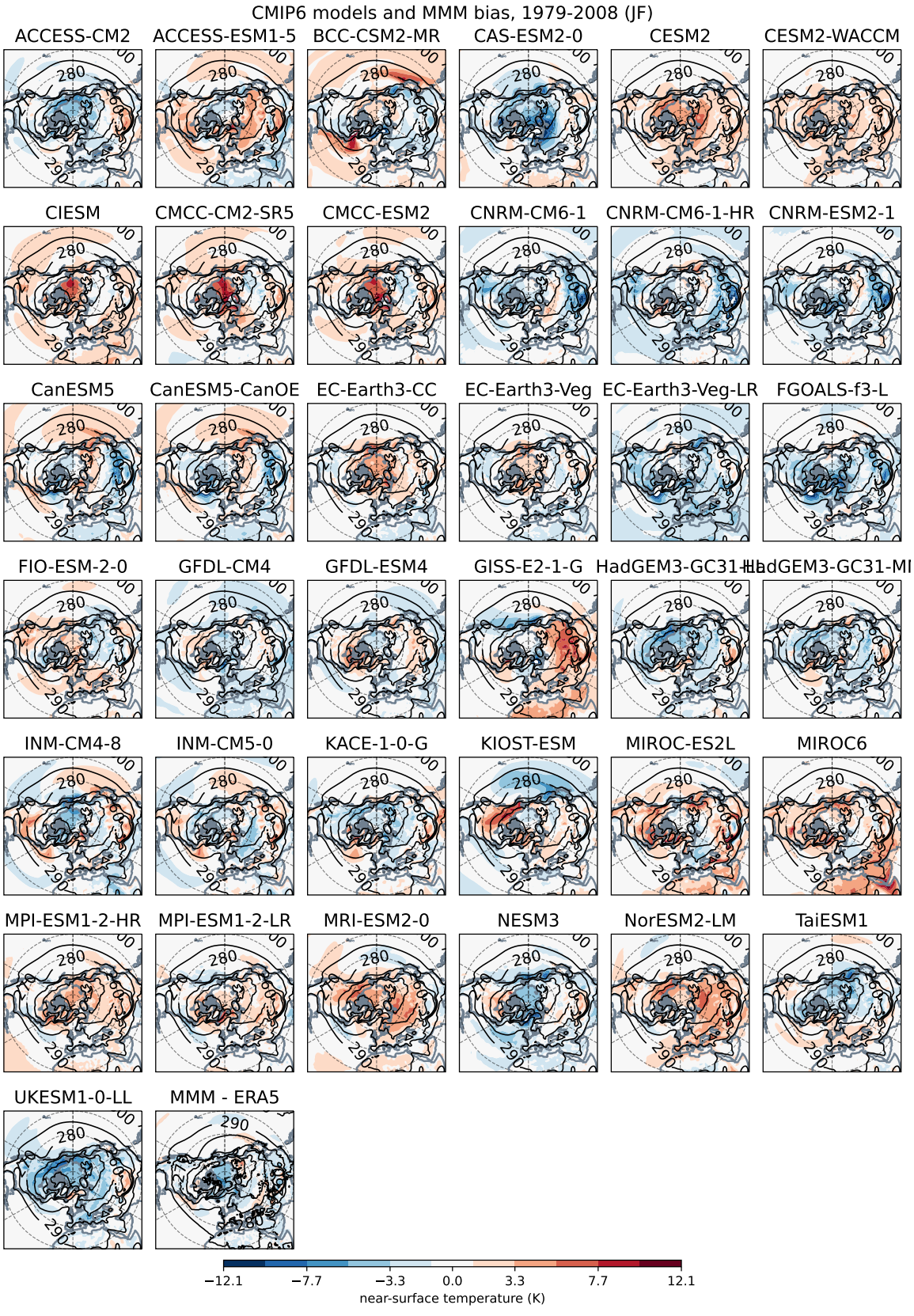

Figure 4.5: The near-surface temperature anomalies in CMIP6 historical runs 1979–2008 for Jan-Feb with respect to the MMM (anomaly in shading and MMM in contours). In the last panel the bias of the MMM with respect to ERA5 skin temperature selected over the same period (MMM bias in shading and ERA5 climatology in contours)

Section 4.1 is adapted from the following manuscript.

Title: Atmospheric response to wintertime Tibetan Plateau cold bias in climate models.

Status: Research article under revision in *Weather and Climate Dynamics* from the 20th of January 2023. DOI: 10.5194/egusphere-2022-1499

Authors: Alice Portal[1,2], Claudia Pasquero[1,3], Fabio D'Andrea[2], Paolo Davini[3], Mostafa Hamouda[4,5].

4.1 Tibetan Plateau land temperature

The impact of orography on the extra-tropical circulation was first proposed by the analytical studies of Bolin (1950) and Smagorinsky (1953), who matched orographic forcing to thermal forcing by land-sea contrast in order to explain the longitudinal variations of the mid-latitude westerlies. Manabe and Terpstra (1974) and Hahn and Manabe (1975) analysed the impact of the Tibetan Plateau on the Asian climate by running an atmospheric general circulation model (AGCM) with and without mountains. They proved that the elevation of central Asia is essential to reproduce the position and strength of the low-level winter anticyclone known as the Siberian High and for the maintenance of the South-East Asia summer monsoon, which, due to the intense uplift from orography, extends from the Indian sector as far as East Asia. The regional dryness and humidity of the aforementioned winter and summer circulation patterns and their association with orography were examined by Broccoli and Manabe (1992).

More recently, starting with Sato (2009), the influence of lower elevation mountain chains on the Asia and Pacific climate was investigated, and their role was considered separately from that of the Tibetan Plateau. This applies in particular to the mountain chains in East Asia, extending north east of Tibet. Similarly to White et al. (2017), we denote the orography between approximately 20 to 40 N and 62 to 120 E as the Tibetan Plateau or TP, and that

[1]Department of Earth and Environmental Sciences, Università di Milano - Bicocca, Milan, Italy
[2]Laboratoire de Météorologie Dynamique/IPSL, École Normale Supérieure, PSL Research University, Sorbonne Université, École Polytechnique, IP Paris, CNRS, Paris, France
[3]Consiglio Nazionale delle Ricerche, Istituto di Scienze dell'Atmosfera e del Clima (CNR-ISAC), Torino, Italy
[4]Astronomy and Meteorology Department, Faculty of Science, Cairo University, Cairo, Egypt
[5]Institute for Atmospheric and Environmental Sciences, Goethe University Frankfurt, Frankfurt am Main, Germany

between approximately 38 to 60 N and 65 to 140 E as the Mongolian Plateau or MP.

In the cold season the Asia-Pacific circulation is dominated by the East-Asia winter monsoon, which consists in north-westerly advection of cold dry continental air from Siberia over the Asian coast and the Pacific ocean (Chan and Li, 2004). The strong winter thermal emission of the TP land and of the air column above generate a tropospheric heat sink over the Plateau (Yanai et al., 1992; Yanai and Wu, 2006; Duan and Wu, 2008) that reinforces the Eurasian mid-tropospheric thermal high (Shi et al., 2015). Moreover, the presence of TP and MP orography reduces the westerlies upstream and enhances the north-westerly winds over East Asia and the Pacific (Shi et al., 2015; Sha et al., 2015). On the lee side of the plateaux, the cold advection strengthens the thermal contrast with the Pacific Ocean and increases the baroclinicity, which in turn fuels the Pacific jet stream downstream, over and east of the East-China Sea (Shi et al., 2015; White et al., 2017). Notwithstanding the lower elevation and extension of the MP compared to the TP, the MP is more relevant for the winter circulation because of its ideal position in terms of impinging low-level winds and meridional potential vorticity gradients for acting as a source of Rossby waves (Held and Ting, 1990; White et al., 2017).

Conversely, the warm season circulation is driven by the East-Asia summer monsoon, modulating rainfall over land and ocean (Yihui and Chan, 2005). This is sustained in strength and extension by the atmospheric uplift produced by Asian orography, which constitutes a tropospheric heat source in summer (Yanai et al., 1992; Hahn and Manabe, 1975; Ye and Wu, 1998). The summer monsoon is mostly controlled by the presence of the TP which, among other things, reinforces the monsoonal circulation and the associated precipitation along the east coast of Asia, with the MP playing only a marginal role (see Figures 6, 9, 10 in Sha et al., 2015).

Considering the importance of the Central Asia orography for the climate of the Asia-Pacific sector, it is not surprising to find examples in literature where orographic surface and near-surface conditions (acting as tropospheric heat sources or sinks, Yanai et al., 1992) have an impact on the atmospheric conditions downstream. Indeed, evidence is found on the relevance of spring and summer temperatures over Asian orography for the successive atmospheric con-

ditions far downstream (see Wu et al. (2015) for a review and Xue et al. (2021, 2022) for recent work on the impact of spring TP land initialisation in subseasonal-to-seasonal predictions). In the extended winter season (October–March) the presence of anomalous snow cover changes the tropospheric energy budget through an increase of the surface albedo, enhancing the reflection of shortwave radiation and the cooling of the land surface and the atmosphere (Yeh et al., 1983). Analyses on the dynamical influence of Tibetan Plateau snow cover indicate that it is relevant for the atmospheric circulation at intraseasonal time scales (Li et al., 2018) and, when anomalies are persistent, it can modulate interannual variability (Chen et al., 2021; Clark and Serreze, 2000) and long-term projections (Liu et al., 2021). Contrary to the impact of autumn Siberian snow cover on the winter circulation, which is widely discussed in literature (e.g. Cohen et al., 2014; Garfinkel et al., 2010), the dynamical role of anomalous surface conditions over the Tibetan and Mongolian plateaux has been poorly investigated. In a more idealised context, winter positive thermal forcing over mid-latitude land - as in a climate with a reduced winter land-sea thermal contrast caused by the faster warming of continents with respect to oceans - was analysed by Portal et al. (2022). It was shown there that the atmospheric response to idealised land warming in East-Asia (including the orography) dominated over a pattern of similar intensity imposed in North America. One possible explanation of the larger impact of Asia surface warming is that the higher average elevation of Asian orography was conductive to the strong hemispheric response to the East-Asian land-forcing, as it acted as a heat source directly in the mid troposphere (Hoskins and Karoly, 1981; Trenberth, 1983; Ting, 1991).

An additional motivation to approach the topic of thermal forcing over the Asian plateaux is the presence of a significant MMM temperature bias in the region of East Asia, which is evident over successive phases of the CMIP and over multiple seasons. Priestley et al. (2022) detect a strong deviation from the reanalysis temperature in the summer season and, based on the modified thermal gradients in the lower troposphere, hypothesise a role of the TP land temperature on the baroclinicity and cyclogenesis downstream. Along the same lines, East-Asia winter conditions are anomalously cold among several climate models (Wei et al., 2014; Gong et al., 2014), although improvements, associated with a closer representation of the winter monsoon, have been detected in the transition from CMIP Phase 3 to Phase 5 (Wei et al.,

2014). The winter bias is specially strong over the TP (Figure 4.2 and Peng et al., 2022; Fan et al., 2020), and limited progress is obtained in the transition from CMIP5 to CMIP6 (Lun et al., 2021; Hu et al., 2022). These studies also highlight the presence of a wide inter-model spread in year-round East-Asia and TP temperatures among the CMIP climate models, which appears to be related with the difficulties in representing surface energy fluxes (Wei et al., 2014), in particular over regions characterised by complex orography and seasonal variations in snow cover (e.g. Su et al., 2013; Chen et al., 2017; Li et al., 2021).

Although the reason for the emergence of the cold Tibetan Plateau temperature bias in many state-of-the-art climate models is examined in some detail by Chen et al. (2017), the dynamical consequences of the cold bias are yet to be explored. The aim of this chapter is to fill this gap by analysing the implications of cold Central Asia orography winter conditions on the large-scale circulation on the lee side of the mountains. Thus, we take advantage of the large temperature spread detected over TP and MP among CMIP6 models to construct a multi-model realisation of the cold bias (the "cold TP composite"), over which we conduct an analysis of the Pacific-sector atmospheric circulation, i.e. the East-Asia winter monsoonal circulation. The results thus obtained are further tested with an intermediate-complexity Atmospheric General Circulation Model (AGCM) forced by land-surface temperature patterns similar to CMIP6 model biases. Finally, to isolate the role of the Mongolian Plateau in the atmospheric response to cold land over Central Asia orography, we consider a separate AGCM experiment where MP forcing is opposed to a widespread TP and MP forcing.

The two approaches (CMIP6 compositing and AGCM idealised simulations) are described in Section 4.1.1, the outcomes and their mutual consistency are examined in the Section 4.1.2 and a final summary and discussion considering previous literature is provided in Section 4.1.3.

4.1.1 Methods

CMIP6 simulations

We use CMIP6 historical runs for years 1979-to-2008 and we compute the January-February climatology over the whole period; the January and February months are referred to as *winter* throughout the chapter. As in Clark and Serreze (2000) the results for an extended winter taking into account the transition months (e.g. October–March) are weaker in intensity, hence are not reported. We select one member per climate model from the CMIP6 dataset, as specified in Table 4.1, giving a sample of 37 historical simulations. Based on an index of Tibetan Plateau temperature (i.e. the climatological weighted-area average of near-surface temperature in the black box of Figure 4.6(b) over the period 1979–2008), the six simulations with temperature below one standard deviation from the CMIP6 multi-model mean form the "cold TP composite" (see models in bold in Table 4.1). The composite fields are shown in terms of the significant anomalies from the climatology of the CMIP6 multi-model mean (MMM), with significance computed according to a permutation test repeated 1000 times over the 37 model realisations, considering the 95% confidence level (Wilks, 2011). Note from Table 4.1 that in the "cold TP composite" multiple models from the same institutions are chosen; the same selection, but based on a single model per institution, produces similar results (not reported).

Wind components and air temperature at levels between 1000 and 700 hPa are extracted from the CMIP6 archive and used in the analysis. Turbulent surface heat fluxes, surface temperature (skin temperature or SST for open ocean) and near-surface temperature (usually 2-meter air temperature) are also used. Due to the lack of availability of daily fields for a large subset of the CMIP6 models, the analyses on the "cold TP composite" are based on monthly-mean variables. Moreover, we report that surface latent heat flux in KIOST-ESM, meridional wind and temperature advection in CAS-ESM2-0, zonal wind, temperature advection and Eady growth rate in FGOALS-f3-L are excluded from the analysis because of the inaccessibility of some datasets from the servers providing the CMIP6 archive.

Idealised experiments

To confirm the causal link between the results obtained from compositing on CMIP6 models we run idealised experiments using an 8-level AGCM developed at the International Centre for Theoretical Physics (ICTP), and known as SPEEDY for Simplified Parametrization, primitivE-Equation DYnamics. The model is spectral on the sphere, with triangular truncation at total wavenumber 30 (T30) and a Gaussian grid of 96 by 48 points, and includes simple parametrisation of moist processes (Molteni, 2003). Despite the low horizontal and vertical resolution, SPEEDY displays an adequate performance for the analysis of large-scale features of the climate system (Kucharski et al., 2006, 2013). SPEEDY is run in perpetual-winter mode (200 January months and 200 February months) with prescribed sea surface temperature (SST), sea-ice cover (SIC) and land surface temperature (LST). Two types of simulations are considered:

- a *control integration* where SST and SIC are equal to the 1979–2008 HadISST climatologies (Rayner et al., 2003). The land surface temperature (LST) corresponds to the climatology obtained from a SPEEDY ensemble-run with a freely evolving LST scheme and with prescribed climatological SIC and evolving SSTs 1979–2008 from HadISST. Details on SPEEDY's LST scheme are available in the Appendix B of Portal et al. (2022);

- two *cold integrations* with SST and SIC as in the *control*, and with LST forcing corresponding to the significant anomalies of surface temperature from the "cold TP composite" within 60–140 E and 20–60 N ("TP+MP experiment") or within 60–140 E and 38–60 N ("MP experiment"), interpolated onto SPEEDY's grid (Figure 4.8(a,e,i)).

The responses of "TP+MP" and "MP" forcing visualised in Section 4.1.2 correspond to the climatological difference "*cold integration* - *control integration*".

Diagnostics

We introduce some diagnostics used in the analysis of the results.

- Temperature advection is

$$-\mathbf{u}\cdot\nabla T = -\left(u\frac{\partial T}{\partial x} + v\frac{\partial T}{\partial y}\right),$$

  where $\mathbf{u} = u\hat{\mathbf{i}} + v\hat{\mathbf{j}}$ is the horizontal wind composed of the zonal u and meridional v components and T is the temperature.

- The Eady growth rate corresponds to

$$\sigma = 0.31\, f\, \frac{du}{dz}\, \mathcal{N}^{-1},$$

  where f is the Coriolis parameter, z is the geopotential height and $\mathcal{N} \equiv \sqrt{(g/\theta)\, d\theta/dz}$ is the Brunt–Väisälä frequency with θ potential temperature and g Earth's gravitational acceleration. Note that the definition is different from that of Section 3.2, where the horizontal velocity vector is considered instead of its zonal component.

- The meridional eddy momentum flux (MEMF), computed for the SPPEDY integrations only, is the product of the 2–6-day Fourier filtered wind components $u^{\mathrm{HF}}v^{\mathrm{HF}}$.

Among these, the temperature advection and the Eady growth rate are computed using mean climatological variables, giving the *temperature advection by the mean flow* and the *Eady growth rate of the mean state*. The climatological MEMF is computed on high-pass filtered daily fields averaged over the total time-span of the model simulations.

4.1.2 Results

The representation of winter (January-February) near-surface temperatures by CMIP6 models in the historical period 1979–2008 shows a strong inter-model spread (Figure 4.6(a)). The spread is generally larger over land than over the ocean, and grows with latitude. The largest amplitude is attained around and poleward of the 60° N latitude circle, with a maximum over the Atlantic and Pacific oceans likely due to the inter-model variability in winter sea-ice cover. An additional hot-spot can be easily identified in the mid-latitude continents over the Tibetan

Plateau (cf. temperature spread and green/yellow boxes over orography in Figure 4.6(b)). Since the atmospheric response to deep mid-latitude heat sources or sinks is specially strong (Trenberth, 1983), and, on top of this, the winter mid-latitude circulation is known to be highly sensitive to East-Asia surface conditions (e.g. Portal et al., 2022; Cohen et al., 2001), in the following we study the dynamical features of a "cold TP composite" obtained by averaging over a model selection based on a TP-temperature index (see Section 4.1.1). The index (one value per CMIP6 model) is the area-weighted spatial and temporal average of near-surface temperature over a region characterised by large temperature spread and high elevation within the Tibetan-Plateau domain (black box in Figure 4.6(b)).

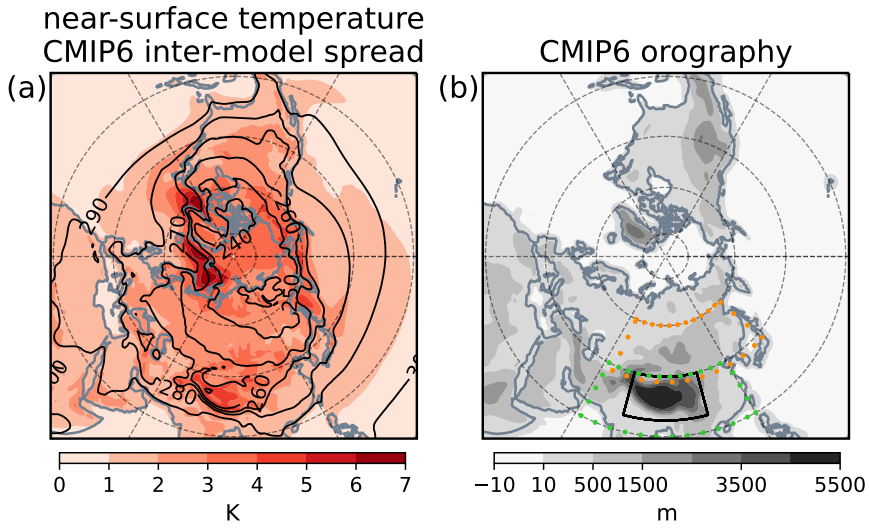

Figure 4.6: (a) The near-surface temperature spread in CMIP6 historical 1979-2008 for Jan-Feb, with the MMM field in contours, and (b) the MMM orographic elevation. The black box in panel (b) is used to compute the Tibetan-Plateau index for near-surface temperature; the "cold TP composite" presented in Figures 4.7–4.9 is based on such index. The dotted boxes in panel (b) indicate the mountainous regions here named Tibetan Plateau or TP (green) and Mongolian Plateau or MP (yellow)

Some relevant surface variables from the "cold TP composite" are presented in Figure 4.7. The near-surface temperature map features an intense cold anomaly over the orography of Central Asia, peaking over the TP and extending north-eastwards to the MP. Significant surface anomalies are also found elsewhere in the North-America / Atlantic sector and are discussed in more detail in the Section *Discussion of the global "cold TP composite"*. By comparing the surface and near-surface temperature patterns over the TP (cf. Figure 4.8(a) and Figure 4.7(a)) we notice that the land-surface temperature anomaly is stronger in intensity than the near-

surface anomaly, and conclude that in the "cold TP composite", as described by Chen et al. (2017), land has a cooling effect on the atmosphere above. This feature is corroborated by negative anomalies of surface sensible and latent heat flux in a region where the MMM fluxes are - on average - weakly positive (Figure 4.7(b,c)), representing a reduced latent and sensible warming of the atmosphere by the land surface in the cold composite models. The signal in sensible heat flux is strong over the center of the TP, the latent heat flux term is significant elsewhere over TP and MP.

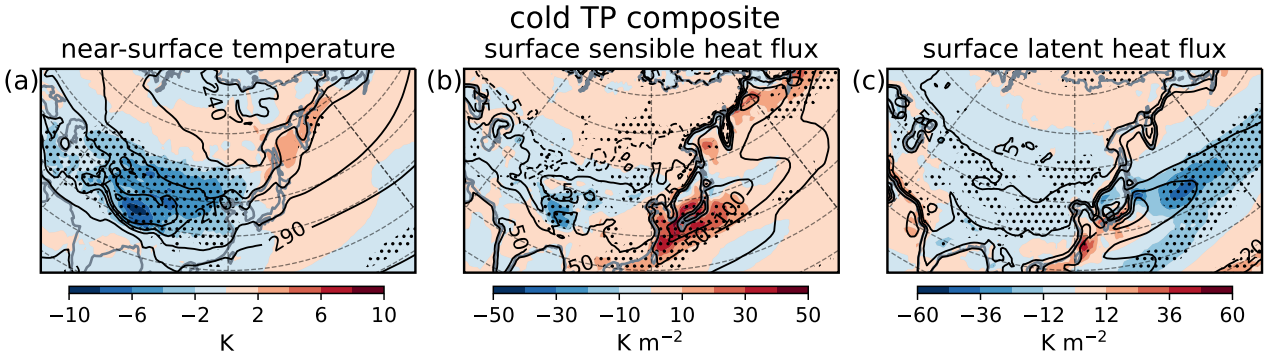

Figure 4.7: From the "cold TP composite" the significant anomalies of (a) near-surface temperature, (b) sensible and (c) latent surface heat flux. The respective MMM climatologies are displayed in contours (cl=[±5,+25,+50,+100,+200,+300] K m^{-2} for the heat fluxes)

In the "cold TP composite" anomalous snow amount is detected in correspondence with the strongest sensible heat flux anomalies (not shown), but, since the anomalies are not significant, this is unlikely to explain on its own the surface-temperature pattern. Chen et al. (2017) decompose the surface energy budget over the TP and show that the processes causing cold biases are physically interlinked, involving anomalous snow cover enhancing the surface albedo with negative effects on the low-level water vapor content and the downward long-wave radiation, which ultimately result in a cooling of the surface. The existence in CMIP6 models of a variety of schemes for land, snow and atmospheric boundary layer and of the mutual interaction between these over complex orography, is at the origin of the wide inter-model spread. Furthermore, based on the results of Figure 4.8 and of Liu et al. (2022), the anomalies do not appear to be driven by the circulation upstream of the TP.

The temperature and wind conditions of the CMIP6 "cold TP composite" at 850 hPa are shown in Figure 4.8(a-d). We note that the negative thermal anomaly expands northeastward of the

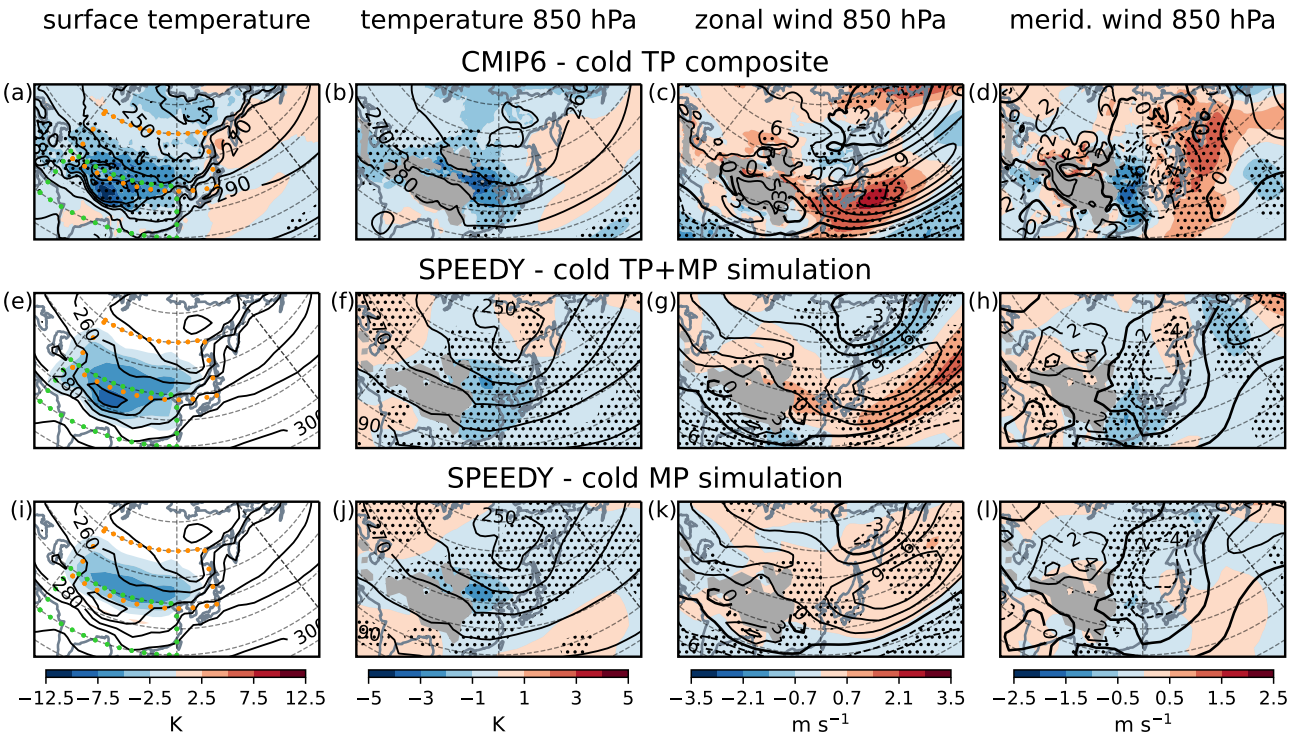

Figure 4.8: The "cold TP composite" significant anomalies of (a) surface temperature and 850-hPa (b) air temperature, (c) zonal wind, (d) meridional wind. The respective MMM climatologies are displayed in contours. The response of the model SPEEDY to "TP+MP" and "MP" surface-temperature forcing (panels (e,i)) in terms of 850-hPa (f,j) temperature, (g,k) zonal wind, (h,l) meridional wind; the control run is shown in contours. Green and yellow dotted boxes in panels (a,e,i) indicate the mountainous regions named TP and MP, respectively. Grey shading masks orography exceeding 1400 m

most elevated area of the Tibetan Plateau - represented by grey patching - and reinforces the thermal cooling induced by the uplift over MP orography, shown in Figure 11 of Sha et al. (2015). East of this region the westerly zonal winds (i.e. Pacific jet) are reinforced. At the same time, southward wind over East China and northward wind over the ocean give rise to a cyclonic anomaly over the Asian coast and reinforce the East-Asia winter monsoon. The advection of cold air downstream of the TP (Figure 4.9(a), see Section 4.1.1 for details on the computation) is supported both by the negative temperature anomaly on the orography and, to the east, by the reinforcement of the north-westerly wind (Figure 4.7(b,d)). These conditions are responsible for intensified meridional temperature gradients east of the TP and along the Pacific coast which enhance the baroclinicity (see positive anomalies in the Eady growth rate west and east of the Chinese coastline, Figure 4.9(b)). Since the Eady growth rate (definition in Section 4.1.1) measures the environmental conditions favourable to instability, we expect

the strengthening of the jet at the entrance of the Pacific basin (Figure 4.8(c)) to be induced by more synoptic disturbances breaking and depositing zonal momentum in the mean westerly flow. Moreover, cyclogenesis is high to the east of the TP and over the East China Sea from mid winter (Priestley et al., 2020; Schemm et al., 2021). In the CMIP6 composite we cannot verify the relation between the transient eddies and the mean flow due to the unavailability of daily frequency data. Nonetheless, the analysis of the eddy feedback on the zonal flow is presented in the discussion of the idealised "TP+MP experiment", which generally confirms the results of the CMIP6 composite analysis and supports the hypothesis that the jet is strengthened by enhanced eddy momentum deposition.

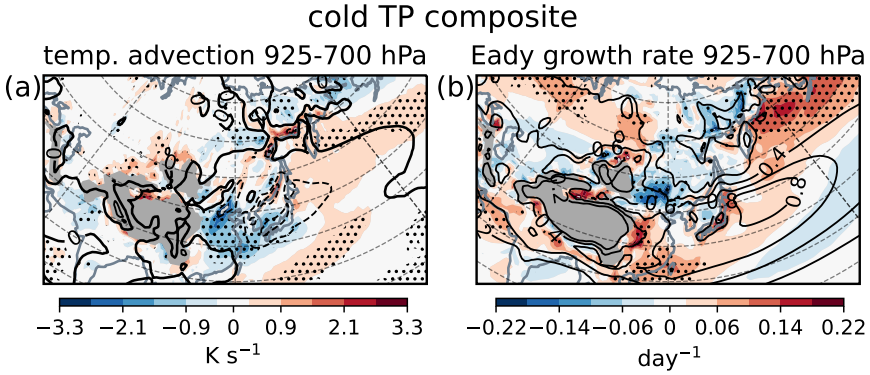

Figure 4.9: The "cold TP composite" significant anomalies of (a) temperature advection by the mean flow ($\mathbf{u} \cdot \nabla T$) averaged over the pressure-levels 925 to 700 hPa, (b) Eady growth rate between 925 and 700 hPa, and the respective MMM climatologies in contours (ci=4e-5 $\mathrm{K\,s^{-1}}$ for temperature advection). Grey shading masks orography exceeding 1400 m

In the "cold TP composite" the strengthening of the Pacific jet over and downstream of the East China Sea (Figure 4.8(c)) extends down to the near-surface level (not shown) and intensifies the advection of cold air masses over the ocean (Figure 4.9(a)), reinforcing the surface sensible heat flux (Figure 4.7(b)). The release of heat into the lower layers of the atmosphere restores the low-level baroclinicity (Hotta and Nakamura, 2011; Papritz and Spengler, 2015), with a positive feedback on the local generation of synoptic eddies, hence on the strength of the Pacific jet. Papritz and Spengler (2015) propose a dominant role of the surface latent heat flux for maintaining the tilt of the isentropic surfaces (i.e. baroclinicity) to the east of the mid-latitude continents. In this case we observe no significant latent heat flux anomaly over the East China Sea, whereas towards the center of the Pacific there is a decrease in the latent heat flux which would be expected to decrease eddy fluxes that maintain the jet east of 150 E (cf. Figure 4.7(c)

and Figure 4.8(c)). The origin of the negative latent heat flux anomaly is unknown, but may be related to a subtropical or tropical Pacific signal emerging from the selection of CMIP6 models (Figures 4.7(a-c), 4.8(b-d)).

To support the existence of a causal relation linking the cold Asian orography and the enhancement of the East-Asia winter monsoon we run an idealised experiment using the model SPEEDY (a perpetual winter simulation with prescribed surface temperatures, for details see Section 4.1.1). The response of SPEEDY to "TP+MP" forcing - a surface cooling over Central Asia orography (Figure 4.8(e)) resembling the pattern of the "cold TP composite" (Figure 4.8(a)) - in terms of air temperature, zonal wind and meridional wind at 850 hPa is shown in panels (f-h) of Figure 4.8. As in the CMIP6 composite, we find a cold anomaly to the north-east of the TP, with enhanced north-westerly winds downstream of the topography advecting excess cold air onto East Asia and over the Pacific (Figure 4.10(a)). The striking similarity between the composite and the "TP+MP experiment" (cf. panels (b-d) and (f-h) in Figure 4.8) supports the idea that also in the "cold TP composite" the circulation anomalies in the Asia / Pacific sector are generated by the cold surface temperatures over Asian orography. Differences in low-level wind are detected over the Pacific: in the composite the significant strengthening of the jet terminates at about 160 E, while it extends zonally to the whole Pacific basin in the "TP+MP experiment" (not shown); the positive meridional wind signal over the North Pacific is also different, with a strong positive signal extending from 20 to 70° N in the CMIP6 composite (Figure 4.8(d)), and a weak positive signal limited to the high latitudes in the SPEEDY experiment (Figure 4.8(h)). Nonetheless, these discrepancies do not undermine the analogy between the two cases, in that they are located relatively far from the TP region and might be related to the presence of additional signals emerging from the selection of CMIP6 models, such as Pacific tropical and subtropical forcing and cold North America land temperatures (see Section *Discussion of the global "cold TP composite"*).

In the "TP+MP experiment" the increase of eddy momentum deposition in the Pacific jet is evident from the map showing the divergence of the meridional eddy momentum flux (MEMF, Figure 4.10(c), see Methods). The increase in low-level baroclinicity to the east of the Chinese coast (Figure 4.10(b)) favours the development of transient eddies which shift the MEMF

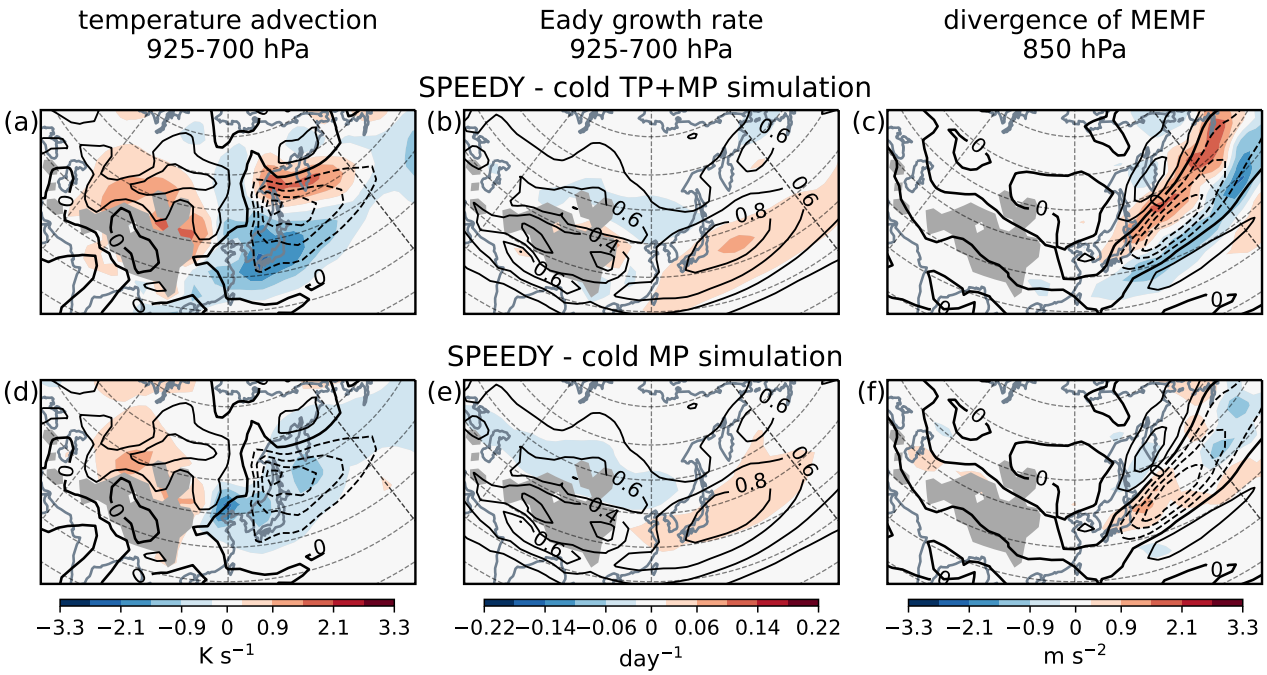

Figure 4.10: The response of the model SPEEDY to "TP+MP" and "MP" surface-temperature forcing in terms of (a,d) temperature advection by the mean flow ($\mathbf{u} \cdot \nabla T$) averaged over the pressure-levels 925 to 700 hPa, (b,e) Eady growth rate between 925 and 700 hPa, (c,f) divergence of the meridional eddy momentum flux (MEMF) at 850 hPa; the control run is shown in contours (ci=4e-5 $\mathrm{K\,s^{-1}}$ for temperature advection, ci=3e-6 $\mathrm{m\,s^{-2}}$ for MEMF divergence). Grey shading masks orography exceeding 1400 m

convergence equatorwards. Such environmental conditions are supported by the cold advection from the orography over the East China Sea (Figure 4.10(a)). In the "cold TP composite" the positive signal in baroclinicity is stronger and localised closer to the coast compared to the "TP+MP experiment" (Figure 4.9(b)); nevertheless it is consistent with the pattern of jet intensification in Figure 4.8(c), also stronger and more localised than in the "TP+MP experiment".

In the papers by White et al. (2017) and Sha et al. (2015) the winter NH circulation is shown to be more impacted by the MP than by the TP due to the former's latitudinal position and interaction with the Pacific low-level jet (Held and Ting, 1990). We briefly consider the role of the former by running the so-called "MP experiment", where the cold anomalies over the Tibetan Plateau are removed (south of 38 N), leaving a residual negative temperature signal over the Mongolian Plateau (Figure 4.8(i)). The low-level response to "MP" forcing shows cold anomalies limited to high mid latitudes (Figure 4.8(j)) and cold advection centered over Japan

(Figure 4.10(d)). Since the baroclinicity is also enhanced at higher latitudes with respect to the "TP+MP experiment" (cf. panels (b) and (e) of Figure 4.10), MP cooling strengthens the Pacific jet on its poleward flank (Figure 4.8(k)), coherently with the changes in MEMF convergence (Figure 4.10(f)). Although the results support the relevance of the MP for the climate of the Pacific sector, TP surface forcing is necessary to have consistency with the "cold TP composite". The latter is in fact fundamental to obtain a strengthening of the baroclinic conditions over East Asia and of the Pacific jet to the east of the Chinese coast, i.e. for the overall intensification the East-Asia winter monsoon.

Discussion of the global "cold TP composite"

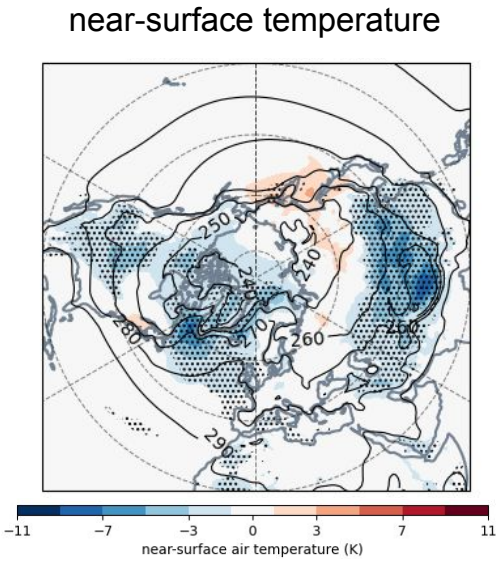

Figure 4.11: The "cold TP composite" anomalies of near-surface temperature (stippled above the 95% significance level), and the respective MMM climatology in contours

We include a brief discussion of the global "cold TP composite" to account for the influence of other large-scale climate patterns (specific to the composite) in setting the dynamical features presented in the Results. Figure 4.11 shows how also the North American continent is affected by a cold mid-latitude anomaly centered over the Rocky Mountains, which corroborates the idea of a biased representation of large-scale mountainous areas by the models in the composite. The high-latitude North Atlantic, Greenland and the confining regions in the Arctic are also characterised by colder than average near-surface conditions. We note that the map of surface

temperature (corresponding to SST over open ocean) shows analogous temperature patterns.

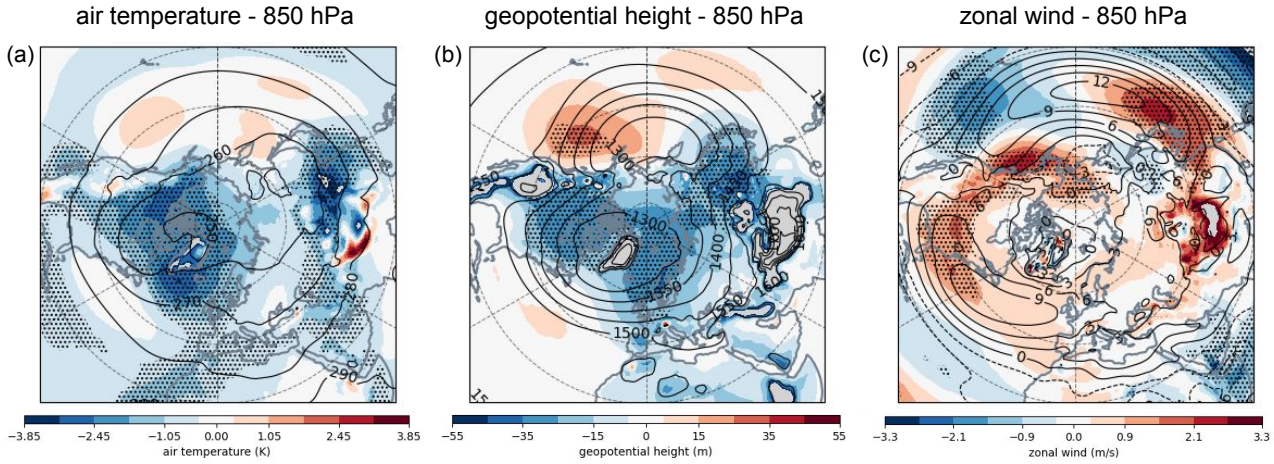

Figure 4.12: The "cold TP composite" anomalies of (a) air temperature, (b) geopotential height and (c) zonal wind at 850 hPa (stippled above the 95% significance level), and the respective MMM climatology in contours

The mid-latitude cold temperature anomaly extends to the lower troposphere (see 850 hPa level in Figure 4.12(a)), where the geopotential height is also contracted over the continents and the Arctic (Figure 4.12(b)). The Atlantic and Pacific eddy-driven jets (zonal wind in Figure 4.12(c)) strengthen upstream of the region of maximum intensity, probably as a result of the reinforced low-level baroclinicity to the east of the continental coastlines. Besides, the "cold TP composite" is affected by a negative 850 hPa temperature anomaly over the tropical Atlantic and Pacific, although barely significant over the Pacific basin (Figure 4.12(a)).

The upper level geopotential height retains the negative anomaly generated by the lower level cooling over the mid-latitude continents and over the Arctic, and the associated strengthening of the jet near the continents (see geopotential height and zonal wind at 300 hPa in Figure 4.13(b,c)). At this level the tropical negative temperature anomaly becomes predominant in the "cold TP composite", and corresponds to a contraction of the Tropics in terms of the geopotential height (Figure 4.13(a,b)). The global map shows evidence of an influence of this upper level tropical cooling on the weakening of the tropospheric jet over the central and eastern section of the Pacific basin. This is a point of interest in the comparison of the "cold TP composite" with the SPEEDY "TP+MP experiment", since the downstream negative wind anomaly in the Pacific jet constitutes one of the main discrepancies from the idealised model

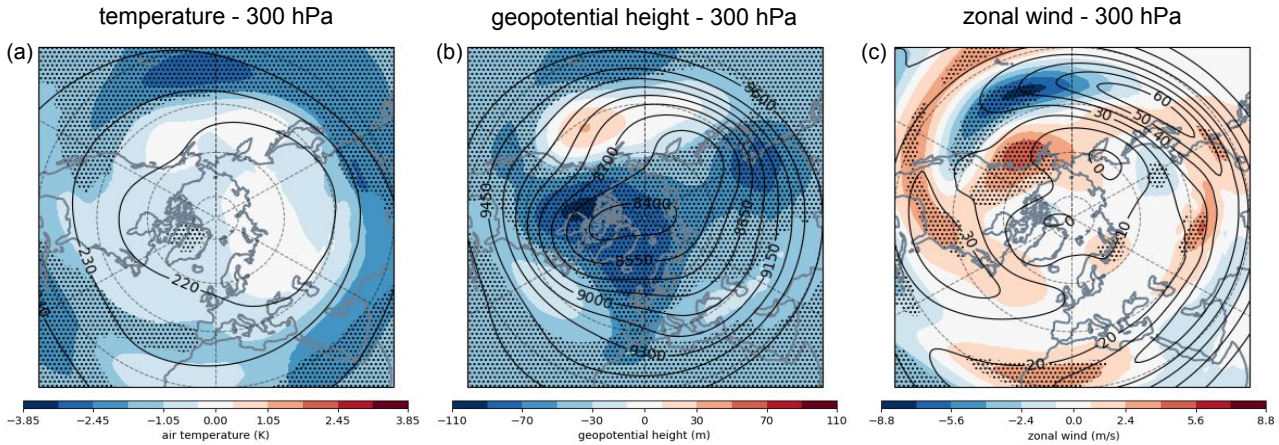

Figure 4.13: The "cold TP composite" anomalies of (a) air temperature, (b) geopotential height and (c) zonal wind at 300 hPa (stippled above the 95% significance level), and the respective MMM climatology in contours

response (cf. panels (c) and (g) in Figure 4.8). In fact, the "TP+MP experiment", which is not subject to tropical forcing, presents a zonally uniform intensification of the jet over the Pacific sector as a response to the cooling of the Central Asia orography. Hence, based on the global CMIP6 composite, we are able to identify the tropical origin of the macroscopic difference in the Pacific low-level jet emerging from the two approaches presented in the Results. However, the link between upper-level tropical cooling and cold mid-latitude continents (specifically in correspondence of orographic features) remains unknown.

4.1.3 Conclusions

By comparing a selection of CMIP6 historical simulations - the "cold Tibetan-Plateau (TP) composite" - with an idealised AGCM simulation we show how cold temperatures over Central Asia orography influence the winter atmospheric circulation over East Asia and the North Pacific. Colder than average Asian plateaux strengthen the tropospheric heat sink and intensify the East-Asia winter monsoon, leading to stronger north-westerly winds and cold advection downstream of the orographic features. Over the East China Sea, the enhancement of the advection of cold northerly air from the continent and of the surface heat flux from the ocean contribute to the intensification of the low-level baroclinicity. The idealised experiment shows

that low-level baroclinic conditions over the East-China Sea favour the development of transient atmospheric perturbations which deposit additional eddy momentum on the mean zonal flow, reinforcing the equatorward flank of the Pacific jet (Hoskins et al., 1983; Hoskins and Valdes, 1990).

Building on previous literature that investigates the relative role of the Tibetan and Mongolian Plateaux on the downstream winter climate by removing or adding regional orography (Shi et al., 2015; Sha et al., 2015; White et al., 2017), we apply a similar approach to surface temperature forcing. A second set of idealised simulations is presented where cold anomalies are confined to the region with Mongolian orography. The intensification of the zonal wind over the Pacific is still present, but is shifted northward with respect to the experiment with extended surface cooling, due to weakened advection of cold air to the east of the Tibetan Plateau. We conclude that the TP region is fundamental for setting the atmospheric conditions conducive to the intensification of the East Asia winter monsoon, as detected in the CMIP6 models contributing to the "cold TP composite". Still, changes in the Mongolian Plateau land temperature are relevant to understand future projections of the winter season over the Pacific sector (Xu et al., 2016).

The results of this work suggest that thermal conditions over high Central Asia plateaux foster significant changes in the large-scale circulation on the lee side of the orography. We relate this to a well-known cold Tibetan Plateau temperature bias measured in many climate models (Peng et al., 2022; Fan et al., 2020) and show how cold conditions are liable to produce atmospheric biases in wind and temperature over East Asia and the western North Pacific. Specifically, a strengthening of the East-Asia winter monsoon, affecting the highly inhabited eastern coast of China and the Pacific jet, is found in models characterised by colder than average temperatures over Central Asia plateaux.

Based on these findings, advances in the representation of surface processes over complex orography are expected to decrease the amplitude of temperature and circulation biases and to improve the modelling of the mean climate downstream of the Central-Asia plateaux. A reduction in the inter-model spread could also improve the confidence of climate projections for

the next decades. Similarly, approaches such as the "emergent costraints" (Hall et al., 2019) applied to the feedback between surface temperatures over orography and the local energy budget may be useful to reduce the uncertainty of the projections. On a different time scale, works analysing subseasonal-to-seasonal forecasts over East Asia find a significant influence by surface anomalies over the Tibetan Plateau (Li et al., 2018; Xue et al., 2021), implying that shorter-term operational forecasting could also benefit from advances in the modelling of land over the Asian high plateaux.

4.2 Siberian land temperature

During the winter season the high-latitude Northern Hemisphere (NH), receiving no or poor insolation, loses heat through thermal emission. Over Siberia this is exacerbated by the high reflectivity of the persistent winter snow cover, which inhibits the absorption of the little shortwave radiation reaching the surface. Therefore, during winter the Siberian surface energy budget is dominated by a strong thermal heat loss that is balanced only by the latent and sensible heat flux from the ground and by a relatively weak sensible heat flux from the atmosphere (see schematics in Fig. 9 of Langer et al., 2011; Serreze and Barry, 2014). The combination of surface and atmospheric radiative cooling generates a wide center of low-level cold and dense air that sits semi-permanently in the North-East Eurasia (southern Siberia), dominating the low-level atmospheric conditions in the mid- and high-latitude regions of East Asia. The pattern is commonly known as the Siberian (sea-level pressure) High (Lydolph, 1977). A shallow winter anticyclone appears with the build-up of the near-surface divergent high-pressure system (Lydolph, 1977; Panagiotopoulos et al., 2005; Cohen et al., 2001) and, at the same time, an upper-level trough is centered on the high-latitude Asian coast, in quadrature with the lower-level Siberian High and Aleutian Low (Takaya and Nakamura, 2005).

Surface based temperature inversion - a vertical temperature increase from the surface (negative lapse rate) caused by strong low-level diabatic cooling - is common in the high latitudes over land and sea, even far from the center of the Siberian High. In Eurasia, the frequency and depth of the inversion and the temperature difference between the top of the inversion layer and the surface increase to the east of the Norwegian Sea, and are stronger inland, reflecting the clearer skies and stronger radiative heat loss conditions (discussed in the following paragraph). The presence of orography in eastern Siberia confines the eastward extension of the cold air pool and exacerbates the temperature inversion (Serreze et al., 1992).

The winter radiative budget in the extratropical and polar NH changes considerably in the presence of humidity and clouds (Groisman et al., 2000; Stramler et al., 2011), setting up a positive feedback with the surface temperature (Pithan and Mauritsen, 2014; Goosse et al., 2018). At Arctic latitudes, low-level clouds and vapour efficiently trap the thermal (longwave)

radiation in the atmosphere and induce a warming of the surface (Curry et al., 1996; Groisman et al., 2000; Langer et al., 2011; Pithan and Mauritsen, 2014; Yihui, 1990; Shupe and Intrieri, 2004; Curry et al., 1995). This effect is amplified if the clouds are relatively low, since the emission temperature is maximised by the presence of the inversion level. Its impact dominates over other cloud-related processes for most of the seasonal cycle, except for summer when the shielding from shortwave radiation induces a weak negative cloud feedback on the surface temperature (Intrieri et al., 2002). For a general review on the complex topic of cloud and water vapour feedbacks see Bony et al. (2006); Held et al. (2000). The positive water vapour feedback is weaker than the cloud feedback but persists throughout the year (Curry et al., 1995; Goosse et al., 2018). In winter, low temperatures and strong low-level stability inhibit the local release of humidity into the atmosphere; water vapour is predominantly advected from lower latitudes (Piao et al., 2018). The presence of cloudy skies may also be associated with the transport of warmer air masses from the mid-latitudes, experiencing adiabatic cooling and water vapour condensation (Woods et al., 2013; Messori et al., 2018). From the point of view of weather systems, the transport of warm air from lower latitudes is often associated with local cyclonic systems, characterised by low surface pressure and local ascent; conversely, anticyclonic systems are characterised by high surface pressure, subsidence and clear skies (Tselioudis et al., 2000).

The relation between energy budget, clouds, humidity and weather systems applies specially well to the NH high latitudes (Groisman et al., 2000) and to Siberia (Kharyutkina et al., 2012). At larger scales it explains the link between the strength of the Siberian High and Northern Eurasia cloud conditions, where rapid radiative cooling and large-scale descent within the clear-sky core of the Siberian anticyclone reinforce the widespread high-pressure system (Chernokulsky et al., 2013; Takaya and Nakamura, 2005). The intensification of the Siberian High, corresponding to a simultaneous intensification of the East-Asia winter monsoon (Zhang et al., 1997; Wu and Wang, 2002; Takaya and Nakamura, 2005), eventually leads to cold-air outbreaks over East China (Ding and Krishnamurti, 1987; Yihui, 1990).

As mentioned above, the snow cover in Northern Eurasia takes part in the surface and atmospheric energy budget by modulating the surface albedo. Cohen and Entekhabi (1999) and

Cohen et al. (2001), based on evidence (in reanalysis data) of the influence of autumn snow cover on the build-up of the Siberian High, hypothesise that the strong (autumn) interannual variability in Eurasian snow may influence the winter NH circulation. Subsequent papers based on reanalysis and modelling experiments (Saito et al., 2001; Gong et al., 2003a; Cohen et al., 2007, 2014) propose that anomalous autumn snow in Eurasia, through the modulation of the Siberian High, is conducive to an amplification of large-scale planetary waves. These are able to propagate to the stratosphere (Charney and Drazin, 1961) and may slow down the stratospheric polar vortex (SPV) at the beginning of the winter season. A downward propagation of the weak stratospheric polar vortex (SPV) anomalies is then liable to reflect on the tropospheric circulation, resulting in a negative phase of the NH annular mode (NAM, Thompson and Wallace, 1998) or of its Atlantic-sector manifestation, the North Atlantic Oscillation (NAO) (Barnston and Livezey, 1987; Hurrell, 1995; Hurrell et al., 2003), in the following months (Baldwin and Dunkerton, 1999; Cohen and Entekhabi, 1999; Cohen et al., 2007; Orsolini and Kvamstø, 2009). These mechanisms are still debated because of the non-stationarity of the observed interaction at decadal time scales and of the uncertainties in the results of climate models forced by snow cover anomalies: the dominant direction of causality - snow inducing atmospheric circulation anomalies or vice versa - continues to be ambiguous (Clark and Serreze, 2000; Henderson et al., 2018).

While the existence of a positive feedback between snow cover anomalies and the NAM is not excluded in Autumn, when the seasonal snow anomalies are located near the center of the Siberian High (Cohen et al., 2001, 2014), a strong interaction of the high-latitude Siberian temperatures on the centers of the NAO / NAM is difficult to imagine (Luo and Wang, 2019, 2018). Indeed, snow and temperature anomalies in high-latitude Eurasia ($> 50^\circ$ N) seem to show mainly local feedbacks (Luo and Wang, 2019), because of the limited impact on the Siberian High and the East Asia winter monsoon modulating the winter weather in East Asia (Zhang et al., 1997; Takaya and Nakamura, 2005; Cohen et al., 2001).

The work presented in the following is motivated by the existence of a wide inter-model spread among CMIP6 climate models in the winter (January-February) climatology of Siberian temperatures (Figure 4.1). Differently from previous literature, we consider here winter Siberian

near-surface temperature conditions, rather than the autumn snow cover. In the historical winter season Siberia is uniformly covered by snow, with weak interannual variability (Estilow et al., 2014) and high uniformity across modelling systems (Zhu et al., 2021). Hence, the inter-model CMIP6 temperature spread likely stems from the different interaction with the atmosphere and from the different model schemes computing surface temperature, rather than from a variable fraction of snow cover. We choose to analyse the near-surface temperature variable[6] in preference to the surface temperature variable[7], because the former is representative of the interactions between land temperatures and the atmosphere ; however, results are consistent independent of the specific choice of variable. For near-surface temperature over Siberia the ensemble shows an inter-model spread of approximately 10 K (Figure 4.3), with regional variations (Figure 4.2). It thus becomes of interest to investigate the reason of the Siberian winter temperature spread among the set of CMIP6 climate systems, and, given the high amplitudes of the anomalies from the MMM, to explore whether the anomalies influence the climatological atmospheric conditions over the Asia / Pacific sector.

Following a description of the datasets used for this study (Section 4.2.1), in the Results (Section 4.2.2) we show composites selected relative to the climatological Siberian temperatures in the CMIP6 models, highlighting the local balance between radiation and surface temperature and the low-level and upper-level atmospheric conditions. The comparison of the multi-model analysis with a composite study based on the interannual variations of Siberian temperatures in reanalysis data provides additional insight on the reasons for and consequences of the CMIP6 multi-model spread, discussed in the Conclusions (Section 4.2.3).

4.2.1 Methods

CMIP6 simulations

As in Section 4.1, we use CMIP6 historical runs for years 1979 to 2008, over which we compute the January-February climatology; the January and February months are referred to as *winter*

[6] usually corresponding to the air temperature at 2 meters from the surface
[7] also known as skin temperature

throughout the chapter. The results for an extended winter taking into account the transition months (e.g. October–March) are consistent but weaker in intensity (not shown). We select one member per climate model from the CMIP6 dataset (Table 4.1), excluding the EC-Earth models because of incongruences between the values of surface and near-surface temperatures (Figure 4.3). The sample is thus made up of 34 historical simulations. Based on an index of Siberian temperature (i.e. the climatological weighted-area average on near-surface temperature in the north-most box of Figure 4.2(b) over the period 1979–2008), the simulations with temperature index above / below one standard deviation from the CMIP6 multi-model mean form the "warm Sib composite" / "cold Sib composite" (see the 7 models in each category from Table 4.1). The composite fields are shown in terms of the anomalies from the climatology of the CMIP6 multi-model mean (MMM), with significance computed according to a permutation test repeated 1000 times over the 34 model realisations, considering the 95% confidence level (Wilks, 2011). Note that the same analysis based on the surface temperature instead of the near-surface temperature produces consistent results.

Atmospheric pressure-level variables are extracted from the CMIP6 archive. Radiative surface heat fluxes in air, surface temperature (skin temperature, corresponding to SST on open ocean), near-surface temperature (usually 2-meter air temperature) are also used. Due to the lack of availability of daily fields for a large subset of the CMIP6 models, the analyses are based on monthly-mean variables. Moreover, we report that FGOALS-f3-L is excluded from the model selection of Figures 4.16, 4.17, 4.18, KACE-1-0-G from the selection of Figure 4.17, ACCESS-CM2, ACCESS-ESM1-5 and CAS-ESM2-0 from the selection of Figure 4.18 because of the inaccessibility of relevant datasets in the servers providing the CMIP6 archive. In the analysis of snow amount (not displayed, but cited in the text) as many as 10 models are missing.

Diagnostics

Specific humidity transport is $\mathbf{u}q_s = uq_s\hat{\mathbf{i}} + vq_s\hat{\mathbf{j}}$, and its divergence is $\nabla \cdot (\mathbf{u}q_s)$. The quantities are computed using the climatological variables u, v and q_s, which give the *specific humidity transport by the mean flow* and its divergence.

Reanalysis

The ERA5 reanalysis dataset (Hersbach et al., 2020b; Bell et al., 2021) is used to represent observations. The common period 1979–2008 is selected for computing multi-model climatological MMM biases. Moreover, the ERA5 composites presented in Section 4.2.2 are based on the interannual variability of the Siberian 2-meter temperature index in the extended period 1959–2021 (as in the CMIP6 index, Siberia corresponds to the north-most box of Figure 4.2(b)). The ten winters (January-February) characterised by a Siberian index anomaly above or below one standard deviation are averaged to give the composites "warm Sib - interan. ERA" and "cold Sib - interan. ERA", represented in Figure 4.19.

4.2.2 Results

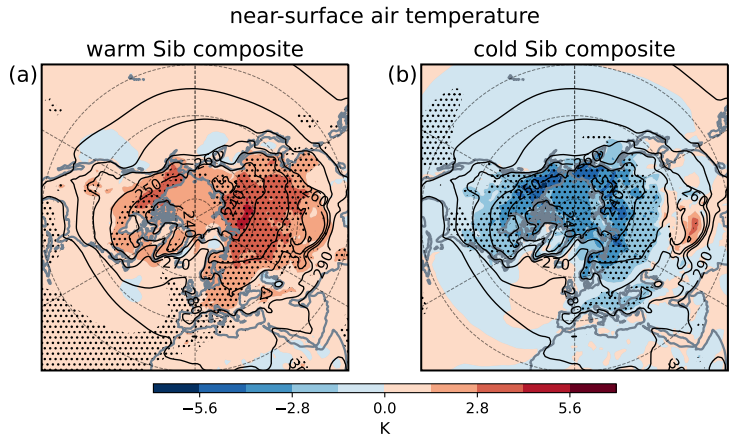

Figure 4.14: The (a) "warm Sib composite" and (b) "cold Sib composite" anomalies of near-surface temperature (stippled above the 95% significance level), with the MMM climatology in contours. The maps are consistent with the surface temperature field (not shown)

We present a composite study based on the climatological winter Siberian (Sib) near-surface temperature index in the CMIP6 historical simulations over the period 1979–2008 (definition in Section 4.2.1). The models with an anomaly from the MMM index greater than one standard deviation are organised in the "cold Sib composite" and in the "warm Sib composite" (Table 4.1). The near-surface temperature patterns of the two composites are displayed in Figure 4.14 and exhibit a coherent land cooling and warming pattern extending from Eurasia to the North American continent, mainly north of 50° N. The peak amplitude is detected at

latitudes 60 to 70° N over Northern Eurasia and Alaska / North-West Canada. In the "cold Sib composite", unlike its "warm" equivalent, the significant thermal anomaly extends to the Arctic Sea bounded by the north coast of Greenland and the Bering Strait. In the "warm Sib composite" the significant pattern spreads to lower latitudes; specifically, it is present in the form of a warm tongue over the subtropical eastern North Atlantic Ocean, where it extends into the Mediterranean region and spreads to most of the Eurasian continent. The surface temperature composites (not shown) are consistent with the near-surface field, but display broader patterns of significant signals in the North Atlantic ("warm Sib composite") and in the tropical eastern North Pacific ("cold" and "warm Sib composite"). Moreover, only in the "warm Sib composite" the SSTs to the south of Japan are warmer than the MMM, in equilibrium with the advection of warmer air from the continent over the sea (cf. Figure 4.3(a) and low-level wind climatology in Figure 4.16(c,d)).

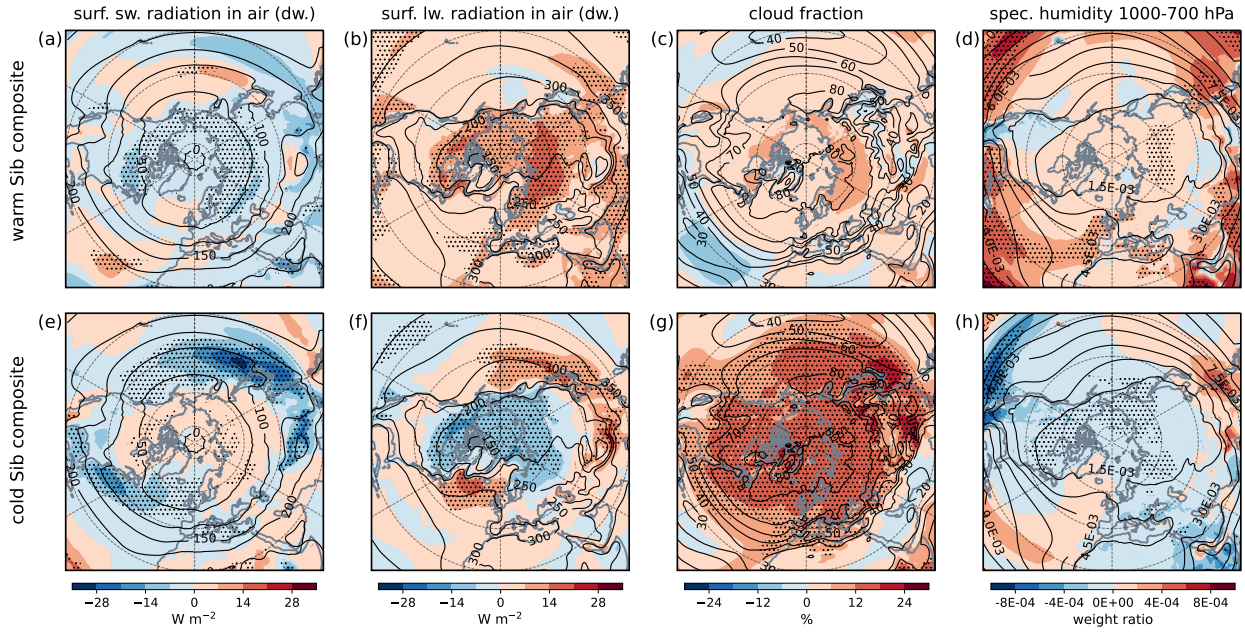

Figure 4.15: Surface radiation, cloud and low-level humidity atmospheric conditions in (a–d) "warm Sib composite" and (e–h) "cold Sib composite". The anomalies of (a,e) surface shortwave radiation, (b,f) surface longwave radiation in air (downward), (c,g) cloud fraction, (d,h) specific humidity in the low levels (1000 to 700 hPa) are displayed in shading (stippled above the 95% significance level), the MMM climatology is shown in contours

As presented in the first paragraphs of Section 4.2, the high-latitude winter climatological temperature lies in a bistable state that is set by the amount of longwave radiation trapped in

the lower levels of the atmosphere by water in the liquid and gaseous phases. In Figure 4.15 we find in the high latitudes a strong consistency between the variables of near-surface temperature (Figure 4.14), longwave radiation into the surface (Figure 4.15(b,f)) and low-level specific humidity (Figure 4.15(d,h)). A warming (cooling) of the land surface associated with stronger (weaker) longwave radiation entering the surface are detected coincidentally with positive (negative) anomaly in low-level humidity. We hypothesise that the increase (decrease) in 1000-700 hPa humidity corresponds also with an analogous change in low-level liquid water content, both enhancing (reducing) the longwave radiation. This is not necessarily associated with a coherent change in the total cloud cover (discussed in the following paragraph). The presence of liquid water cannot be verified across CMIP6 climatologies because of the unavailability of the relevant data. Note that in the high latitudes of panels (b,f) in Figure 4.15 the anomaly in longwave radiation into the surface is compensated by a corresponding anomaly in the longwave emission by the warmer surface (not shown).

The cloud fraction or cloud cover (Figure 4.15(c,g)) is a variable representing the fraction of sky area covered by clouds integrated over the vertical extent of the atmosphere. Note that there exists no unique relation between cloud-fraction and surface temperatures, since the latter depends on the clouds' distribution in the vertical direction and on their opacity to longwave radiation, to which the cloud fraction is partially insensitive (Curry et al., 1996; Shupe and Intrieri, 2004). Otherwise, the cloud fraction determines the shielding from solar (shortwave) radiation.

In the "cold Sib composite" a positive anomaly in cloud fraction occupies most of the NH poleward of 20° N. The strong signal over the climatological locations of the mid-latitude storm tracks (i.e. the western sections of the Pacific and Atlantic basins) likely indicates a link with the large-scale condensation associated with the warm sectors of extratropical cyclones (Held et al., 2000; Curry and Herman, 1985). This is expected to extend to the high latitudes in the form of mid- and upper-level clouds (Curry and Herman, 1985; Held et al., 2000). Hence, two different causes for excess cloud cover can be hypothesised. The first is related to an enhanced synoptic variability and cyclone frequency, or to the specific features of the models' extratropical cyclones (not verifiable within the present dataset); the second hypothesis is linked

to the models' physics producing more large-scale cloud cover than the MMM. The positive cloudiness anomaly in the "cold Sib composite" is consistent with the decrease in shortwave radiation entering the mid-latitude surface (Figure 4.15(e)) and is compensated by the net longwave radiation entering the surface (not shown). The same does not apply to the subpolar regions of Eurasia, where the climatologically low winter insolation is substantially unaffected by the extensive cloud-cover anomaly (cf. panels (e) and (g) in Figure 4.15) and the cloud and water-vapour feedbacks with the surface temperature are dominant. The reason for the Arctic anomalies in the "cold Sib composite" remains unclear since we are not able to link it directly to the cloud cover anomaly. This topic deserves further investigation, possibly including the role of transient atmospheric heat and moisture transport.

The inter-model snow cover variability is not expected to be relevant for the January-February near-surface temperature anomalies (Figure 4.14) because during the whole winter season the high latitudes of the Eurasian continent are uniformly covered by snow; inter-model differences are weak (Zhu et al., 2021). The variable describing the quantity of snow (*snow weight per square meter*, not shown) reveals a weak but positive anomaly in Northern Eurasia for the "warm Sib composite", which is consistent with the higher low-level specific humidity in Figure 4.15 and with the stronger precipitation flux (not shown). We note that the results for snow amount, even though significant, are not completely reliable because based on a limited model ensemble (details in Section 4.2.1).

The dynamical features of the "warm" and "cold" CMIP6 composites are represented in Figure 4.16. In panels (a,e) we observe that the sea-level pressure decreases (increases) in the regions where the temperature is warmest (coldest) (cf. with Figure 4.14), corresponding to a weakening (strengthening) of the inversion layer. In the polar and subpolar latitudes the 850 hPa geopotential height anomaly (panels (b,f)) essentially corresponds with the surface pressure pattern. The pressure response is restricted to the low levels (below 700 hPa), consistently with the shallow temperature anomalies (cf. Figure 4.16(c,g) and Figure 4.14). The geopotential height and temperature signals (Figure 4.16(b,f) and (c,g)) are particularly sensitive to temperature anomalies located over the sea surface (cf. with Figure 4.14): the presence of the sea induces a deeper thermal impact on the atmosphere because of the presence of

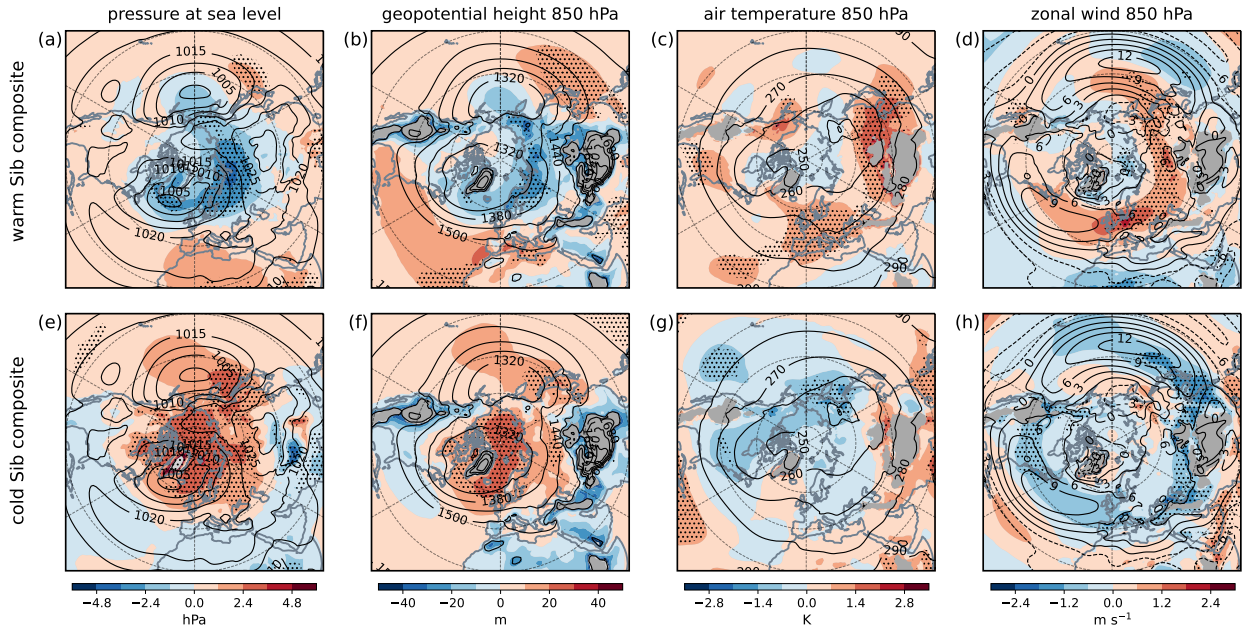

Figure 4.16: Low-level atmospheric conditions in (a–d) "warm Sib composite" and (e–h) "cold Sib composite". The anomalies of (a,e) sea-level pressure, (b,f) geopotential height, (c,g) air temperature, (d,h) zonal wind are displayed in shading (stippled above the 95% significance level), the MMM climatology is shown in contours. Grey shading masks orography exceeding 1400 m

stronger turbulent mixing and dynamic instability (associated with storms) releasing latent and sensible heat through the air column (Lau, 1979; Peixoto et al., 1992; Held et al., 2002). The continental temperature anomaly influences the mid troposphere only where the orography elevates the pattern towards lower pressure surfaces, i.e. extratropical East Asia in the "warm Sib composite" (Figure 4.16(c,g)).

The wind patterns (Figure 4.16(d,h)), in quadrature with the geopotential height anomalies (Figure 4.16(b,f)), display a weakening of the Eurasian zonal component in presence of the high-latitude continental cooling in the "cold Sib composite" and nearly opposite conditions, though shifted to the north, for continental warming in the "warm Sib composite". Although this appears counterintuitive in terms of the thermal-wind relation - linearly linking meridional temperature gradients to vertical gradients in the zonal winds (pp. 81–84 Holton and Hakim, 2013) - the dynamical conditions are justified by the interference between the orographic profile (Figure 4.6(b)) and the near-surface temperature patterns (Figure 4.14(a)) over extratropical East Asia. In the "warm Sib composite" the shallow warming affects the 850 hPa isobaric

surface where the orography is sufficiently elevated (i.e. on the Mongolian Plateau and around the north of the Tibetan Plateau, Figure 4.16(c)), producing a strengthening of the climatological temperature gradients, hence of the thermal wind, on the 850 hPa pressure level, to the north of the orography. Similar conclusions based on geostrophy (pp. 71–72 Holton and Hakim, 2013) are obtained by considering the 850 hPa geopotential height anomaly (Figure 4.16(b)). In the "cold Sib composite", where the Siberian cooling is restricted to the boundary layer (not shown), the deepening of the polar low pressure, restricted to the north of the orographic barrier, weakens the meridional pressure gradient (Figure 4.16(e,f)); the negative zonal wind anomaly is in geostrophic equilibrium (Figure 4.16(h)).

The North Pacific eddy-driven[8] jet stream is only lightly affected by the upstream conditions: the zonal wind changes reach the entrance region of the Pacific jet only in the "cold Sib composite" (Figure 4.16(g)), where the continental anomalies are located further south with respect to the warm composite (Figure 4.16(c)) and are associated with reduced northerly winds downstream of the Tibetan Plateau (not shown). Such conditions correspond to a weakening of the low-level East Asia winter monsoon (the climatological trough residing between the Siberian High and the Aleutian Low responsible for north-westerly advection of cold air into eastern China, see Panagiotopoulos et al. (2005)).

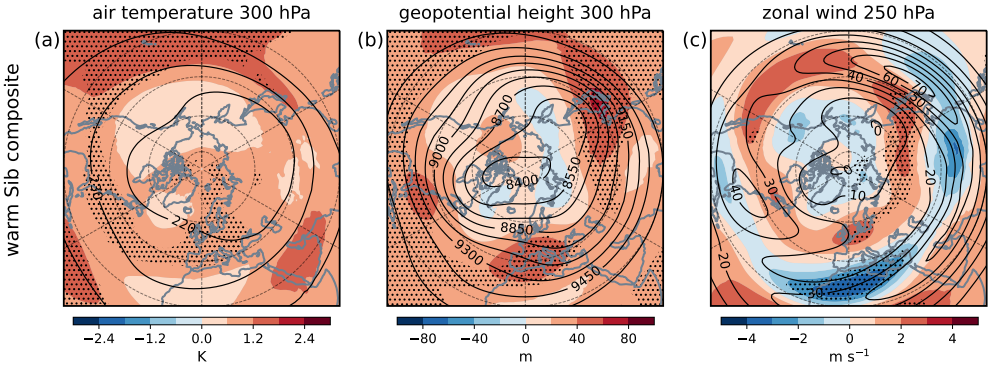

Figure 4.17: Atmospheric conditions in the upper troposphere for the "warm Sib composite". The anomalies of (a) 300 hPa air temperature, (b) 300 hPa geopotential height and (c) 250 hPa zonal wind are displayed in shading (stippled above the 95% significance level), the MMM climatology is shown in contours

The mid-latitude warming over East Asia in the "warm Sib composite" penetrates deep into the

[8]equivalent to low-level

troposphere (up to 300 hPa, Figure 4.17(a)), affecting the upper-level jet over the continent - see following paragraph. On the contrary, in the "cold Sib composite" the high-latitude cooling and the weakening of the mean flow are restricted to the lower levels. The differences in the depth of the changes over the Eurasian continent are most probably due to the diverse (latitudinal) extension of the warming and cooling patterns, which, in the "warm Sib composite" extend simultaneously to lower latitudes and higher surface elevation. This, together with the deep atmospheric warming over the Pacific south of Japan, generates "warm Sib" temperature (and geopotential height) anomalies that are able to interact with the mid-latitude flow.

We show the upper-level signal relative to the "warm Sib composite" in Figure 4.17 ("cold Sib composite" anomalies are not presented because not significant). The 300 hPa temperature map (Figure 4.17(a)) reveals an intensive tropical and subtropical warming, which is not restricted to the near surface (Figure 4.14(a)), but rather peaks in the upper troposphere. This type of signal is reminiscent of the Tropical Amplification predicted for the future climate (Butler et al., 2010; Barnes and Polvani, 2013). While the maps of near-surface temperature (Figure 4.14(a)) and surface temperature (not shown) indicate a connection between the tropical Atlantic and Eurasia, in parallel Figure 4.17 supports the existence of a strong atmospheric link with the Tropical Pacific, through zonal westerly advection of tropical temperature anomalies towards the Mediterranean region (cf. climatology of Figure 4.17(c) with anomaly of Figure 4.17(a)). Hence, our results highlight the fact that in climate models a Tropical-Amplification-like signal may be also associated with warmer conditions over Siberia. The mechanism involves a higher availability of heat and humidity in the Tropics (humidity is discussed in the following) that is transported remotely to the European region and eventually to Siberia, where the surface energy budget changes and the surface temperature increases.

The winter transport of specific humidity by the climatological flow, represented in Figure 4.18(a), shows how the North Pacific and North Atlantic jets carry humid air into the high latitudes and over the continents. In the "warm Sib composite" (Figure 4.18(b)) we observe a strong increase in the humidity transport from the North Atlantic into the Eurasian continent. This originates from the positive anomaly in low-level North Atlantic specific humidity (Figure 4.15(d)), which is advected by the north westerly winds into the European region, then towards the interior of

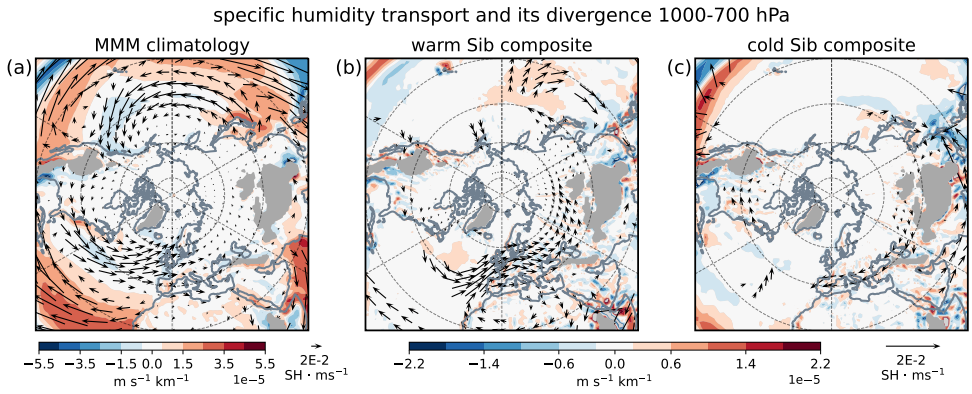

Figure 4.18: Specific humidity transport (arrows) and its divergence (shading) averaged from 1000 to 700 hPa in (a) MMM climatology, (b) "warm Sib composite" and (c) "cold Sib composite". Only the significant transport anomalies from the MMM are represented in panels (b,c)

the continent and Siberia by the strengthened zonal flow (Figure 4.16(c)). The transport into Siberia (Figure 4.18(b)) is consistent with the positive specific humidity anomaly detected in the region (Figure 4.15(d)), and is expected to produce low-level clouds by radiative cooling (variable not available, see Curry (1983)). Differently, the "cold Sib composite" (Figure 4.18(c)) displays a reduced low-level humidity transport towards and into the Eurasian continent, which is induced by the weaker zonal winds shown in Figure 4.16(g).

The tropical influence on the Siberian surface and near-surface conditions through atmospheric transport is restricted to the "warm Sib composite". In this particular case, the widespread Eurasian temperature anomalies feed back on the atmospheric circulation: the warming over the orographic region of Central Asia increases the low- and mid-troposphere meridional pressure gradients (deepening of the high-latitude pressure low in Figure 4.16(a,b) and expansion of the air column above and downstream of the mid-latitude orography in Figure 4.17(b)) causing a strengthening of the mid-latitude zonal flow across the depth of the troposphere (Figures 4.17(c) and 4.16(c)). Consequently the moisture transport into Northern Eurasia is enhanced, feeding the local temperature anomaly. We again stress that the effects on the jet and mean circulation over the Pacific basin are limited (see the Pacific sector in Figure 4.17(c)).

A different analysis, where compositing is done based on the interannual variability of winter Siberian near-surface temperature[9], is performed on the ERA5 reanalysis dataset over the

[9]2-m temperature averaged over the same region as the CMIP6 climatological model indices for each January-February

extended historical period 1959–2021. The results, synthesised in Figure 4.19, are relatively different from those obtained by compositing on the CMIP6 historical climatologies, but provide useful insight with regard to the inter-model spread over the Siberian region.

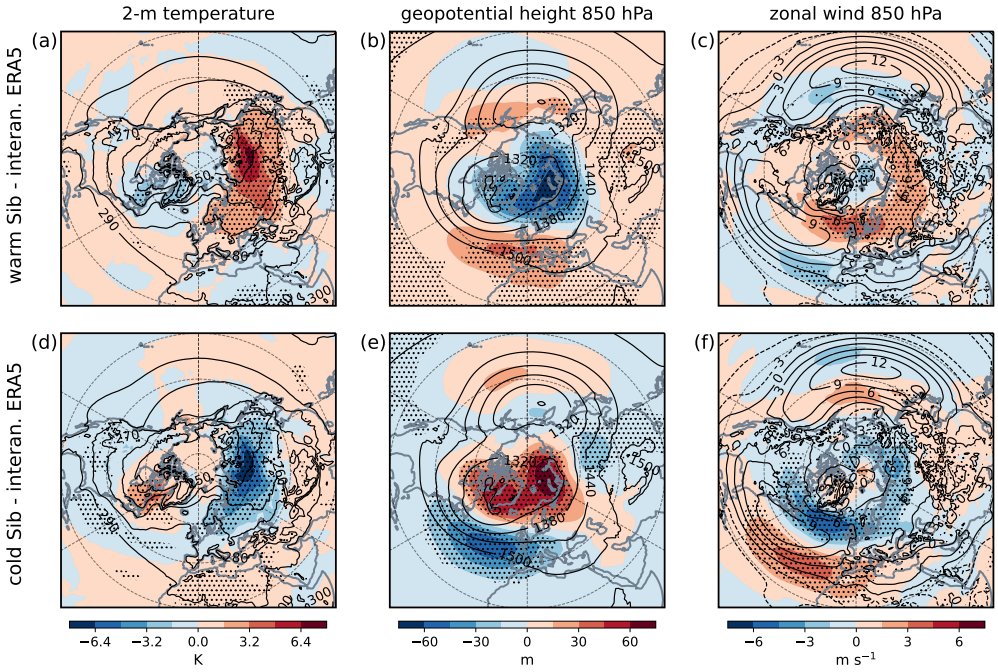

Figure 4.19: Atmospheric conditions in composites (a–c) "warm Sib - interannual ERA5" and (d–f) "cold Sib - interannual ERA5". The anomalies of (a,d) 2-meter temperature, (b,e) 850 hPa geopotential height, (c,f) 850 hPa zonal wind are displayed in shading (stippled above the 95% significance level), the MMM climatology is shown in contours. Note that the colorbars have different intervals with respect to those used to represent the CMIP6 composites

The first peculiarity of the "warm Sib - interan. ERA5" ("cold Sib - interan. ERA5") is that the temperature anomalies in Figure 4.19(a,c) are associated with clear upstream atmospheric patterns (Figure 4.19(b,c) and 4.19(e,f)) ascribable to positive (negative) NAO (Hurrell et al., 2003). The meridional pressure gradients induced by NAO-like anomalies over the North Atlantic (Figure 4.19(b,e)) tune the strength of the westerly flow over the Eurasian continent (Figure 4.19(c,f)), modulating the interannual variations in the Siberian surface temperatures (Figure 4.19(a,d) and Wu and Wang, 2002). The hemispheric geopotential height anomalies are more annular compared to those found in the CMIP6 analysis (cf. Figure 4.19(b,e) and Figure 4.16(b,f)) and organised in a dipole structure that is strong over the North Atlantic and weak but significant over East Asia.

The East Asia geopotential anomaly dipole (Figure 4.19(b,e)) extends the NAO-forced zonal

flow into high-latitude eastern Siberia (Figure 4.19(c,f)), and resembles the 850 hPa signal in the CMIP6 "warm Sib composite" - the analogue signal in the "cold Sib composite" is shifted to the south. Note that the geopotential pattern does not superpose with the classic Arctic Oscillation (AO) features over the Pacific sector (Thompson and Wallace, 1998), but at the same time is more zonally symmetric than the NAO (Hurrell et al., 2003). We believe that the peculiarities in the NAO arising in the ERA5 interannual composites are related to the temperature anomalies over the Eurasian continent, i.e. the starting point for the composite selection. Positive temperature anomalies over Northern Eurasia ("warm Sib - interan. ERA5" in Figure 4.19(a)) correspond to a decrease in the low-level atmospheric pressure (Figure 4.19(b)) - in agreement with the CMIP6 analysis where the low-level geopotential height decreases (increases) with warmer (colder) near-surface conditions (Figure 4.16(a,b) or 4.16(e,f)). In the mid latitudes the vertical expansion induced by the warming produces a signal of opposite sign extending deeper in the troposphere (not shown). Similarly to the results of the CMIP6 models' compositing, and differently from the classic AO patterns (e.g. Thompson and Wallace, 1998), the Pacific jet remains substantially unaffected. Note that symmetric conclusions (reversed in sign) apply to "cold Sib - interan. ERA5" (Figure 4.19(d–f)).

We briefly mention that in the composite "warm Sib - interan. ERA5" ("cold Sib - interan. ERA5") the near-surface temperatures over north-eastern North America are colder (warmer) than the climatological average. This feature is dynamically consistent with a stronger (weaker) zonal flow increasing (decreasing) the eastward transport of cold air from the continent towards the ocean (Hurrell et al., 2003); furthermore, it is expected to produce a positive feedback on the meridional temperature gradient supporting the jet in the western North Atlantic.

4.2.3 Conclusions

The strong inter-model spread in Siberian temperatures among CMIP6 climatologies prompted us to investigate the links with the models' local atmospheric conditions and mean circulation. Based on an index representing the average climatological near-surface temperature of the region, we compute a composite analysis in which we select the models featuring warmest

and coldest Siberian temperatures, and compute their anomalies from the multi-model mean (MMM) conditions. We find that the two composites ("warm Sib" and "cold Sib") show antisymmetric atmospheric conditions only locally, i.e. in the "warm Sib composite" higher temperatures in the subpolar latitudes are consistent with stronger incoming and outgoing longwave radiation flux near the surface and slightly enhanced low-level moisture; the "cold Sib composite" displays anomalies of opposite sign.

The "cold Sib composite" shows excess cloud cover extending uniformly poleward of the 20° N line. Based on the correspondence of the peak anomaly with the geographical location of the storm tracks, we can hypothesise that it is connected either with the models' mid-latitude dynamics or with the models' cloud physics. At present we are unable to infer the reasons for the cloud anomalies nor the links with the Arctic heat budget, since we lack information on the vertical distribution of the clouds, and on the transient transport of moisture and heat towards the Arctic (important for exchanges between mid and high latitudes, see Woods et al., 2013; Messori et al., 2018).

In the "warm Sib composite" anomalously high temperatures at tropical latitudes, peaking in the upper troposphere as in the well-known Tropical Amplification, are detected concomitantly with warm conditions in North Eurasia. The two can be related through the identification of a positive feedback between the transport of heat and humidity from the tropical latitudes and the local Siberian temperature. In fact, warmer high-latitude temperatures reinforce the flow that carries anomalous moisture and heat into the Eurasian continent.

In the CMIP6 composites of both signs, the low-level circulation anomalies over Eurasia - mainly limited to the continental regions - depend on the attenuation or amplification of the low-level inversion layer in the high latitudes. The geopotential height anomalies are shallow in the high latitudes, but extend deep into the mid-troposphere when the temperature anomalies reach lower-latitude regions characterised by elevated orography (the East Asia mountain chains, cf. near temperature map in Figure 4.14 and orographic elevation map in Figure 4.6). The hypothesis of near-surface temperature being more impactful when located at high elevation in the Extratropics (rather than low-level at subpolar latitudes) is based on the spatial proximity

of surface-based heat sources or sinks to the strong mid-tropospheric winds characterising the mid latitudes (Trenberth, 1983; White et al., 2017; Held and Ting, 1990).

An alternative composite analysis based on the reanalysis yearly winter Siberian temperature reveals that the mechanism forcing or being forced by (see the introduction of the Section *Siberian land temperature*) its interannual variability is identifiable as the NAO. However, neither NAO nor NAM are important in explaining the spread in the CMIP6 climatological temperatures. The major similarity between the outcomes of the two compositing approaches (CMIP6 model climatologies and interannual reanalysis) lies in the significant interaction of the Siberian temperature anomalies with the circulation over East Asia, with the detection of two types of response depending on the latitude and elevation of the anomaly (low-level in the high latitudes, deep in the orographically elevated mid latitudes). Both composite approaches support the lack of impact of winter Siberian temperatures on the Pacific large-scale circulation.

We reserve an additional comment for the North American near-surface temperatures. While in the interannual composites the temperature over high-latitude North America is coherent with the dynamical NAO conditions (cold east-coast temperature with positive NAO and warm Siberia), in the CMIP6 composites the surface temperature anomalies are zonally coherent over Siberia and North America. In the "warm Sib composite" the only dynamical feature justifying the North America temperature pattern is the generalised, albeit non-significant, warming of the Arctic Sea. The possibility of model errors in the calculation of land temperatures or in the land–atmosphere interaction over the high latitudes is not excluded, and prompts towards a deeper exploration of the problem. Also, we note that the near-surface (and surface) temperature anomalies are distinctly more extended and statistically robust than the associated changes in radiative fluxes and low-level humidity, again hinting to a potential bias in surface temperature giving rise to consistent local atmospheric conditions. Nevertheless, because of the wide extent of the Eurasian anomalies with respect to those found over North America, the connection between North Eurasia warming and Tropical Amplification in the "warm Sib composite" constitutes a robust results of this analysis.

4.3 Storyline approach to climate projections

The last part of Chapter 4 is dedicated to the analysis of CMIP6 projections of the future climate (details on the dataset are provided in the Methods). In Chapter 3 and in Section 4.1 it is shown that land temperature - or land-induced changes in the land-sea thermal contrast - influence significantly the mid-latitude circulation, especially when the land warming or cooling is located in specific hotspots of land–atmosphere interaction. Hence, it is conceivable that land temperature may play a role in explaining the dynamical uncertainties detected in model projections of the future climate.

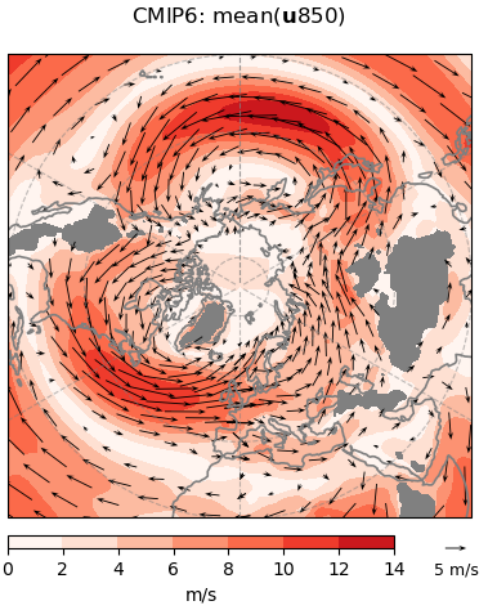

Figure 4.20: The MMM January-February climatology of the horizontal wind at 850 hPa in CMIP6 historical simulations 1860–1889. Arrows indicate the direction and intensity, shading again represents the intensity

The starting point is taken as the atmospheric circulation at the end of the XIX century, represented in Figure 4.20 in terms of the horizontal wind at 850 hPa. We focus here on the future model projections of the 850 hPa zonal wind, i.e. the difference between the end of the XXI ("future") and the end of the XIX century ("past"). In Figure 4.21, where the difference is scaled by global warming, the wind change per degree of global near-surface temperature increase is represented. The map displays the well-documented, zonally asymmetric northward shift of the eddy-driven jet, which is however scarcely significant because of the wide inter-model spread (see right panel of Figure 4.21 and Harvey et al., 2020).

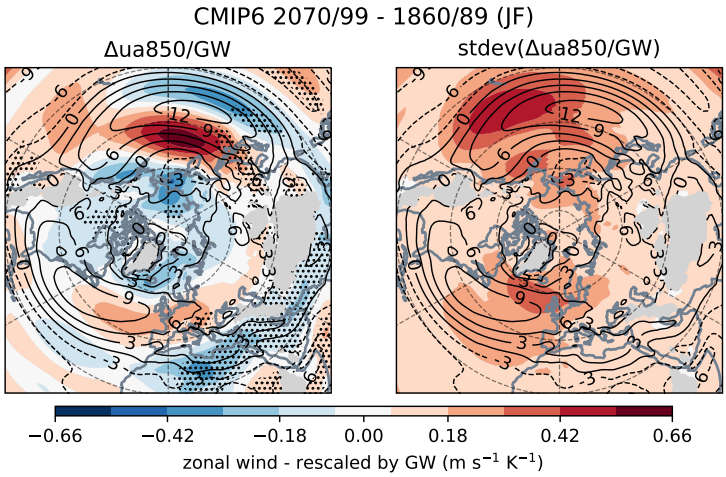

Figure 4.21: (Left) The MMM January-February projections of the horizontal wind at 850 hPa as the difference "future - past", with stippling representing the 95% significance level according to a two-sided t-test. (Right) The spread (standard deviations) among the different models. In contours the "past" MMM

Recently, a separation of the different factors driving the circulation changes across CMIP models has been attempted. The so-called "storyline approach", in the form introduced by Zappa and Shepherd (2017), takes advantage of the high number of models available within the CMIP framework to provide a range of plausible trajectories conditional on the occurrence of particular aspects of climate change. The main drivers of mid-latitude zonal wind uncertainty are identified based on existing knowledge of climate and of the internal interactions between its components (Manzini et al., 2014); an attempt to separate their influence on the large-scale atmospheric circulation by means of a multilinear regression across models was accomplished by Zappa and Shepherd (2017).

Our analysis is an extension of the work by Zappa and Shepherd (2017), following the example of Oudar et al. (2020), aiming to analyse the contribution of the future changes in land temperatures over East Asia to the uncertainty in the 850 hPa zonal wind projections. To the remote drivers of mid-latitude zonal wind changes identified in Manzini et al. (2014), i.e. Arctic Amplification, Tropical Amplification and stratospheric polar vortex, we add Siberia and Tibetan Plateau near-surface temperature (ΔtasSib and ΔtasTP).

4.3.1 Methods

The projections of the future winter climate are computed based on the CMIP6 scenario with highest radiative forcing by the end of the XXI century, identified as SSP585 for RCP8.5 global forcing pathway with SSP5 socioeconomic conditions (O'Neill et al., 2016). The zonal wind projections and the indices representing the changes in the drivers are computed based on the difference "future - past", where "future" corresponds to JF (January-February) in the period 2070–2099, "past" to JF the period 1860–1889. The estimate of global warming (GW) is based on the annual mean temperature.

The indices (or drivers) used in the analyses are:

- global warming (GW): annual warming in global mean near-surface temperature;
- Arctic Amplification (ΔAA): air temperature warming between 1000–700 hPa and 60–90° N;
- Tropical Amplification (ΔTA): air temperature warming between 400–150 hPa and 20° S–20° N;
- stratospheric polar vortex (ΔSPV): zonal-mean zonal wind change averaged between 250–30 hPa and 70–90° N;
- Siberian temperature (ΔtasSib): near-surface temperature warming over the region of Siberia (north-most box in Figure 4.2);
- Tibetan Plateau temperature (ΔtasTP): near-surface temperature warming over the Tibetan Plateau region (south-most box in Figure 4.2).

The first four indices follow the same definitions given by (Oudar et al., 2020).

For the multilinear regression we follow the approach by Zappa and Shepherd (2017). The wintertime 850 hPa zonal wind projection is expressed in terms of the drivers listed above.

Indicating with s a specific point of the longitude-latitude grid and the model with m:

$$(\Delta \mathrm{ua850}/\,GW)_{s,m} = a_s + b_{\mathrm{AA},s}\left(\frac{\Delta \mathrm{AA}}{GW}\right)_m + b_{\mathrm{TA},s}\left(\frac{\Delta \mathrm{TA}}{GW}\right)_m + b_{\mathrm{SPV},s}\left(\frac{\Delta \mathrm{SPV}}{GW}\right)_m + b_{\mathrm{LSCPac},s}\left(\frac{\Delta \mathrm{LSCPac}}{GW}\right)_m + b_{\mathrm{tasTP},s}\left(\frac{\Delta \mathrm{tasTP}}{GW}\right)_m + c_{s,m}$$

where the $b_{\mathrm{driver},s}$ are the regression coefficients associated with each driver, a_s is the intercept, and $c_{s,m}$ is the residual term. Even though the multiple linear regression does not imply causality between the drivers and the zonal wind projections, this method diagnoses the fraction of the inter-model spread associated with the selected indices. Furthermore, the drivers and the zonal wind projections are all scaled by global warming (GW), allowing a separation of the uncertainty due to the amplitude of global warming from the dynamical uncertainty (Zappa and Shepherd, 2017). The multilinear regression assumes independence between the explanatory variables (drivers); this is verified by computing the correlation coefficients between the indices (Table 4.2), which are generally low after scaling by GW.

4.3.2 Results

By comparing the regression of the zonal wind changes on the original drivers selected by Manzini et al. (2014) (Figure 4.22) with the equivalent in Zappa and Shepherd (2017) (Figure 3) and Oudar et al. (2020) (Figure 2), we observe a similar sensitivity of the eddy-driven

Table 4.2: Correlation coefficients between drivers of mid-latitude circulation changes: Arctic Amplification (ΔAA), Tropical Amplification (ΔTA), stratospheric polar vortex (ΔSPV), Siberian temperature (ΔtasSib), and Tibetan Plateau temperature (ΔtasTP). In the two bottom rows the MMM projection for each driver and the inter-model standard deviation around the MMM. The values in parenthesis are computed after scaling by global warming (GW)

Corr. coef.	ΔAA	ΔTA	ΔSPV	ΔtasSib	ΔtasTP	GW
ΔAA	-	0.84 (-0.10)	-0.38 (-0.27)	0.71 (0.09)	0.77 (-0.02)	0.90
ΔTA		-	-0.31 (0.02)	0.70 (0.05)	0.83 (0.21)	0.93
ΔSPV			-	-0.04 (0.38)	-0.21 (0.21)	-0.33
ΔtasSib				-	0.66 (0.24)	0.85
ΔtasTP					-	0.85
MMM	8.8 K	7.7 K	-1.8 m s^{-1}	9.4 K	6.4 K	4.7 K
stdev	1.9 K	1.4 K	1.6 m s^{-1}	1.8 K	1.1 K	0.9 K

jet to Tropical Amplification (i.e. a northward shift of the Pacific jet) and to strong SPV (i.e. a northerly shift of the annular jet). The main differences consist in the lack of the eastward extension of the Atlantic jet with Tropical Amplification and in the regression on Arctic Amplification, which does not display the continental signal over Eurasia shown in Zappa and Shepherd (2017) and Oudar et al. (2020), but exhibits significant patterns in the tropical regions. While the tropical component of the regression is probably a statistical artifact as it is unjustified in terms of causal connections (see also the low correlation between ΔTA and ΔAA in Table 4.2), the residual jet weakening over northern Europe and over the North Pacific sector is consistent with a thermal wind response to sea ice loss. The percentage of explained variance (last panel in Figure 4.22) also shows differences with respect to the previous studies, particularly over the North Atlantic sector, where the larger inter-model spread (Figure 4.21) is weakly explained by the three drivers. The divergences with respect to the multilinear regression in Figure 2 of Oudar et al. (2020), using the same indices and roughly the same periods to compute the projections, are likely attributable to the different model dataset (their 29 CMIP5 and 22 CMIP6 models against our 37 CMIP6 models) and to the choice of winter months (their ONDJFM against our JF).

The introduction of the Siberian warming among the drivers of 850 hPa zonal wind changes (bottom-left panel in Figure 4.23) is useful to explain the dynamical changes over the continent, as testified by the increase of explained variance (bottom-right panel in Figure 4.23). In this context is interesting to note the large amplitude of Siberian temperature changes with respect to global warming (Table 4.2). In the regression, amplified continental warming strengthens the circulation across North Eurasia; this is consistent with the dynamical effects of Siberian temperatures found in Section 4.2. However, unlike in the "Sib composites" of Section 4.2 where the Pacific sector was not significantly affected, the northern flank of the Pacific jet stream experiences a weakening associated with an intense high-latitude inland warming.

The Tibetan Plateau region (TP) is also a hotspot of winter global warming (cf. the MMM tasTP and GW in Table 4.2, see You et al., 2020). Within the multilinear regression framework, a strong TP near-surface temperature change induces a poleward shift of the Pacific eddy-driven jet (bottom-centre panel in Figure 4.23) and is close (but reversed in sign) to the

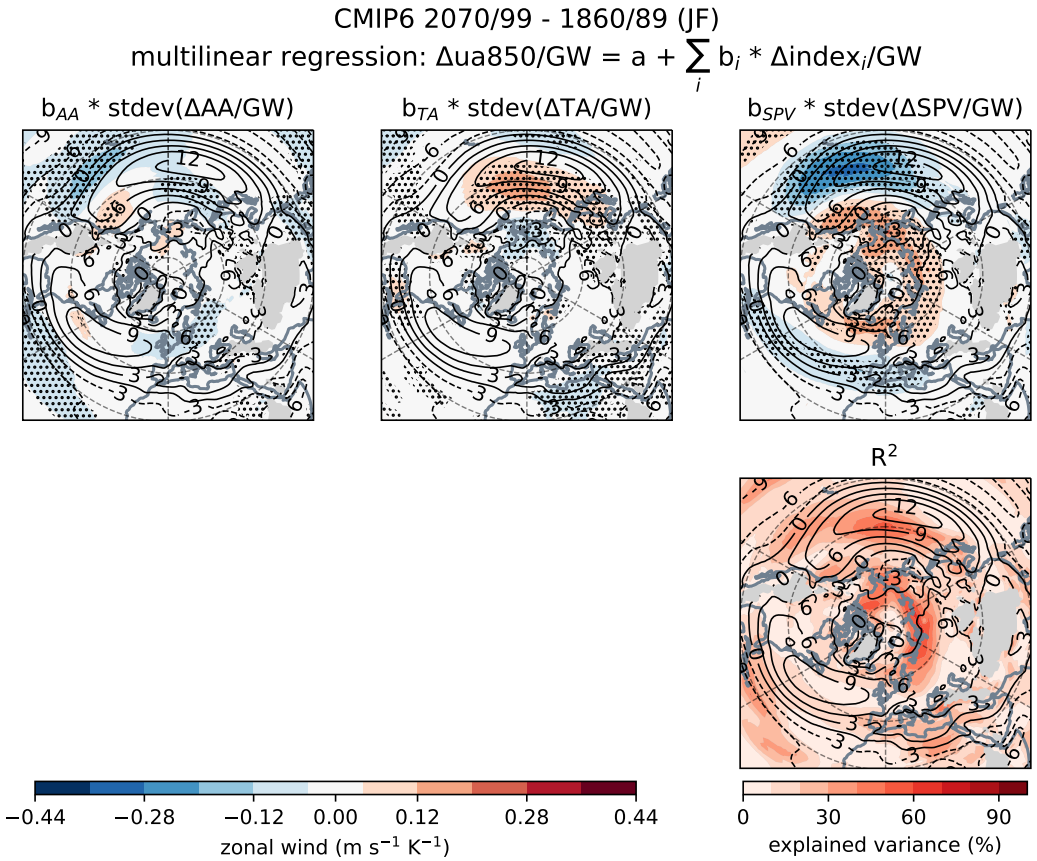

Figure 4.22: (Top) Multilinear regression (across models) of the January-February 850 hPa zonal wind projections (Δu850) on the indices of Arctic Amplification (ΔAA), Tropical Amplification (ΔTA) and stratospheric polar vortex strength (ΔSPV). The zonal wind and the indices are scaled by each models' global warming (GW). (Bottom) The inter-model variance explained by the multilinear regression. In stippling the 95% significance level according to a two-sided t-test, in contours the "past" MMM

response to TP cooling identified in Section 4.1. In comparison with the "cold TP composite" of Section 4.1 the regression extends further east, to most of the North Pacific basin - it is consistent with the idealised response to the cooling of East Asia orography by the AGCM SPEEDY in Figure 4.8(g) (reversed in sign). An additional easterly wind anomaly along the Eurasian continent at subtropical latitudes, which may be connected to a regional northward expansion of the Tropics or to the heating of the southern flank of the Tibetan Plateau, is detected in response to strong TP warming. Overall, the introduction of the Tibetan Plateau warming in the multilinear regression allows us to explain a greater fraction of 850 hPa zonal wind variance in the southern part of Eurasia and in the North Pacific sector (bottom-right panel in Figure 4.23). This is specially important in the entrance region of the Pacific jet, where the circulation uncertainty was poorly constrained even considering the additional drivers in

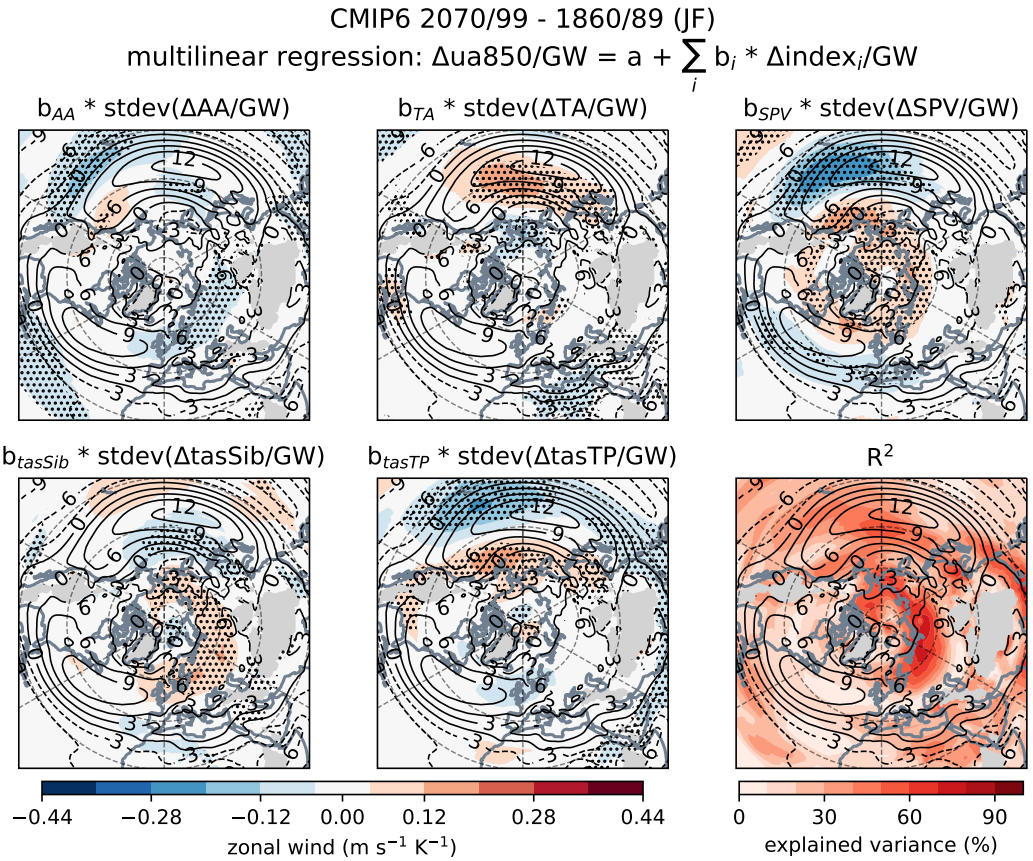

Figure 4.23: (Top and bottom) Multilinear regression (across models) of the January-February 850 hPa zonal wind projections (Δu850) on the indices of Arctic Amplification (ΔAA), Tropical Amplification (ΔTA), stratospheric polar vortex strength (ΔSPV), Siberian warming (ΔtasSib) and Tibetan Plateau warming (ΔtasTP). (Bottom-right) The inter-model variance explained by the multilinear regression. In stippling the 95% significance level according to a two-sided t-test, in contours the "past" MMM

Oudar et al. (2020), Figure 6.

In summary, we find that the application of Zappa and Shepherd's "storyline approach" to future winter climate projections using two new drivers representative of the changes in East Asia land temperatures allows us to constrain circulation changes over the Eurasian continent and over the North Pacific. In particular, models predicting a stronger warming in North Eurasia show a strengthening of the local low-level zonal winds and a weakening of the high-latitude Pacific jet. On the other hand, models with stronger Tibetan Plateau warming produce a northward jet shift and easterly wind anomalies to the south of the Asian orography. We note that the independent inclusion of the two additional drivers (ΔtasSib and ΔtasTP) in the regression produces the same circulation patterns obtained by considering both simultaneously.

Chapter 5

Conclusion

Summary

The response and interactions of the winter mid-latitude atmosphere with forcing by large scale continental temperature anomalies are investigated here.

In Chapter 3, motivated by the recent and projected decrease in winter land-sea thermal contrast (LSC) induced by a higher land warming rate, we devise a set of idealised experiments where the LSC is artificially reduced by prescribing warmer land conditions. An intermediate-complexity AGCM known as SPEEDY is used for the purpose. While in previous literature LSC was regarded as only a hemispheric-scale feature and its atmospheric influence was studied accordingly, here we differentiate between sectors (Pacific LSC reduced by Asia warming and Atlantic LSC by North America warming). Notwithstanding the similarity in the extension and intensity of the warming patterns over the two continents, the results indicate a clear dominance of the atmospheric response to the Pacific LSC reduction (i.e. to Asian warming). The Asian continent is ostensibly more important in setting thermal large-scale stationary waves - a particular sensitivity of wavenumber 1 perturbation is found. Its downstream interaction with orographic waves is mediated by the influence on the Pacific jet which, being strongly reduced and shifted poleward as a response to the warming of East Asia, weakens the orographic wave pattern over the Rocky mountains and North America.

The influence of the temperature conditions of Asia and North America on the large-scale tropospheric waves also changes the vertical wave propagation to the stratosphere. In the case of Asian and combined (Asia + North America) thermal forcing, wavenumber 1 and 2 are reduced up to the stratosphere and this results in a stronger stratospheric polar vortex (SPV); North America warming, which produces a strengthening of wavenumber 1 and a weakening of wavenumber 2, is associated with a slower SPV. The SPV anomalies eventually project on the mean tropospheric conditions below.

In Chapter 4, by analysing the historical simulations from a large set of state-of-the-art climate models participating in CMIP6, we find a strong inter-model variability in the representation of winter temperatures over mid- and high-latitude land extensions. East Asia, identified in the previous chapter for its strong impact on the mid-latitude atmosphere, is characterised by two hotspots of inter-model temperature spread:

1. the Tibetan Plateau, where the modelling of the surface and low-level energy budget is made difficult by the presence of complex orography. The region is reported to be affected by a cold bias in the majority of climate models;

2. North Eurasia (Siberia in particular), where the surface temperature and the local low-level atmospheric conditions are usually tightly interconnected, because of feedbacks between the longwave radiation and the low-level water content.

Based on a comparison between an analysis of the CMIP6 model climatologies and idealised simulations (run with SPEEDY using prescribed surface conditions), we find a strong influence of cold Tibetan Plateau winter conditions on the atmospheric circulation over East Asia and the Pacific Ocean. The cold bias over the orography is advected downstream, where an intensified baroclinicity increases the strength of the East Asia winter monsoon, hence of the jet stream over the East China Sea. Based on results of the idealised simulations, we are able to show that the intensification of the low-level jet in this region is induced by a positive signal in the eddy momentum deposition.

Across the CMIP6 ensemble winter Siberian temperatures are shown to be linked with the low-

level conditions, in that anomalously warm temperatures are associated with excess moisture trapping longwave radiation in the lower part of the atmosphere. By analysing a warm and a cold composite based on Siberian climatological conditions across CMIP6 models, warm conditions appear to be related to a Tropical Amplification-like signal inducing anomalous moisture transport into Eurasia, while cold conditions co-occur with anomalously high mid- and high-latitude cloud cover. The causal connection between cloud cover and high-latitude temperature anomalies cannot be identified in the present study; we intend to investigate the topic further by considering the high-frequency variability on a limited selection of climate models.

The Siberian composites also show a strengthening (weakening) of the zonal winds north of the Tibetan Plateau in response to high-latitude warming (cooling), or equivalently to a decline (intensification) of the high-latitude inversion layer. However, we notice a different atmospheric signal depending on the latitude and elevation of the temperature anomalies. While high-latitude anomalies are restricted to the lower atmospheric levels, the warm Siberia pattern, extending southwards to Central Asia orography and to a small section of the Pacific basin, is associated with a deep atmospheric response, coinciding with an upper level expansion of the air column. No robust signal is detected over the Pacific basin, downstream of Siberia, indicating a low relevance of winter high-latitude Asian temperatures for the Pacific jet and circulation.

The results for both cold and warm Siberia composites support the idea that the origin of the local temperature spread is unrelated to the Atlantic jet or to the NAO / NAM patterns (otherwise associated with the interannual variability of observed winter Siberian temperature conditions) and has weak downstream impacts. The inter-model temperature biases may originate from mis-representations in other regions of the globe (e.g. the Tropics and Extratropics, which eventually affect the transport of moisture into the region), or even from high uncertainty in the modelling of the local surface temperature.

The role of Tibetan Plateau and Siberia temperature patterns in determining dynamical uncertainties in model projections of the future climate is also analysed. By computing a multilinear

regression across the same set of CMIP6 models, we show that the models featuring strongest warming over Siberia present an intensification of the continental low-level winds, while an enhanced temperature increase in the Tibetan Plateau region is associated with a poleward shift of the eddy-driven jet. These features are consistent with the outcomes of the study of the CMIP6 historical simulations.

General Outlook

An interesting theme arising from the results of Chapters 3 and 4 is that of the role of the orographic elevation of the thermal anomalies in determining the amplitude and extension of the tropospheric response. As shown in the works by Hoskins and Karoly (1981) and Trenberth (1983), the vertical distribution of mid-latitude heat sources is critical in determining the amplitude of the response, which increases as the heating is shifted towards the mid troposphere. This and the dependence of the temperature pattern on the interaction of the mean flow with mountain barriers, support the non-linearity of the atmospheric response to surface thermal forcing and orographic (intended as mechanical) forcing (Chang, 2009). Ringler and Cook (1999) show that the stationary wave generated by an isolated orographic feature suggestive of the Tibetan Plateau embedded in the average 33° N winds is reinforced by the superposition of a winter-like low-level cooling (low-level with respect to the elevated surface). Furthermore, the atmospheric response is non-linear in that it is greater than the sum of the responses to individual thermal and orographic forcing. Conversely, the wave response is reduced when a warming pattern is imposed over the orography. See Trenberth (1983) for an analytic treatment of the interaction between thermal and orographic (mechanical) forcing and of the dependence of the response on the phase difference between the forcings.

In light of this, the stronger stationary response to Asian than to North American warming in Chapter 3 and the importance of Tibetan Plateau cooling for the downstream circulation patterns in CMIP6 models shown in Chapter 4 are naturally attributable to the interaction with the orography, which raises the warming and cooling patterns to higher elevations. This

statement is based on the theoretical and idealised modelling studies to which we refer above, and are not based on a systematic evaluation of the role of the elevation in the response to a geographically confined low-level thermal forcing. A similar conclusion was given by Gong et al. (2003b, 2004) to motivate the high sensitivity of the winter atmospheric state to autumn snow anomalies in southern Siberia (e.g. Cohen et al., 2014). Basing their reasoning on the importance of Asian orography for the vertical wave connection between troposphere and stratosphere, they show that snow-related atmospheric anomalies in a Siberian region encircled by lower mountain ranges than those effectively present fail to propagate in the vertical direction and do not determine the classical negative AO response (Gong et al., 2003a).

The idea brought forward by Gong and co-authors, together with the theoretical studies by Trenberth (1983) and Ringler and Cook (1999), explain why the Asian continent can be considered as an amplifier of land–atmosphere interaction. The proximity to the Pacific basin (and on its jet) potentially extends the impacts of the interactions far downstream. Our analysis in Chapter 3 and the work by Henderson et al. (2013) use a similar approach to compare the influence of mid- and high-latitude anomalies over Asia and North America (considering temperature in the former and snow in the latter as surface forcing). The results of the two works, showing a strong response to surface forcing over Asia, which is not equaled neither in scale nor in intensity by the response to North America surface forcing, fit perfectly with the perspective of regionally and orographically dependent amplification of land–atmosphere interaction.

The presence of an extended mountain range on the North American continent - the Rockies - questions this interpretation. The idealised simulations by Ringler and Cook (1999) and the findings by Held and Ting (1990) solve this point by indicating that the tilt and structure of the Rockies and the intense mean flow impinging on the mountains determine a strong wave response which is mostly orographic. The elevated heat sink appears to be more relevant for the downstream temperature field more than for the structure and intensity of the atmospheric wave. The position of the Rockies with respect to the mid-latitude jet structures (downstream of the Pacific jet and far upstream of the Atlantic jet) is thus expected to play a role in the orography–heating interaction.

Future Work

To conclude the discussion started in the previous Section, we believe it would be of wide interest to study the sensitivity of the atmosphere to regionally confined thermal anomalies over Asia. While this has been done relative to snow anomalies (Luo and Wang, 2019) and to orography (White et al., 2017), we are not aware of works systematically treating the role of low-level thermal sources and sinks located on different mountain chains of Central-East Asia, and the importance of elevation in setting the atmospheric response. This may be relevant in the context of Climate Change projections and Paleoclimate simulations.

In fact, the sensitivity of the atmosphere to regionally varying land warming is particularly important when talking of climate projections. As demonstrated in Section 4.3, land-sea thermal contrast and land warming may be relevant, in some regions more than others, for understanding the dynamical response of the atmospheric system to anthropogenic emissions of greenhouse gases.

In the idealised experiments run with the model SPEEDY, used to understand the atmospheric response to surface temperature anomalies over the mid-latitude continents (in Chapter 3) and over the Tibetan Plateau (in Section 4.1), the surface conditions are prescribed. This precludes a two-way interaction between surface conditions (over land or sea) and the atmosphere. We consider the possibility of running short-term experiments using an ensemble with similarly perturbed initial land conditions and freely evolving surface temperature, or alternatively long-term experiments with prescribed land temperature and an active ocean model. Approaches of this type would allow to delve deeper in the complexity of the feedbacks between the atmosphere and the surface conditions.

Glossary

AGCM atmospheric general circulation model.

AO Arctic Oscillation.

CGCM coupled general circulation model.

CMIP6 Coupled Model Intercomparison Project - Phase 6.

LHS left hand side.

LSC land-sea thermal contrast.

LST land surface temperature.

MEMF meridional eddy momentum convergence.

MMM CMIP6 multi-model mean.

MP Mongolian Plateau.

NAM Northern Annular Mode.

NAO North Atlantic Oscillation.

NH Northern Hemisphere.

RHS right hand side.

Sib Siberia.

SPEEDY Simplified Parametrization, primitivE-Equation DYnamics, an intermediate complexity AGCM developed by the International Centre for Theoretical Physics (ICTP).

SPV stratospheric polar vortex.

SST sea surface temperature.

TP Tibetan Plateau.

Bibliography

D. G. Andrews, J. R. Holton, and C. B. Leovy. *Middle atmosphere dynamics*. Number 40. Academic press, 1987. 9, 49

B. Ayarzagüena, E. Manzini, N. Calvo, and D. Matei. Interaction between decadal-to-multidecadal oceanic variability and sudden stratospheric warmings. *Annals of the New York Academy of Sciences*, 2021. 61

M. P. Baldwin and T. J. Dunkerton. Propagation of the arctic oscillation from the stratosphere to the troposphere. *Journal of Geophysical Research: Atmospheres*, 104(D24):30937–30946, 1999. 30, 58, 92

E. A. Barnes and L. Polvani. Response of the midlatitude jets, and of their variability, to increased greenhouse gases in the cmip5 models. *Journal of Climate*, 26(18):7117–7135, 2013. 62, 101

A. G. Barnston and R. E. Livezey. Classification, seasonality and persistence of low-frequency atmospheric circulation patterns. *Monthly weather review*, 115(6):1083–1126, 1987. 92

B. Bell, H. Hersbach, A. Simmons, P. Berrisford, P. Dahlgren, A. Horányi, J. Muñoz-Sabater, J. Nicolas, R. Radu, D. Schepers, et al. The era5 global reanalysis: Preliminary extension to 1950. *Quarterly Journal of the Royal Meteorological Society*, 147(741):4186–4227, 2021. 95

A. K. Betts, J. H. Ball, A. C. Beljaars, M. J. Miller, and P. A. Viterbo. The land surface-atmosphere interaction: A review based on observational and global modeling perspectives. *Journal of Geophysical Research: Atmospheres*, 101(D3):7209–7225, 1996. 27

R. Blackport and J. A. Screen. Insignificant effect of arctic amplification on the amplitude of midlatitude atmospheric waves. *Science advances*, 6(8):eaay2880, 2020. 34

J. A. Boffi. Effect of the andes mountains on the general circulation over the southern part of south america. *Bulletin of the American Meteorological Society*, 30(7):242–247, 1949. 3

B. Bolin. On the influence of the earth's orography on the general character of the westerlies. *Tellus*, 2(3):184–195, 1950. 3, 72

S. Bony, R. Colman, V. M. Kattsov, R. P. Allan, C. S. Bretherton, J.-L. Dufresne, A. Hall, S. Hallegatte, M. M. Holland, W. Ingram, et al. How well do we understand and evaluate climate change feedback processes? *Journal of Climate*, 19(15):3445–3482, 2006. 91

G. Branstator. Organization of storm track anomalies by recurring low-frequency circulation anomalies. *Journal of the atmospheric sciences*, 52(2):207–226, 1995. 25

D. J. Brayshaw, B. Hoskins, and M. Blackburn. The basic ingredients of the north atlantic storm track. part i: Land–sea contrast and orography. *Journal of the Atmospheric Sciences*, 66(9):2539–2558, 2009. 33, 53, 60

A. J. Broccoli and S. Manabe. The effects of orography on midlatitude northern hemisphere dry climates. *Journal of Climate*, 5(11):1181–1201, 1992. 72

A. H. Butler, D. W. Thompson, and R. Heikes. The steady-state atmospheric circulation response to climate change–like thermal forcings in a simple general circulation model. *Journal of Climate*, 23(13):3474–3496, 2010. 58, 62, 101

J. C. Chan and C. Li. The east asia winter monsoon. In *East Asian Monsoon*, pages 54–106. World Scientific, 2004. 73

E. K. Chang. Downstream development of baroclinic waves as inferred from regression analysis. *Journal of the atmospheric sciences*, 50(13):2038–2053, 1993. 54

E. K. Chang. Diabatic and orographic forcing of northern winter stationary waves and storm tracks. *Journal of climate*, 22(3):670–688, 2009. 21, 25, 43, 53, 117

E. K. Chang, S. Lee, and K. L. Swanson. Storm track dynamics. *Journal of climate*, 15(16): 2163–2183, 2002. 25

W. C. Chao and B. Chen. The origin of monsoons. *Journal of the Atmospheric Sciences*, 58 (22):3497–3507, 2001. 29

J. G. Charney and J. G. DeVore. Multiple flow equilibria in the atmosphere and blocking. *Journal of Atmospheric Sciences*, 36(7):1205–1216, 1979. 33, 60

J. G. Charney and P. G. Drazin. Propagation of planetary-scale disturbances from the lower into the upper atmosphere. *Journal of Geophysical Research (1896-1977)*, 66(1):83–109, 1961. doi: https://doi.org/10.1029/JZ066i001p00083. 15, 49, 92

J. G. Charney and A. Eliassen. A numerical method for predicting the perturbations of the middle latitude westerlies. *Tellus*, 1(2):38–54, 1949. 3, 8, 16, 17, 21

X. Chen, Y. Liu, and G. Wu. Understanding the surface temperature cold bias in cmip5 agcms over the tibetan plateau. *Advances in Atmospheric Sciences*, 34(12):1447–1460, 2017. 75, 80

Z. Chen, R. Wu, and Z. Wang. Impact of autumn-winter tibetan plateau snow cover anomalies on the east asian winter monsoon and its interdecadal change. *Frontiers in Earth Science*, 9:569, 2021. 30, 74

A. Chernokulsky, I. I. Mokhov, and N. Nikitina. Winter cloudiness variability over northern eurasia related to the siberian high during 1966–2010. *Environmental Research Letters*, 8(4): 045012, 2013. 91

M. P. Clark and M. C. Serreze. Effects of variations in east asian snow cover on modulating atmospheric circulation over the north pacific ocean. *Journal of Climate*, 13(20):3700–3710, 2000. 74, 76, 92

J. Cohen and D. Entekhabi. Eurasian snow cover variability and northern hemisphere climate predictability. *Geophysical Research Letters*, 26(3):345–348, 1999. 91, 92

J. Cohen and D. Rind. The effect of snow cover on the climate. *Journal of Climate*, 4(7): 689–706, 1991. 30

J. Cohen, K. Saito, and D. Entekhabi. The role of the siberian high in northern hemisphere climate variability. *Geophysical Research Letters*, 28(2):299–302, 2001. 45, 79, 90, 92

J. Cohen, M. Barlow, P. J. Kushner, and K. Saito. Stratosphere–troposphere coupling and links with eurasian land surface variability. *Journal of Climate*, 20(21):5335–5343, 2007. 92

J. Cohen, J. C. Furtado, J. Jones, M. Barlow, D. Whittleston, and D. Entekhabi. Linking siberian snow cover to precursors of stratospheric variability. *Journal of Climate*, 27(14): 5422–5432, 2014. 30, 61, 74, 92, 118

J. Cohen, X. Zhang, J. Francis, T. Jung, R. Kwok, J. Overland, T. Ballinger, U. Bhatt, H. Chen, D. Coumou, et al. Divergent consensuses on arctic amplification influence on midlatitude severe winter weather. *Nature Climate Change*, 10(1):20–29, 2020. 34

J. Curry. On the formation of continental polar air. *Journal of the Atmospheric Sciences*, 40 (9):2278–2292, 1983. 102

J. Curry and G. Herman. Relationships between large-scale heat and moisture budgets and the occurrence of arctic stratus clouds. *Monthly weather review*, 113(9):1441–1457, 1985. 97

J. Curry, J. Schramm, M. Serreze, and E. Ebert. Water vapor feedback over the arctic ocean. *Journal of Geophysical Research: Atmospheres*, 100(D7):14223–14229, 1995. 91

J. A. Curry, J. L. Schramm, W. B. Rossow, and D. Randall. Overview of arctic cloud and radiation characteristics. *Journal of Climate*, 9(8):1731–1764, 1996. 91, 97

A. Czaja, C. Frankignoul, S. Minobe, and B. Vannière. Simulating the midlatitude atmospheric circulation: what might we gain from high-resolution modeling of air-sea interactions? *Current Climate Change reports*, 5(4):390–406, 2019. 27

J. J. Day and K. I. Hodges. Growing land-sea temperature contrast and the intensification of arctic cyclones. *Geophysical Research Letters*, 45(8):3673–3681, 2018. 34

H. de Vries, R. J. Haarsma, and W. Hazeleger. Western european cold spells in current and future climate. *Geophysical Research Letters*, 39(4), 2012. 34

A. Díaz-Durán, E. Serrano, B. Ayarzagüena, M. Abalos, and A. de la Cámara. Intra-seasonal variability of extreme boreal stratospheric polar vortex events and their precursors. *Climate Dynamics*, 49(9):3473–3491, 2017. 49

Y. Ding and T. N. Krishnamurti. Heat budget of the siberian high and the winter monsoon. *Monthly Weather Review*, 115(10):2428–2449, 1987. 91

D. I. Domeisen, A. H. Butler, A. J. Charlton-Perez, B. Ayarzagüena, M. P. Baldwin, E. Dunn-Sigouin, J. C. Furtado, C. I. Garfinkel, P. Hitchcock, A. Y. Karpechko, et al. The role of the stratosphere in subseasonal to seasonal prediction: 2. predictability arising from stratosphere-troposphere coupling. *Journal of Geophysical Research: Atmospheres*, 125(2):e2019JD030923, 2020. 61

S. Drijfhout, G. J. Van Oldenborgh, and A. Cimatoribus. Is a decline of amoc causing the warming hole above the north atlantic in observed and modeled warming patterns? *Journal of Climate*, 25(24):8373–8379, 2012. 34

M. Drouard, G. Rivière, and P. Arbogast. The link between the north pacific climate variability and the north atlantic oscillation via downstream propagation of synoptic waves. *Journal of Climate*, 28(10):3957–3976, 2015. 43

A. Duan and G. Wu. Weakening trend in the atmospheric heat source over the tibetan plateau during recent decades. part i: Observations. *Journal of Climate*, 21(13):3149–3164, 2008. 73

T. Estilow, A. Young, and D. Robinson. A long-term northern hemisphere snow cover extent data record for climate studies and monitoring. *Earth System Science Data Discussions*, 7 (2), 2014. 93

X. Fan, C. Miao, Q. Duan, C. Shen, and Y. Wu. The performance of cmip6 versus cmip5 in simulating temperature extremes over the global land surface. *Journal of Geophysical Research: Atmospheres*, 125(18):e2020JD033031, 2020. 75, 88

C. I. Garfinkel, D. L. Hartmann, and F. Sassi. Tropospheric precursors of anomalous northern hemisphere stratospheric polar vortices. *Journal of Climate*, 23(12):3282–3299, 2010. 74

C. I. Garfinkel, I. White, E. P. Gerber, M. Jucker, and M. Erez. The building blocks of northern hemisphere wintertime stationary waves. *Journal of Climate*, 33(13):5611–5633, 2020. 33, 60

G. Gong, D. Entekhabi, and J. Cohen. Modeled northern hemisphere winter climate response to realistic siberian snow anomalies. *Journal of Climate*, 16(23):3917–3931, 2003a. 30, 92, 118

G. Gong, D. Entekhabi, and J. Cohen. Relative impacts of siberian and north american snow anomalies on the winter arctic oscillation. *Geophysical Research Letters*, 30(16), 2003b. 118

G. Gong, D. Entekhabi, and J. Cohen. Orographic constraints on a modeled siberian snow–tropospheric–stratospheric teleconnection pathway. *Journal of Climate*, 17(6):1176–1189, 2004. 30, 118

H. Gong, L. Wang, W. Chen, R. Wu, K. Wei, and X. Cui. The climatology and interannual variability of the east asian winter monsoon in cmip5 models. *Journal of Climate*, 27(4): 1659–1678, 2014. 74

H. Goosse, J. E. Kay, K. C. Armour, A. Bodas-Salcedo, H. Chepfer, D. Docquier, A. Jonko, P. J. Kushner, O. Lecomte, F. Massonnet, et al. Quantifying climate feedbacks in polar regions. *Nature communications*, 9(1):1–13, 2018. 90, 91

R. G. Graversen and M. Burtu. Arctic amplification enhanced by latent energy transport of atmospheric planetary waves. *Quarterly Journal of the Royal Meteorological Society*, 142 (698):2046–2054, 2016. 47

J. M. Gregory and J. Mitchell. Simulation of daily variability of surface temperature and precipitation over europe in the current and 2× co2 climates using the ukmo climate model. *Quarterly Journal of the Royal Meteorological Society*, 121(526):1451–1476, 1995. 34

P. Y. Groisman, R. S. Bradley, and B. Sun. The relationship of cloud cover to near-surface temperature and humidity: Comparison of gcm simulations with empirical data. *Journal of Climate*, 13(11):1858–1878, 2000. 90, 91

D. G. Hahn and S. Manabe. The role of mountains in the south asian monsoon circulation. *Journal of the Atmospheric Sciences*, 32(8):1515–1541, 1975. 72, 73

A. Haklander, P. Siegmund, and H. Kelder. Interannual variability of the stratospheric wave driving during northern winter. *Atmospheric Chemistry and Physics*, 7(10):2575–2584, 2007. 49

A. Hall, P. Cox, C. Huntingford, and S. Klein. Progressing emergent constraints on future climate change. *Nature Climate Change*, 9(4):269–278, 2019. 89

N. M. Hall, J. Derome, and H. Lin. The extratropical signal generated by a midlatitude sst anomaly. part i: Sensitivity at equilibrium. *Journal of Climate*, 14(9):2035–2053, 2001. 24, 25

M. E. Hamouda, C. Pasquero, and E. Tziperman. Decoupling of the arctic oscillation and north atlantic oscillation in a warmer climate. *Nature Climate Change*, 11(2):137–142, 2021. 62

B. Harvey, P. Cook, L. Shaffrey, and R. Schiemann. The response of the northern hemisphere storm tracks and jet streams to climate change in the cmip3, cmip5, and cmip6 climate models. *Journal of Geophysical Research: Atmospheres*, 125(23):e2020JD032701, 2020. 62, 107

K. F. Haualand and T. Spengler. Relative importance of tropopause structure and diabatic heating for baroclinic instability. *Weather and Climate Dynamics Discussions*, 2021: 1–28, 2021. doi: 10.5194/wcd-2021-13. URL `https://wcd.copernicus.org/preprints/wcd-2021-13/`. 58

Y. He, J. Huang, and M. Ji. Impact of land–sea thermal contrast on interdecadal variation in circulation and blocking. *Climate dynamics*, 43(12):3267–3279, 2014. 34

Y. He, J. Huang, D. Li, Y. Xie, G. Zhang, Y. Qi, S. Wang, and S. Totz. Comparison of the effect of land-sea thermal contrast on interdecadal variations in winter and summer blockings. *Climate Dynamics*, 51(4):1275–1294, 2018. 34

I. M. Held. Stationary and quasi-stationary eddies in the extratropical troposphere: Theory. *Large-scale dynamical processes in the atmosphere*, 127:168, 1983. xiii, 18, 21, 33, 34, 45, 46, 60

I. M. Held and M. Ting. Orographic versus thermal forcing of stationary waves: The importance of the mean low-level wind. *Journal of Atmospheric Sciences*, 47(4):495–500, 1990. 21, 33, 34, 45, 46, 54, 73, 84, 106, 118

I. M. Held, B. J. Soden, et al. Water vapor feedback and global warming. *Annual review of energy and the environment*, 25(1):441–475, 2000. 91, 97

I. M. Held, M. Ting, and H. Wang. Northern winter stationary waves: Theory and modeling. *Journal of climate*, 15(16):2125–2144, 2002. xiv, 21, 24, 25, 26, 33, 34, 35, 43, 54, 60, 99

G. R. Henderson, D. J. Leathers, and B. Hanson. Circulation response to eurasian versus north american anomalous snow scenarios in the northern hemisphere with an agcm coupled to a slab ocean model. *Journal of climate*, 26(5):1502–1515, 2013. 118

G. R. Henderson, Y. Peings, J. C. Furtado, and P. J. Kushner. Snow–atmosphere coupling in the northern hemisphere. *Nature Climate Change*, 8(11):954–963, 2018. 30, 67, 92

I. Herceg-Bulić, B. Mezzina, F. Kucharski, P. Ruggieri, and M. P. King. Wintertime enso influence on late spring european climate: the stratospheric response and the role of north atlantic sst. *International Journal of Climatology*, 37:87–108, 2017. 36

H. Hersbach, B. Bell, P. Berrisford, S. Hirahara, A. Horányi, J. Muñoz-Sabater, J. Nicolas, C. Peubey, R. Radu, D. Schepers, et al. The era5 global reanalysis. *Quarterly Journal of the Royal Meteorological Society*, 146(730):1999–2049, 2020a. 41

H. Hersbach, B. Bell, P. Berrisford, S. Hirahara, A. Horányi, J. Muñoz-Sabater, J. Nicolas, C. Peubey, R. Radu, D. Schepers, et al. The era5 global reanalysis. *Quarterly Journal of the Royal Meteorological Society*, 146(730):1999–2049, 2020b. 95

J. Holton and G. Hakim. An introduction to dynamic meteorology. waltham, ma, 2013. 10, 24, 99, 100

B. J. Hoskins and D. J. Karoly. The steady linear response of a spherical atmosphere to thermal and orographic forcing. *Journal of the atmospheric sciences*, 38(6):1179–1196, 1981. xiv, 22, 23, 24, 74, 117

B. J. Hoskins and M. J. Rodwell. A model of the asian summer monsoon. part i: The global scale. *Journal of Atmospheric Sciences*, 52(9):1329–1340, 1995. 29

B. J. Hoskins and P. J. Valdes. On the existence of storm-tracks. *Journal of Atmospheric Sciences*, 47(15):1854–1864, 1990. 25, 33, 42, 88

B. J. Hoskins, I. N. James, and G. H. White. The shape, propagation and mean-flow interaction of large-scale weather systems. *Journal of Atmospheric Sciences*, 40(7):1595–1612, 1983. 88

D. Hotta and H. Nakamura. On the significance of the sensible heat supply from the ocean in the maintenance of the mean baroclinicity along storm tracks. *Journal of Climate*, 24(13): 3377–3401, 2011. 82

Q. Hu, W. Hua, K. Yang, J. Ming, P. Ma, Y. Zhao, and G. Fan. An assessment of temperature simulations by cmip6 climate models over the tibetan plateau and differences with cmip5 climate models. *Theoretical and Applied Climatology*, 148(1):223–236, 2022. 75

J. W. Hurrell. Decadal trends in the north atlantic oscillation: Regional temperatures and precipitation. *Science*, 269(5224):676–679, 1995. 92

J. W. Hurrell, Y. Kushnir, G. Ottersen, and M. Visbeck. An overview of the north atlantic oscillation. *Geophysical Monograph-American Geophysical Union*, 134:1–36, 2003. 92, 103, 104

M. Inatsu, H. Mukougawa, and S.-P. Xie. Atmospheric response to zonal variations in midlatitude sst: Transient and stationary eddies and their feedback. *Journal of climate*, 16(20): 3314–3329, 2003. 27

J. Intrieri, C. Fairall, M. Shupe, P. Persson, E. Andreas, P. Guest, and R. Moritz. An annual cycle of arctic surface cloud forcing at sheba. *Journal of Geophysical Research: Oceans*, 107 (C10):SHE–13, 2002. 91

IPCC-*WGI. Climate Change 2021: The Physical Science Basis. Contribution of Working Group I to the Sixth Assessment Report of the Intergovernmental Panel on Climate Change.* Cambridge University Press. In press., 2021. 34, 40, 62

I. N. James and U. Burkhardt. A sidelong look at storm tracks. *Atmospheric Science Letters*, 7(3):69–74, 2006. 54

Y. Kamae, M. Watanabe, M. Kimoto, and H. Shiogama. Summertime land–sea thermal contrast and atmospheric circulation over east asia in a warming climate—part i: Past changes and future projections. *Climate dynamics*, 43(9-10):2553–2568, 2014. 34

Y. Kaspi and T. Schneider. Winter cold of eastern continental boundaries induced by warm ocean waters. *Nature*, 471(7340):621–624, 2011. 25, 43, 60

Y. Kaspi and T. Schneider. The role of stationary eddies in shaping midlatitude storm tracks. *Journal of the atmospheric sciences*, 70(8):2596–2613, 2013. 25

P. Keil, T. Mauritsen, J. Jungclaus, C. Hedemann, D. Olonscheck, and R. Ghosh. Multiple drivers of the north atlantic warming hole. *Nature Climate Change*, 10(7):667–671, 2020. 41

E. Kharyutkina, I. Ippolitov, and S. Loginov. The variability of radiative balance elements and air temperature over the asian region of russia. *Biogeosciences*, 9(3):1113–1123, 2012. 91

J. Kidston, A. A. Scaife, S. C. Hardiman, D. M. Mitchell, N. Butchart, M. P. Baldwin, and L. J. Gray. Stratospheric influence on tropospheric jet streams, storm tracks and surface weather. *Nature Geoscience*, 8(6):433–440, 2015. 30, 58

M. P. King, F. Kucharski, and F. Molteni. The roles of external forcings and internal variabilities in the northern hemisphere atmospheric circulation change from the 1960s to the 1990s. *Journal of climate*, 23(23):6200–6220, 2010. 36

F. Kucharski, F. Molteni, and A. Bracco. Decadal interactions between the western tropical pacific and the north atlantic oscillation. *Climate dynamics*, 26(1):79–91, 2006. 35, 77

F. Kucharski, F. Molteni, M. P. King, R. Farneti, I.-S. Kang, and L. Feudale. On the need of intermediate complexity general circulation models: A "speedy" example. *Bulletin of the American Meteorological Society*, 94(1):25–30, 2013. 35, 62, 77

Y. Kushnir, W. Robinson, I. Bladé, N. Hall, S. Peng, and R. Sutton. Atmospheric gcm response to extratropical sst anomalies: Synthesis and evaluation. *Journal of Climate*, 15(16):2233–2256, 2002. 24, 27, 45

Z. Labe, Y. Peings, and G. Magnusdottir. Warm arctic, cold siberia pattern: role of full arctic amplification versus sea ice loss alone. *Geophysical Research Letters*, 47(17):e2020GL088583, 2020. 34

M. Langer, S. Westermann, S. Muster, K. Piel, and J. Boike. The surface energy balance of a polygonal tundra site in northern siberia–part 2: Winter. *The Cryosphere*, 5(2):509–524, 2011. 90, 91

N.-C. Lau. The observed structure of tropospheric stationary waves and the local balances of vorticity and heat. *Journal of Atmospheric Sciences*, 36(6):996–1016, 1979. 99

N.-C. Lau and E. O. Holopainen. Transient eddy forcing of the time-mean flow as identified by geopotential tendencies. *Journal of the Atmospheric Sciences*, 41(3):313–328, 1984. 25

J. Li, C. Miao, W. Wei, G. Zhang, L. Hua, Y. Chen, and X. Wang. Evaluation of cmip6 global climate models for simulating land surface energy and water fluxes during 1979–2014. *Journal of Advances in Modeling Earth Systems*, 13(6):e2021MS002515, 2021. 75

W. Li, W. Guo, B. Qiu, Y. Xue, P.-C. Hsu, and J. Wei. Influence of tibetan plateau snow cover on east asian atmospheric circulation at medium-range time scales. *Nature communications*, 9(1):1–9, 2018. 30, 74, 89

Y. Li and N.-C. Lau. Impact of enso on the atmospheric variability over the north atlantic in late winter—role of transient eddies. *Journal of Climate*, 25(1):320–342, 2012. 54

A. Liu, Y. Huang, and D. Huang. Inter-model spread of the simulated winter surface air temperature over the eurasian continent and the physical linkage to the jet streams from the

cmip6 models. *Journal of Geophysical Research: Atmospheres*, page e2022JD037172, 2022. 80

L. Liu, W. Zhang, Q. Lu, and G. Wang. Variations in the sensible heating of tibetan plateau and related effects on atmospheric circulation over south asia. *Asia-Pacific Journal of Atmospheric Sciences*, 57(3):499–510, 2021. 74

S. Liu, Q. Wu, X. Ren, Y. Yao, S. R. Schroeder, and H. Hu. Modeled northern hemisphere autumn and winter climate responses to realistic tibetan plateau and mongolia snow anomalies. *Journal of Climate*, 30(23):9435–9454, 2017. 30

Y. Lun, L. Liu, L. Cheng, X. Li, H. Li, and Z. Xu. Assessment of gcms simulation performance for precipitation and temperature from cmip5 to cmip6 over the tibetan plateau. *International Journal of Climatology*, 41(7):3994–4018, 2021. 75

X. Luo and B. Wang. Predictability and prediction of the total number of winter extremely cold days over china. *Climate dynamics*, 50(5):1769–1784, 2018. 92

X. Luo and B. Wang. How autumn eurasian snow anomalies affect east asian winter monsoon: A numerical study. *Climate Dynamics*, 52(1):69–82, 2019. 92, 119

P. E. Lydolph. *Climates of the Soviet Union*. Elsevier Scientific Publishing Company, 1977. 90

S. Manabe and T. B. Terpstra. The effects of mountains on the general circulation of the atmosphere as identified by numerical experiments. *Journal of Atmospheric Sciences*, 31(1): 3–42, 1974. 21, 72

E. Manzini, A. Y. Karpechko, J. Anstey, M. Baldwin, R. Black, C. Cagnazzo, N. Calvo, A. Charlton-Perez, B. Christiansen, P. Davini, et al. Northern winter climate change: Assessment of uncertainty in cmip5 projections related to stratosphere-troposphere coupling. *Journal of Geophysical Research: Atmospheres*, 119(13):7979–7998, 2014. 108, 110

J. Marshall and D. W. So. Thermal equilibration of planetary waves. *Journal of Atmospheric Sciences*, 47(8):963–978, 1990. 33

T. Matsuno. A dynamical model of the stratospheric sudden warming. *Journal of Atmospheric Sciences*, 28(8):1479–1494, 1971. 4

G. Messori, C. Woods, and R. Caballero. On the drivers of wintertime temperature extremes in the high arctic. *Journal of Climate*, 31(4):1597–1618, 2018. 91, 105

H. L. Mitchell and J. Derome. Blocking-like solutions of the potential vorticity equation: their stability at equilibrium and growth at resonance. *Journal of Atmospheric Sciences*, 40(10): 2522–2536, 1983. 33

F. Molteni. Atmospheric simulations using a gcm with simplified physical parametrizations. i: Model climatology and variability in multi-decadal experiments. *Climate Dynamics*, 20(2-3): 175–191, 2003. 35, 77

F. Molteni and F. Kucharski. Description of the ictp agcm (speedy) version 40. *Abdus Salam International Centre for Theoretical Physics, Trieste, Italy. Consulted in March*, 2016. 36

F. Molteni, M. P. King, F. Kucharski, and D. M. Straus. Planetary-scale variability in the northern winter and the impact of land–sea thermal contrast. *Climate dynamics*, 37(1-2): 151–170, 2011. 34, 38

H. Nakamura, T. Sampe, A. Goto, W. Ohfuchi, and S.-P. Xie. On the importance of midlatitude oceanic frontal zones for the mean state and dominant variability in the tropospheric circulation. *Geophysical Research Letters*, 35(15), 2008. 27

S. Nigam, I. M. Held, and S. W. Lyons. Linear simulation of the stationary eddies in a gcm. part ii: The "mountain" model. *Journal of the atmospheric sciences*, 45(9):1433–1452, 1988. 21

N.-E. Omrani, F. Ogawa, H. Nakamura, N. Keenlyside, S. W. Lubis, and K. Matthes. Key role of the ocean western boundary currents in shaping the northern hemisphere climate. *Scientific reports*, 9(1):1–12, 2019. 27

B. C. O'Neill, C. Tebaldi, D. P. Van Vuuren, V. Eyring, P. Friedlingstein, G. Hurtt, R. Knutti,

E. Kriegler, J.-F. Lamarque, J. Lowe, et al. The scenario model intercomparison project (scenariomip) for cmip6. *Geoscientific Model Development*, 9(9):3461–3482, 2016. 109

J. Opsteegh and A. Vernekar. A simulation of the january standing wave pattern including the effects of transient eddies. *Journal of the Atmospheric Sciences*, 39(4):734–744, 1982. 25

Y. J. Orsolini and N. G. Kvamstø. Role of eurasian snow cover in wintertime circulation: Decadal simulations forced with satellite observations. *Journal of Geophysical Research: Atmospheres*, 114(D19), 2009. 92

T. Oudar, J. Cattiaux, and H. Douville. Drivers of the northern extratropical eddy-driven jet change in cmip5 and cmip6 models. *Geophysical Research Letters*, 47(8):e2019GL086695, 2020. 62, 108, 109, 110, 111, 113

F. Panagiotopoulos, M. Shahgedanova, A. Hannachi, and D. B. Stephenson. Observed trends and teleconnections of the siberian high: A recently declining center of action. *Journal of climate*, 18(9):1411–1422, 2005. 90, 100

L. Papritz and T. Spengler. Analysis of the slope of isentropic surfaces and its tendencies over the north atlantic. *Quarterly Journal of the Royal Meteorological Society*, 141(693): 3226–3238, 2015. 82

J. P. Peixoto, A. H. Oort, and E. N. Lorenz. *Physics of climate*, volume 520. Springer, 1992. 27, 99

Y. Peng, A. Duan, W. Hu, B. Tang, X. Li, and X. Yang. Observational constraint on the future projection of temperature in winter over the tibetan plateau in cmip6 models. *Environmental Research Letters*, 2022. 75, 88

S. Petterssen and S. Smebye. On the development of extratropical cyclones. *Quarterly Journal of the Royal Meteorological Society*, 97(414):457–482, 1971. 56

J. Piao, W. Chen, Q. Zhang, and P. Hu. Comparison of moisture transport between siberia and northeast asia on annual and interannual time scales. *Journal of Climate*, 31(18):7645–7660, 2018. 91

F. Pithan and T. Mauritsen. Arctic amplification dominated by temperature feedbacks in contemporary climate models. *Nature geoscience*, 7(3):181–184, 2014. 90, 91

L. M. Polvani and P. J. Kushner. Tropospheric response to stratospheric perturbations in a relatively simple general circulation model. *Geophysical Research Letters*, 29(7):18–1, 2002. 58

A. Portal, P. Ruggieri, F. M. Palmeiro, J. García-Serrano, D. I. Domeisen, and S. Gualdi. Seasonal prediction of the boreal winter stratosphere. *Climate Dynamics*, pages 1–22, 2021. 61

A. Portal, C. Pasquero, F. D'Andrea, P. Davini, M. E. Hamouda, and G. Rivière. Influence of reduced winter land–sea contrast on the midlatitude atmospheric circulation. *Journal of Climate*, 35(19):2637–2651, 2022. 74, 77, 79

M. Previdi, K. L. Smith, and L. M. Polvani. Arctic amplification of climate change: a review of underlying mechanisms. *Environmental Research Letters*, 2021. 34

M. D. Priestley, D. Ackerley, J. L. Catto, K. I. Hodges, R. E. McDonald, and R. W. Lee. An overview of the extratropical storm tracks in cmip6 historical simulations. *Journal of Climate*, 33(15):6315–6343, 2020. 82

M. D. Priestley, D. Ackerley, J. L. Catto, and K. I. Hodges. Drivers of biases in the cmip6 extratropical storm tracks. part 1: Northern hemisphere. *Journal of Climate*, pages 1–37, 2022. 74

S. Rahmstorf, J. E. Box, G. Feulner, M. E. Mann, A. Robinson, S. Rutherford, and E. J. Schaffernicht. Exceptional twentieth-century slowdown in atlantic ocean overturning circulation. *Nature climate change*, 5(5):475–480, 2015. 41

N. Rayner, D. E. Parker, E. Horton, C. K. Folland, L. V. Alexander, D. Rowell, E. C. Kent, and A. Kaplan. Global analyses of sea surface temperature, sea ice, and night marine air temperature since the late nineteenth century. *Journal of Geophysical Research: Atmospheres*, 108(D14), 2003. 38, 77

T. D. Ringler and K. H. Cook. Understanding the seasonality of orographically forced stationary waves: Interaction between mechanical and thermal forcing. *Journal of the atmospheric sciences*, 56(9):1154–1174, 1999. 24, 117, 118

G. Rivière. A dynamical interpretation of the poleward shift of the jet streams in global warming scenarios. *Journal of the Atmospheric Sciences*, 68(6):1253–1272, 2011. 58

G. Rivière and I. Orlanski. Characteristics of the atlantic storm-track eddy activity and its relation with the north atlantic oscillation. *Journal of the Atmospheric Sciences*, 64(2): 241–266, 2007. 54

P. Ruggieri, F. Kucharski, R. Buizza, and M. Ambaum. The transient atmospheric response to a reduction of sea-ice cover in the barents and kara seas. *Quarterly Journal of the Royal Meteorological Society*, 143(704):1632–1640, 2017. 36, 62

P. Rupp and T. Birner. Tropospheric eddy feedback to different stratospheric conditions in idealised baroclinic life cycles. *Weather and Climate Dynamics*, 2(1):111–128, 2021. 58

K. Saito, J. Cohen, and D. Entekhabi. Evolution of atmospheric response to early-season eurasian snow cover anomalies. *Monthly Weather Review*, 129(11):2746–2760, 2001. 92

B. Saltzman. Empirical forcing functions for the large-scale mean disturbances in the atmosphere. *Geofisica pura e applicata*, 52(1):173–188, 1962. 25

T. Sato. Influences of subtropical jet and tibetan plateau on precipitation pattern in asia: Insights from regional climate modeling. *Quaternary International*, 194(1-2):148–158, 2009. 72

S. Schemm, H. Wernli, and H. Binder. The storm-track suppression over the western north pacific from a cyclone life-cycle perspective. *Weather and Climate Dynamics*, 2(1):55–69, 2021. 82

R. Seager, D. S. Battisti, J. Yin, N. Gordon, N. Naik, A. C. Clement, and M. A. Cane. Is the gulf stream responsible for europe's mild winters? *Quarterly Journal of the Royal Me-*

teorological Society: A journal of the atmospheric sciences, applied meteorology and physical oceanography, 128(586):2563–2586, 2002. 60

S. I. Seneviratne, T. Corti, E. L. Davin, M. Hirschi, E. B. Jaeger, I. Lehner, B. Orlowsky, and A. J. Teuling. Investigating soil moisture–climate interactions in a changing climate: A review. *Earth-Science Reviews*, 99(3-4):125–161, 2010. 27, 29

M. C. Serreze and R. G. Barry. Processes and impacts of arctic amplification: A research synthesis. *Global and planetary change*, 77(1-2):85–96, 2011. 34

M. C. Serreze and R. G. Barry. *The Arctic climate system*. Cambridge University Press, 2014. 90

M. C. Serreze, J. D. Kahl, and R. C. Schnell. Low-level temperature inversions of the eurasian arctic and comparisons with soviet drifting station data. *Journal of Climate*, 5(6):615–629, 1992. 90

Y. Sha, Z. Shi, X. Liu, and Z. An. Distinct impacts of the mongolian and tibetan plateaus on the evolution of the east asian monsoon. *Journal of Geophysical Research: Atmospheres*, 120 (10):4764–4782, 2015. 73, 81, 84, 88

T. Shaw and A. Voigt. Tug of war on summertime circulation between radiative forcing and sea surface warming. *Nature Geoscience*, 8(7):560–566, 2015. 34

T. Shaw, M. Baldwin, E. A. Barnes, R. Caballero, C. Garfinkel, Y.-T. Hwang, C. Li, P. O'gorman, G. Rivière, I. Simpson, et al. Storm track processes and the opposing influences of climate change. *Nature Geoscience*, 9(9):656–664, 2016. 62

Z. Shi, X. Liu, Y. Liu, Y. Sha, and T. Xu. Impact of mongolian plateau versus tibetan plateau on the westerly jet over north pacific ocean. *Climate Dynamics*, 44(11):3067–3076, 2015. 73, 88

M. D. Shupe and J. M. Intrieri. Cloud radiative forcing of the arctic surface: The influence of cloud properties, surface albedo, and solar zenith angle. *Journal of climate*, 17(3):616–628, 2004. 91, 97

J. Smagorinsky. The dynamical influence of large-scale heat sources and sinks on the quasi-stationary mean motions of the atmosphere. *Quarterly Journal of the Royal Meteorological Society*, 79(341):342–366, 1953. xiii, 1, 2, 5, 8, 18, 19, 20, 21, 24, 33, 34, 72

L. Smy and R. Scott. The influence of stratospheric potential vorticity on baroclinic instability. *Quarterly Journal of the Royal Meteorological Society: A journal of the atmospheric sciences, applied meteorology and physical oceanography*, 135(644):1673–1683, 2009. 58

K. Stramler, A. D. Del Genio, and W. B. Rossow. Synoptically driven arctic winter states. *Journal of Climate*, 24(6):1747–1762, 2011. 90

F. Su, X. Duan, D. Chen, Z. Hao, and L. Cuo. Evaluation of the global climate models in the cmip5 over the tibetan plateau. *Journal of climate*, 26(10):3187–3208, 2013. 75

R. T. Sutton, B. Dong, and J. M. Gregory. Land/sea warming ratio in response to climate change: Ipcc ar4 model results and comparison with observations. *Geophysical research letters*, 34(2), 2007. 34

K. Takaya and H. Nakamura. Mechanisms of intraseasonal amplification of the cold siberian high. *Journal of the Atmospheric Sciences*, 62(12):4423–4440, 2005. 90, 91, 92

K. E. Taylor, R. J. Stouffer, and G. A. Meehl. An overview of cmip5 and the experiment design. *Bulletin of the American meteorological Society*, 93(4):485–498, 2012. 41

D. W. Thompson and J. M. Wallace. The arctic oscillation signature in the wintertime geopotential height and temperature fields. *Geophysical research letters*, 25(9):1297–1300, 1998. 92, 104

M. Ting. The stationary wave response to a midlatitude sst anomaly in an idealized gcm. *Journal of the atmospheric sciences*, 48(10):1249–1275, 1991. 24, 74

K. E. Trenberth. Interactions between orographically and thermally forced planetary waves. *Journal of Atmospheric Sciences*, 40(5):1126–1153, 1983. 24, 74, 79, 106, 117, 118

G. Tselioudis, Y. Zhang, and W. B. Rossow. Cloud and radiation variations associated with northern midlatitude low and high sea level pressure regimes. *Journal of climate*, 13(2): 312–327, 2000. 91

P. J. Valdes and B. J. Hoskins. Linear stationary wave simulations of the time-mean climatological flow. *Journal of Atmospheric Sciences*, 46(16):2509–2527, 1989. 21, 34

G. K. Vallis. *Atmospheric and oceanic fluid dynamics*. Cambridge University Press, 2017. 17

B. Van den Hurk, H. Kim, G. Krinner, S. I. Seneviratne, C. Derksen, T. Oki, H. Douville, J. Colin, A. Ducharne, F. Cheruy, et al. Ls3mip (v1. 0) contribution to cmip6: the land surface, snow and soil moisture model intercomparison project–aims, setup and expected outcome. *Geoscientific Model Development*, 9(8):2809–2832, 2016. 29

C. Wallace and M. Joshi. Comparison of land–ocean warming ratios in updated observed records and cmip5 climate models. *Environmental Research Letters*, 13(11):114011, 2018. 34

H. Wang and M. Ting. Seasonal cycle of the climatological stationary waves in the ncep–ncar reanalysis. *Journal of the atmospheric sciences*, 56(22):3892–3919, 1999. 40, 43

P. X. Wang, B. Wang, H. Cheng, J. Fasullo, Z. Guo, T. Kiefer, and Z. Liu. The global monsoon across time scales: Mechanisms and outstanding issues. *Earth-Science Reviews*, 174:84–121, 2017. 29

P. J. Webster. The variable and interactive monsoon. *Monsoon*, pages 269–330, 1986. 29

K. Wei, T. Xu, Z. Du, H. Gong, and B. Xie. How well do the current state-of-the-art cmip5 models characterise the climatology of the east asian winter monsoon? *Climate dynamics*, 43:1241–1255, 2014. 74, 75

R. White, D. Battisti, and G. Roe. Mongolian mountains matter most: Impacts of the latitude and height of asian orography on pacific wintertime atmospheric circulation. *Journal of Climate*, 30(11):4065–4082, 2017. 24, 72, 73, 84, 88, 106, 119

D. S. Wilks. *Statistical methods in the atmospheric sciences*, volume 100. Academic press, 2011. xv, 44, 46, 76, 94

R. C. Wills, R. H. White, and X. J. Levine. Northern hemisphere stationary waves in a changing climate. *Current climate change reports*, 5(4):372–389, 2019. 62

M. A. Wittman, A. J. Charlton, and L. M. Polvani. The effect of lower stratospheric shear on baroclinic instability. *Journal of the atmospheric sciences*, 64(2):479–496, 2007. 58

C. Woods, R. Caballero, and G. Svensson. Large-scale circulation associated with moisture intrusions into the arctic during winter. *Geophysical Research Letters*, 40(17):4717–4721, 2013. 91, 105

B. Wu and J. Wang. Winter arctic oscillation, siberian high and east asian winter monsoon. *Geophysical research letters*, 29(19):3–1, 2002. 91, 103

G. Wu, Y. Liu, Q. Zhang, A. Duan, T. Wang, R. Wan, X. Liu, W. Li, Z. Wang, and X. Liang. The influence of mechanical and thermal forcing by the tibetan plateau on asian climate. *Journal of Hydrometeorology*, 8(4):770–789, 2007. 29

G. Wu, A. Duan, Y. Liu, J. Mao, R. Ren, Q. Bao, B. He, B. Liu, and W. Hu. Tibetan plateau climate dynamics: recent research progress and outlook. *National Science Review*, 2(1): 100–116, 2015. 74

M. Xu, H. Xu, and J. Ma. Responses of the east asian winter monsoon to global warming in cmip5 models. *International Journal of Climatology*, 36(5):2139–2155, 2016. 88

Y. Xue, T. Yao, A. A. Boone, I. Diallo, Y. Liu, X. Zeng, W. K. Lau, S. Sugimoto, Q. Tang, X. Pan, et al. Impact of initialized land surface temperature and snowpack on subseasonal to seasonal prediction project, phase i (ls4p-i): organization and experimental design. *Geoscientific Model Development*, 14(7):4465–4494, 2021. 74, 89

Y. Xue, I. Diallo, A. A. Boone, T. Yao, Y. Zhang, X. Zeng, J. David Neelin, W. K. Lau, Y. Pan, Y. Liu, et al. Spring land temperature in tibetan plateau and global-scale summer precipitation–initialization and improved prediction. *Bulletin of the American Meteorological Society*, 2022. 30, 74

M. Yanai and G.-X. Wu. Effects of the tibetan plateau. In *The Asian Monsoon*, pages 513–549. Springer, 2006. 73

M. Yanai, C. Li, and Z. Song. Seasonal heating of the tibetan plateau and its effects on the evolution of the asian summer monsoon. *Journal of the Meteorological Society of Japan. Ser. II*, 70(1B):319–351, 1992. 73

D.-Z. Ye and G.-X. Wu. The role of the heat source of the tibetan plateau in the general circulation. *Meteorology and Atmospheric Physics*, 67(1):181–198, 1998. 73

T. Yeh, R. Wetherald, and S. Manabe. A model study of the short-term climatic and hydrologic effects of sudden snow-cover removal. *Monthly Weather Review*, 111(5):1013–1024, 1983. 74

D. Yihui. Build-up, air mass transformation and propagation of siberian high and its relations to cold surge in east asia. *Meteorology and Atmospheric Physics*, 44(1):281–292, 1990. 91

D. Yihui and J. C. Chan. The east asian summer monsoon: an overview. *Meteorology and Atmospheric Physics*, 89(1):117–142, 2005. 73

Q. You, D. Chen, F. Wu, N. Pepin, Z. Cai, B. Ahrens, Z. Jiang, Z. Wu, S. Kang, and A. AghaKouchak. Elevation dependent warming over the tibetan plateau: Patterns, mechanisms and perspectives. *Earth-Science Reviews*, 210:103349, 2020. 111

C. Youngblut and T. Sasamori. The nonlinear effects of transient and stationary eddies an the winter mean circulation. part i: Diagnostic analysis. *Journal of the Atmospheric Sciences*, 37(9):1944–1957, 1980. 25

G. Zappa and T. G. Shepherd. Storylines of atmospheric circulation change for european regional climate impact assessment. *Journal of Climate*, 30(16):6561–6577, 2017. 69, 108, 109, 110, 111, 113

Y. Zhang, K. R. Sperber, and J. S. Boyle. Climatology and interannual variation of the east asian winter monsoon: Results from the 1979–95 ncep/ncar reanalysis. *Monthly weather review*, 125(10):2605–2619, 1997. 91, 92

X. Zhu, S.-Y. Lee, X. Wen, Z. Wei, Z. Ji, Z. Zheng, and W. Dong. Historical evolution and future trend of northern hemisphere snow cover in cmip5 and cmip6 models. *Environmental Research Letters*, 16(6):065013, 2021. 93, 98

M. Zhuang, A. Duan, R. Lu, P. Li, and J. Yao. Relative impacts of the orography and land–sea contrast over the indochina peninsula on the asian summer monsoon between early and late summer. *Journal of Climate*, pages 1–35, 2022. 34